1-1-2004

# Fatigue life prediction in a door hinge system under uni-axial and multi-axial loading conditions

Sacheen Bekah
*Ryerson University*

# FATIGUE LIFE PREDICTION IN A DOOR HINGE SYSTEM UNDER UNI-AXIAL AND MULTI-AXIAL LOADING CONDITIONS

by

**SACHEEN BEKAH, B. Eng. (AEROSPACE)**

**RYERSON UNIVERSITY, 2002**

A thesis

presented to Ryerson University

in partial fulfillment of the requirement for the degree of

Master of Applied Science

in the Program of

Mechanical Engineering

Toronto, Ontario, Canada, 2004

*Your file Votre référence*
*ISBN: 0-494-08195-3*
*Our file Notre référence*
*ISBN: 0-494-08195-3*

# AUTHOR'S DECLARATION

I hereby declare that I am the sole author of this thesis.

I authorize Ryerson University to lend this thesis to other institutions or individuals for the purpose of scholarly research.

I further authorize Ryerson University to reproduce this thesis by photocopying or by other means, in total or in part, at the request of other institutions or individuals for the purpose of scholarly research.

# ABSTRACT

*FATIGUE LIFE PREDICTION IN A DOOR HINGE SYSTEM UNDER UNI-AXIAL AND MULTI-AXIAL LOADING CONDITIONS*

© Sacheen Bekah, 2004

Master of Applied Science

in the Program of

Mechanical Engineering

Ryerson University

This thesis presents the use of Finite Element (FE) based fatigue analysis to locate the critical point of crack initiation and predict life in a door hinge system that is subjected to both uni-axial and multi-axial loading. The results are experimentally validated. The FE model is further used to obtain an optimum design per the standard requirement in the ground vehicle industry. The accuracy of the results showed that FE based fatigue analysis can be successfully employed to reduce costly and time-consuming experiments in the preliminary design stage. Numerical analysis also provides the product design engineers with substantial savings, enabling the testing of fewer prototypes.

# ACKNOWLEDGEMENTS

I would like to extend my sincerest gratitude to my principal supervisor Dr. Kamran Behdinan and Co-supervisor, Dr. Zouheir Fawaz for their continuous support and guidance before, during and after the process of this research. My gratitude also goes to Dr. Kornel Farkas, Jake Xu, Dave McCabe and Malisha Djokic of Van-Rob Stampings Inc. who provided valuable suggestions in the Finite Element and Experimental Fatigue aspect of this research. Special thanks are also granted to my colleagues at the Advanced Computational Laboratory of Ryerson University: Kin-Pong Louis Lam, Primoz Cresnik for their priceless support in the Finite Element Modeling and Analysis aspect of this research and Masoud Alimardani, Simon Chan, Yigui Xu for their beneficial discussions in Solid Mechanics. Finally, I would like to extend my appreciation to Materials and Manufacturing Ontario (MMO), NCE-AUTO-21 and Van-Rob Stampings Inc. for their joint support in the collaborative research and development grant for this project.

# DEDICATION

I would like to dedicate this thesis to my family: My father and mother, Doodave and Woormeela Bekah, my uncle and aunt, Loondeo and Anuradha Bekah, my brother, Devesh Bekah and my cousins, Nandishi and Dhilan Bekah. ***Their unfailing support and continuous words of encouragement throughout these years will always be remembered…***

# TABLE OF CONTENTS

# LIST OF FIGURES

# LIST OF TABLES

# NOMENCLATURE

## Roman

| | |
|---|---|
| $a$ | area of triangular element |
| $a_e$ | mean bi-axiality ratio |
| $b$ | fatigue strength exponent |
| $c$ | fatigue ductility exponent |
| $D$ | Miner's rule damage parameter |
| $e$ | engineering strain |
| $e_f^1$ | engineering cyclic strain at fracture |
| $E$ | elastic modulus |
| $F$ | applied force in beam |
| $h$ | distance between the midpoints of opposite faces in a hex or wedge element |
| $H$ | height of beam |
| $i$ | numerical increment |
| $I$ | area moment of inertia for the beam |
| $J_2$ | Von Mises stress deviator |
| $J$ | jacobian |
| $K^1$ | cyclic strength coefficient |
| $K_t$ | stress concentration factor |
| $L$ | length of beam |
| $M$ | applied moment in beam |

| | |
|---|---|
| n | number of cycles of operation |
| $n^1$ | cyclic strain hardening exponent |
| $N$ | total number of cycles of operation |
| $N_f$ | total number of cycles to failure |
| $S$ | engineering stress |
| $S_a$ | allowable engineering stress amplitude |
| $S_m$ | mean engineering stress |
| $S_o$ | allowable engineering stress amplitude at zero mean stress |
| $S_u$ | ultimate engineering tensile stress |
| $S_{0.2}$ | 0.2% proof strength |
| $SRI$ | stress range intercept |
| W | width of beam |
| y | vertical height from beam neutral axis |

## Greek

| | |
|---|---|
| $\alpha$ | skew angle |
| $\Delta$ | differential change |
| $\varepsilon$ | true strain |
| $\varepsilon_a$ | true cyclic strain amplitude |
| $\varepsilon_t$ | total strain |
| $\varepsilon_f^1$ | fatigue ductility coefficient |
| $\phi_p$ | angle of spread |
| $\sigma$ | true stress |

| | |
|---|---|
| $\sigma_f$ | true fracture strength |
| $\sigma_f^1$ | fatigue strength coefficient |
| $\sigma_{\max}$ | maximum true stress |
| $\sigma_0$ | Morrow mean stress |
| $\sigma_x$ | maximum principal stress in the x-direction |
| $\sigma_y$ | maximum principal stress in the y-direction |
| $\sigma_z$ | maximum principal stress in the z-direction |
| $\tau_{\max}$ | maximum shear stress (Tresca) |
| $\tau_{xy}$ | maximum principal stress in the xy-direction |
| $\tau_{xz}$ | maximum principal stress in the xz-direction |
| $\tau_{yz}$ | maximum principal stress in the yz-direction |
| $\theta$ | warp angle |

# CHAPTER 1 INTRODUCTION

## 1.1 Objective

The major challenge in today's ground vehicle industry is to overcome the increasing demands of higher performance, lower weight, and longer life of components, all this at a reasonable cost and in a short period of time. Fatigue failure is a multi-stage process that begins with crack initiation, propagating with continued cyclic loading and finally, rupture of the component or specimen. It is estimated that fatigue is responsible for 85% to 90% of all structural failures [1]. As such, early engineers used many cut-and-try practices in their machine designs in an attempt to minimize these failures [2]. This has led to the development of experimentally oriented tests and development procedures [2]. For many years, structural designers spent a considerable amount of time performing experimental testing, which in some occasions appeared to be quite expensive. As the engineering profession developed further, analytical techniques were introduced to improve the design procedures. As the components became more complex, the more difficult it was to apply analytical techniques to predict fatigue life. Instead, numerical approaches have been developed, which make it possible to effectively analyze complex structures and obtain solutions faster. These numerical approaches use both the data obtained from multiple experimental testing together with the analytical correlations developed.

For the effective use of these numerical approaches, knowledge of Finite Element Analysis (FEA) is required. In the same progressive manner as fatigue,

FEA is now an integral part of structural design. FEA allows design analysts and engineers to create virtual models and perform simulations in the preliminary design stage. As such, a considerable amount of time and cost is saved.

The majority of investigations into the fatigue process are concerned with locating critical points where cracks might occur in components under specific loading conditions. This is followed by the estimation of the total life expectancy of that component [1]. The aim of this thesis is to effectively combine the methods involved in fatigue and FEA to predict the life in a 60-degree front door hinge assembly system. Finite Element (FE) is used as a tool to create the virtual model of the hinge and perform a static analysis. The stresses and strains from the static analysis are then used as input to locate the critical point and predict the life expectancy of the hinge under uni-axial and multi-axial loadings. The uni-axial and multi-axial fatigue results are then validated from experiments conducted at Van-Rob Stampings Inc. Moreover, only numerical approaches are used to improve the fatigue life of the hinge. As such, the outcome of these results provide the product development specialists at Van-Rob Stampings Inc. with tremendous savings in time and cost because of a reduction in the number of prototypes to be tested in the preliminary design stage.

## 1.2 Background on Fatigue

Modern engineering structures and components are rarely subjected to purely static loading. The majority of structures involve fluctuating or cyclic

loads [1]. These fluctuating or cyclic loads induce cyclic stresses in theses structures causing failure through fatigue.

For centuries, it has been known that a piece of metal can fail under repeated loading at a stress level well below the ultimate tensile strength of the material. Hence came fatigue, from a French engineer Monsieur Poncelet, who related fatigue to its biological counterpart meaning tired [2]. However, the first fatigue investigations came from a German engineer, W.A.S. Albert in 1829, who conducted repeated loading tests on iron chains [1]. When fatigue failure began to develop rapidly in railway axles in the middle of the nineteenth century, numerous engineers began to draw their attention to cyclic loading effects [1]. As such, attempts were made to correlate these failures to experiments conducted in the laboratories.

Between 1852 and 1870, the German railway engineer August Wöhler successfully conducted fatigue tests on full-scale railway axles and small scale bending, torsion and axial cyclically loaded specimens for different materials [1-3]. Thereon, he plotted the results of stress amplitude against life cycles to failure, which is commonly known today as the Stress-Life (S-N) curve. R.R. Moore later followed the same principles as Wöhler and modified the S-N diagram. The currently available S-N data are based under Moore's fatigue tests [1-3].

By 1900, engineers put more effort into understanding the mechanisms of fatigue failure rather than just observing the results [1,2]. As a result, in the late 1950s and early 1960s, two new approaches to fatigue life estimation

emerged. The first one is known as the Manson-Coffin Local Strain approach or Strain-Life (ε-N) approach [1-4]. The ε-N approach attempts to describe and predict crack initiation. The second approach is based on Linear Elastic Fracture Mechanics (LEFM) and attempts to explain crack growth [1]. All the aforementioned approaches reflect structures under uni-axial stress states.

More recently, Miller has been working on ways of finding a unified theory of metal fatigue by describing failure of components under multi-axial loading [1,3]. Hence, a new approach emerged known as the critical plane approach [1-8]. The critical plane approach recognizes that fatigue is essentially a directional process where failure occurs through the thickness of the component instead of the surface [1,2]. Bannantine-Socie and Wang-Brown later developed their own theories following the work of Miller [1-3,5-9]. Presently, there is no general agreement about how to fully deal with multi-axial fatigue failure. The theories developed by Bannantine-Socie and Wang-Brown are still unvalidated [1].

## 1.3 Background Information on the Door Hinge

The door hinge under investigation is a 60-degree door hinge commonly used in trucks. The 60-degree movement of the hinge embodies the range of motion from a fully-closed to a fully-opened position. The 60-degree hinge is also available in 45 and 90-degree configurations. The three components comprising the hinge are a Door-Side (DS) bracket, a Body-Side (BS) bracket and a circular cross-sectional pin (see figure 1-1) are stamped together. This allows a free rotation of the DS and BS brackets about the pin, hence simulating

the open/close door movement. Each bracket consists of two cut-outs to allow for fasteners to attach the BS and DS brackets to the body and door of the vehicle respectively.

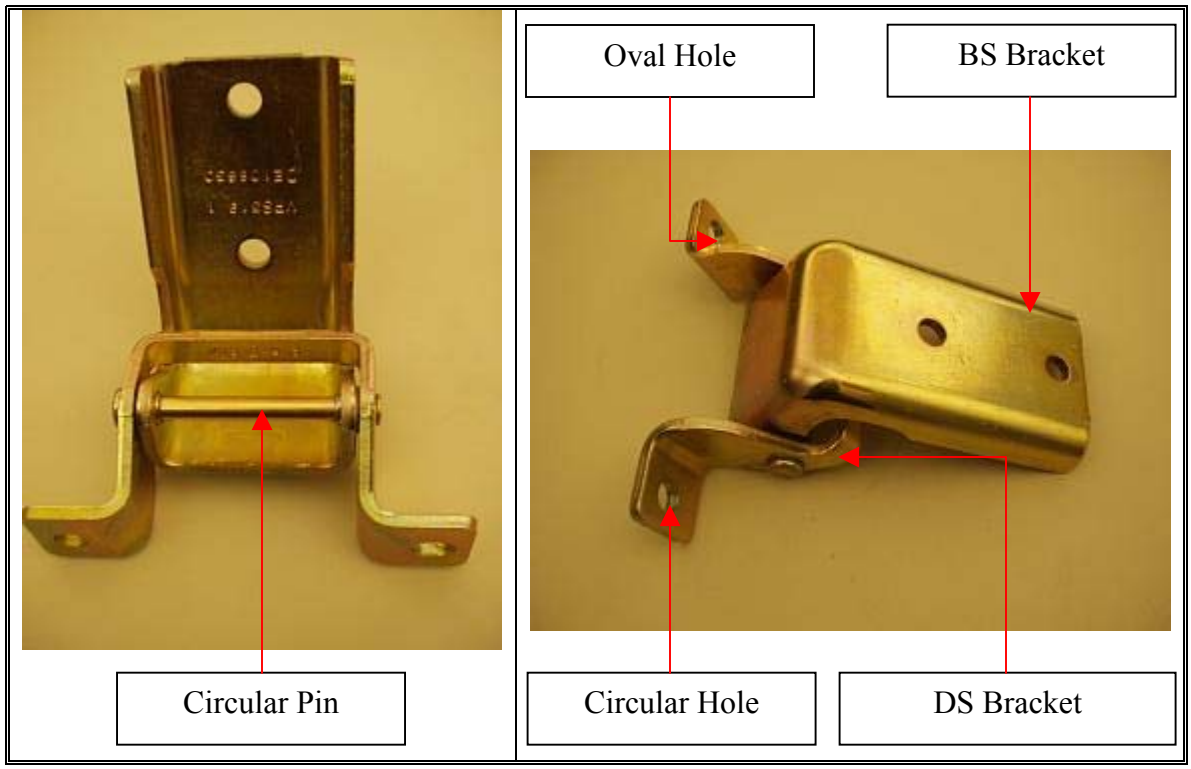


**Figure 1-1 A 60-Degree Door Hinge**

## 1.4 Thesis Contributions

There are three major contributions in this thesis:

I. Development of an effective FE model for a door hinge under uni-axial and multi-axial loading conditions.

II. Computational uni-axial and multi-axial fatigue life predicted for the door hinge is experimentally validated.

III. The accuracy of the results shows that there is no need for developing costly, time consuming experiments and FE fatigue analysis will suffice.

## 1.5 Thesis Outline

This thesis is organized as follows. Chapter two provides the theoretical approaches on fatigue, outlining the different methods used herein. Chapter three focuses on the uni-axial and multi-axial fatigue experiment. In contrast, chapters four and five are dedicated to numerical analysis, FEA and Fatigue respectively. Moreover, in chapter four, a detailed description of FE modeling of the hinge is also portrayed. Chapter six deal with the improvement in the fatigue life of the hinge through traditional optimization techniques. Finally, chapter seven reports the findings and provides a brief discussion and recommendation for this research.

# CHAPTER 2 FATIGUE, A THEORETICAL APPROACH

## 2.1 Overview

This chapter focuses on both the basic and advanced forms of fatigue failure in structures. Although this research is mainly based on fatigue pertaining to complex loading conditions, it is important to understand the basic and traditional theories involved in fatigue behaviour such as the stress-life and strain-life curves. The onset of uni-axial and multi-axial fatigue behaviours and their limitations are followed by detailed explanation on the various mechanisms that cause them. Further, environmental factors that adversely effects fatigue life are also succinctly discussed.

Before discussing into the different approaches to describe fatigue mechanisms, a brief introduction on the two dissimilar domains adopted by the uni-axial and multi-axial stress states is provided. The two domains herewith mentioned are referred to as high and low cycle fatigue respectively.

## 2.2 High Cycle versus Low Cycle Fatigue

Throughout years of investigations in fatigue theory, it has been found that the fatigue process embraces two distinct domains whereby the cyclic stresses and strains follow different paths to failure. In the first domain, the stresses and strains for the material under investigation are largely confined to the elastic region. As a result, failure will occur after large number of cycles, implying long lives [1,4,5,11]. This mechanism is commonly referred as high

cycle fatigue. As duty cycles become more severe and components more complicated, another failure mechanism occurs whereby the material endures significant plastic straining leading to short lives. This type of behaviour is referred to low cycle fatigue.

Recent investigations have led to believe that high and low cycle fatigue behaviour can be distinguished by observing the monotonic stress-strain curve for the particular material under static loading. The fact is that for an applied static load, the material will fall in the high cycle region if the magnitude of the maximum stress is lower than the tensile elastic limit or yield strength. On the other hand, low cycle fatigue is characterized by a maximum stress higher than the yield strength. In summary, high cycle fatigue is typically associated with lives greater than 100,000 cycles whereas low cycle fatigue involves lives between 1,000 to 100,000 cycles [1].

These observations are important as they provide a guideline for the selection of the appropriate methods in life prediction. The aforementioned methods are thoroughly discussed in sections 2.3 through 2.6.

## 2.3 Stress-Life Approach

It has been recognized, since 1830, that a metal subjected to a repeated or fluctuating load will fail at a stress level considerably lower than that required to cause fracture on a single application of that load [1,2,4,12]. The nominal stress or S-N approach was the first method developed to describe this phenomenon. Throughout years, it has been recognized that the S-N method works best in the high cycle regime where elastic events dominate plastic ones.

Hence, the S-N curve yields conservative results up to the yield point of the material where plastic effect is insignificant. The S-N method is inappropriate in the low cycle region, where applied strains have significant plastic component.

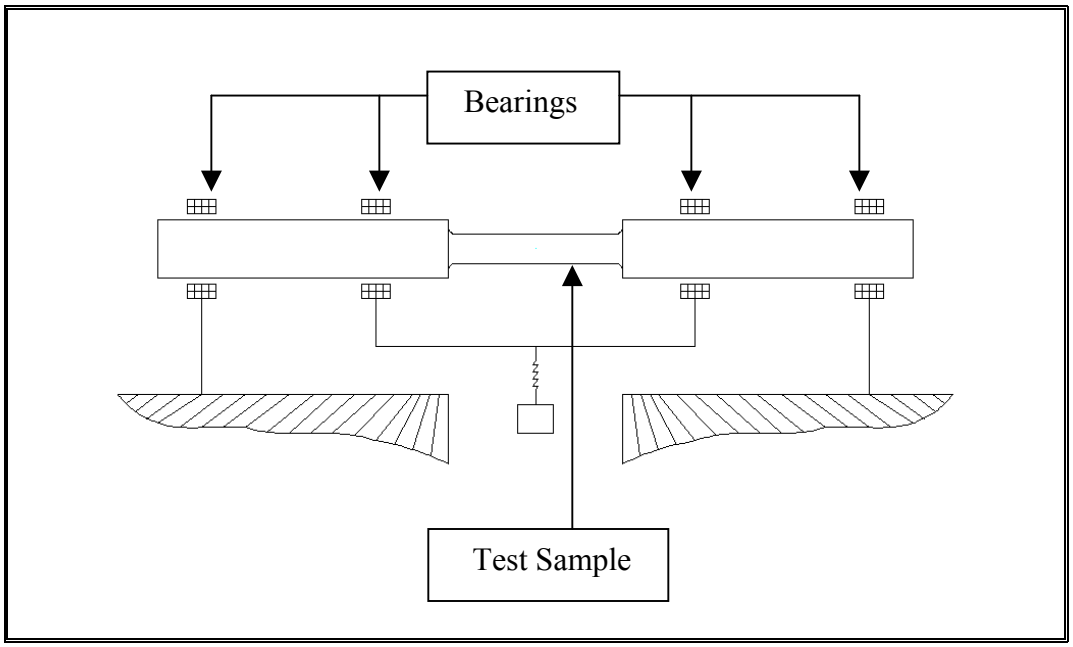


**Figure 2-1 The R. R. Moore Fatigue Testing Machine[1]**

A German engineer Wöhler was the first to conduct fatigue tests on specimens to characterize the material fatigue performance of metals [1,2,4,12]. Using a rotating bending test machine, Wöhler performed tests on notched and unnotched specimens and plotted stress amplitude versus cycles to failure, known today as the S-N diagram. Extensive efforts have been made over the years to understand the fatigue behaviour of metals along the lines of Wöhler. More recently, Moore conducted rotating bending tests. Using the R.R. Moore Fatigue Testing Machine as shown in figure 2-1, fatigue tests were conducted whereby a constant moment was applied to hourglass-shaped specimen polished to a mirror finish prior to testing [1].

### 2.3.1 The Stress-Life Curve

Figure 2-2 shows a typical S-N curve based on Moore's test. The fact is that for most materials used nowadays, the S-N curves are characterized by Moore's tests. The usual laboratory procedure for determining the S-N curve is to test the first specimen at a very high stress, usually about two thirds of its material's static tensile strength, where failure is expected to occur in fairly small number of cycles [1,2]. The stress is subsequently reduced until the point where no failure occurs, i.e., the endurance or fatigue limit (EL) [1]. It should be noted that the curve in figure 2-2 does not have the influence of mean stresses, notches, environment and surface finish. These effects will be discussed later.

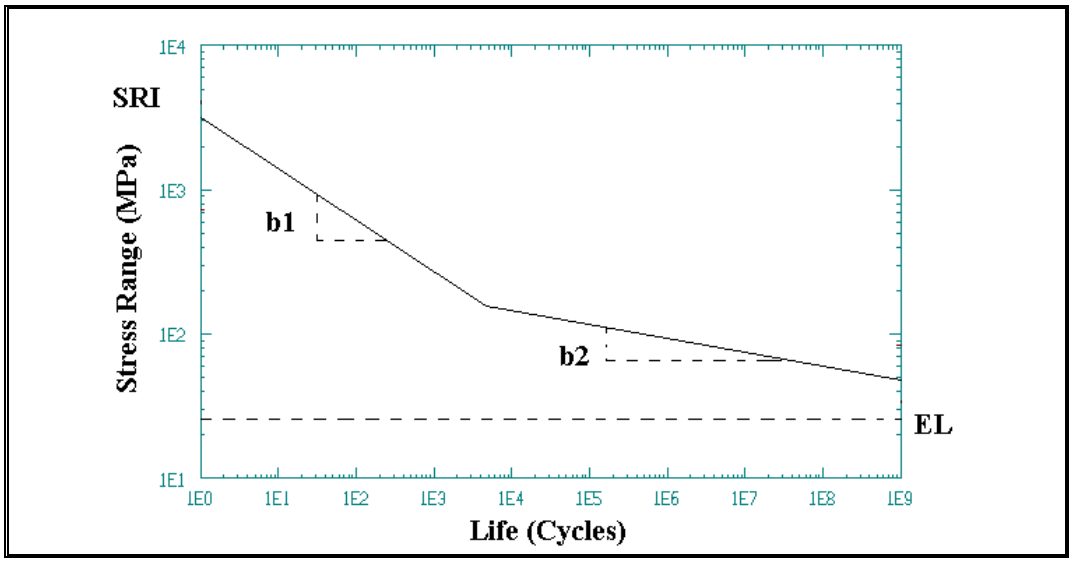


**Figure 2-2 The S-N Curve**[1]

The basic equation for the S-N curve as portrayed in figure 2-2 is:

$$\Delta S = SRIi\left(N_f\right)^{bi} \tag{2.1}$$

where, $\Delta S$ is the nominal stress range, SRI is the stress range intercept of the life line, $N_f$ is the number of cycles to failure, b1 and b2 are the slopes of life

lines 1 and 2 respectively and i is 1, 2 for the two slopes respectively. The interesting point to note here is when b2 is equal to zero, the corresponding material is said to have reached the endurance limit (EL). Materials such as mild steel do have the occurrence of an endurance limit of about $10^6$ cycles as opposed to nonferrous materials such as aluminum alloys. For this type of material, we have a designated life of $10^7$ cycles as the endurance limit [1].

The S-N approach is applicable to situations where cyclic loading is essentially elastic, meaning that the S-N curve should be used in regions where lives greater than 100,000 cycles are expected [1]. This is because the S-N curve is essentially flat in the low cycle region, and would yield an inaccurate estimation of life. The reason for this apparent flatness is the large plastic strain, which results from the high load levels. Low cycle fatigue analysis is best treated by strain-based procedures that account for the effects of plasticity [1,2,4].

### 2.3.2 The Influence of Mean Stress

Before examining the influence of mean stress on the S-N curve, it is important to consider the general types of cyclic stresses that contribute to the fatigue process. Most fatigue data collected in the laboratory employed fully reversed loading conditions [1,2,4,13,14] as shown in figure 2-3 (a). However most service loading conditions employ tensile loading, compressive loading or a combination of both. Figure 2-3 (b) and 2-3 (c) show a fully tensile loading and a combined tensile-compressive loading respectively.

Most realistic service situations involve non-zero mean stress [1].

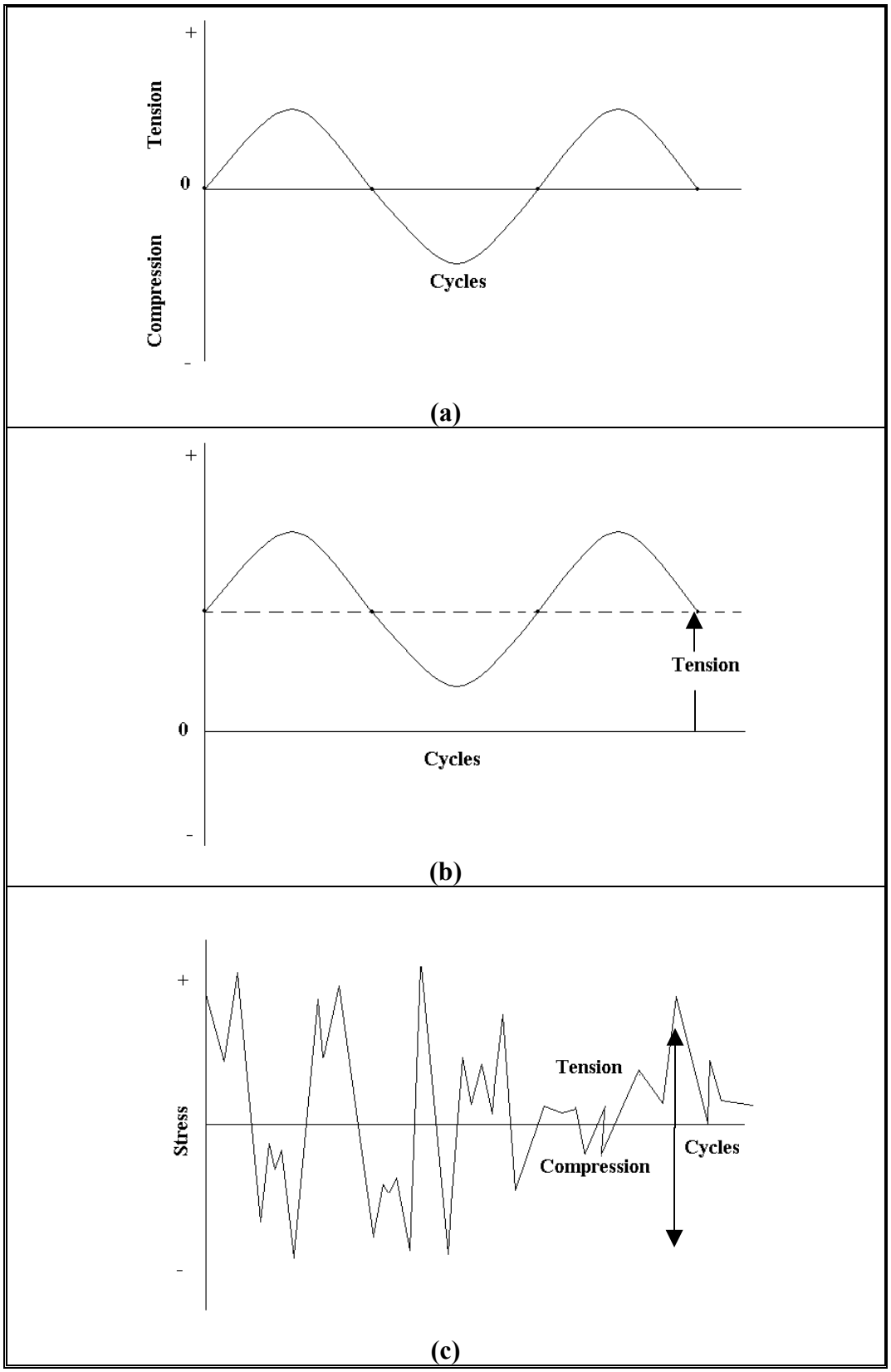


**Figure 2-3 Typical Fatigue Stress Cycles[1]**

Therefore, it is very important to fully characterize the effect mean stresses has on the fatigue process so that laboratory data can be efficiently employed in determining life calculations. Several empirical relations that characterize the effect of mean stress on fatigue life have been developed. Of all the proposed relationships, two has been most widely accepted, those of Goodman and Gerber [1,2,4,13,14].

According to Goodman, the effect of mean stress will reduce the applied stress amplitude in a linear way for both tensile and compressive mean stresses [1,14]. This procedure can be summarized as follows:

$$S_a = S_0\left[1-\frac{S_m}{S_u}\right] \tag{2.2}$$

where, $S_a$ is the allowable stress amplitude, $S_o$ is the allowable stress amplitude at zero mean stress, $S_m$ is the mean stress and $S_u$ is the ultimate tensile stress.

Gerber, on the other hand hypothesizes that the mean stress will reduce the applied stress amplitude in a quadratic way for both tensile and compressive state of mean stresses [1,13]. Hence Gerber's relation can be summarized as:

$$S_a = S_0\left[1-\left(\frac{S_m}{S_u}\right)^2\right] \tag{2.3}$$

Experience has shown that the actual data falls between the Goodman and Gerber's relationships [1]. Unfortunately, little or no experimental data exists to support one approach over the other. It is therefore recommended that the approach yielding the most conservative life be selected.

## 2.4 Strain-Life Approach

The stress-life approach has been used extensively to investigate the premature failure of structures or components subjected to fluctuating loads [1]. Traditionally, the magnitude of the stresses was low, hence the life cycles to failure greater than 100,000 cycles. This type of behaviour as previously mentioned is strictly confined within the elastic region of the material, before the yield point. However, as duty cycles have become more severe and the components more complicated, another pattern of fatigue behaviour has emerged [1]. In this regime, the cyclic stresses are very high, and a significant amount of plastic deformation is associated with the component. As a result, the component has short lives in the range of 100 to 100,000 cycles. This type of behaviour is commonly referred to as low cycle fatigue or strain controlled fatigue.

Strain controlled fatigue is based on the observation that in critical locations such as notches, the material response is strain rather than load controlled [1]. This observation comes from the fact that since most structures are designed to confine to the elastic regions, critical locations such as notches often cause significant amount of plastic deformation to occur locally. Hence, the deformation at the root of a notch is considered to be strain controlled.

The strain-life method assumes that the extent of plastic deformation at the root of a notch will be similar to that of a smooth specimen tested under strain controlled. Since the extent of plastic deformation is assumed to be similar, their lives will also be similar [1,2,4,5]. A strain transducer attached to

an hourglass smooth specimen is used to sense and control the appropriate strain limits. Thus, both stress and strain can be simultaneously monitored throughout the test, such that the deformation response of a material can be completely documented from initial cyclic shakedown, through mid-life steady-state response, to the formation and growth of a critical fatigue crack [2]. Unlike the nominal stress approach, the strain life methodology is characterized by two curves, namely the cyclic stress-strain curve and the strain-life curve.

### 2.4.1 Cyclic Stress-Strain Curve

To fully understand the characteristics of a cyclic stress-strain curve, it is important to comprehend the behaviour of a material when it is loaded monotonically. Tension tests on certain materials provide basic design data such as yield strength, ultimate tensile strength and ductility. In fatigue analyses, it provides baseline stress-strain curve for evaluating the nature and extent of any subsequently cyclically induced changes in deformation resistance (such as cyclic hardening of softening) [1,2,16].

In a tension test, a smooth cylindrical specimen is continually loaded with a tensile uni-axial load. The elongation of the specimen is simultaneously monitored throughout this process until the specimen fails. Figure 2-4 shows a typical monotonic stress-strain curve. The stress in the engineering stress-strain curve is calculated by subsequently dividing the applied load by the original cross-sectional area of the specimen. However, in reality, a true stress-strain curve yields the true behaviour of the material when loaded monotonically. In the latter case, the applied load is divided by the instantaneous cross-sectional

area. Figure 2-5 shows a true stress-strain curve as compared to its engineering counterpart. The empirical correlations that characterize the engineering and true stress-strain curves can be found in [1,2,4,16].

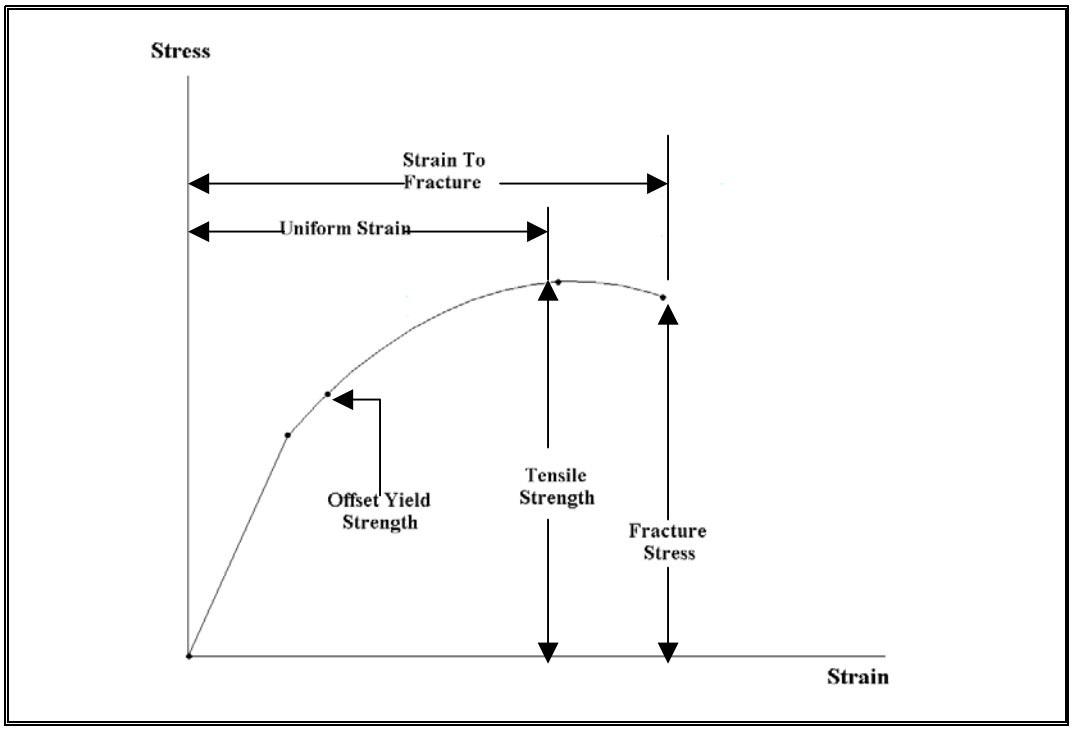


**Figure 2-4 The Engineering Stress-Strain Curve[1]**

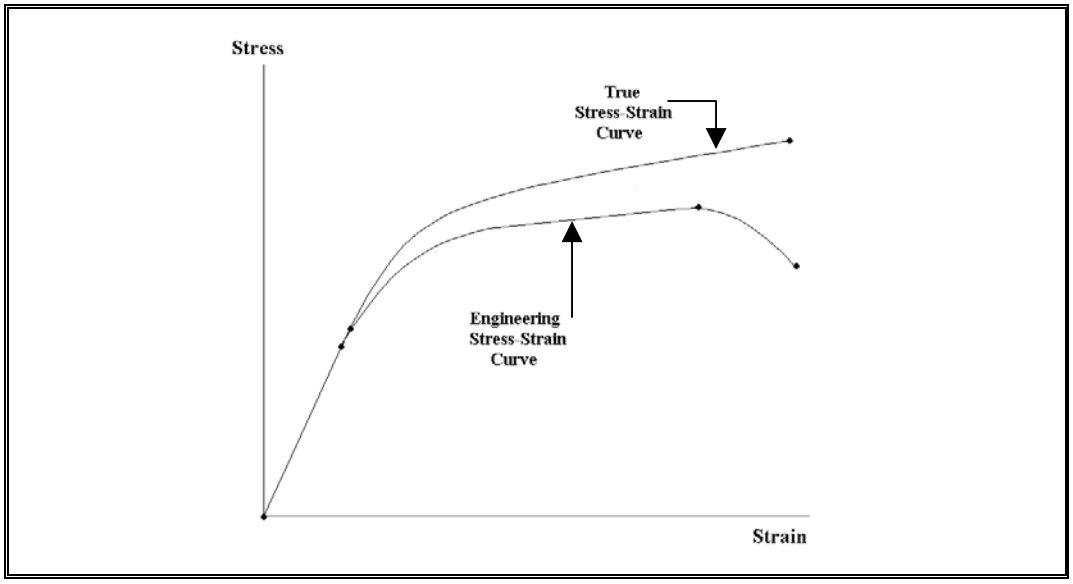


**Figure 2-5 A Comparison between True and Engineering Stress-Strain Curves[1]**

If during the course of a monotonic tension test the material is loaded to point B (see fig. 2-6 below) and the load removed, the curve will follow a straight line denoted by line BC. The slope of BC is equivalent to the elastic modulus represented by OA. Indeed, the calculation of slope BC is the most accurate way of measuring the elastic modulus of the material [1].

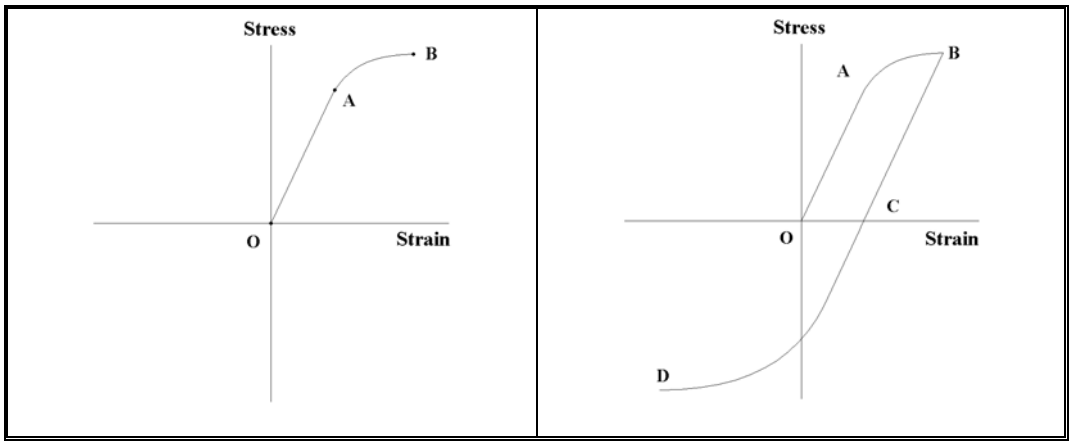


**Figure 2-6 Loading Reversed into Compression[1]**

Line OC represents the zero stress line, positive stress being tensile loading and negative, compressive loading. If the loading process OB is reversed at point C, the material will be in compression up to point D. It should be noted that point O is equidistant from points B and D both horizontally and vertically. At point D, the process OB is repeated, both in magnitude and direction. The curve will then follow the trend DB, forming a complete stress-strain cycle also known as a hysteresis loop (see figure 2-7). The above procedure is the first step towards a cyclic stress-strain curve.

If the material is continuously cycled between fixed strain limits, one of the following four events may happen. Depending on the type of material in terms of its properties and heat treatment, the material may [1,2,4]:

- cyclically soften
- cyclically harden
- remain stable
- cyclically harden and soften depending on strain range (mixed behaviour)

The onset of cyclic softening and hardening is illustrated in figure 2-8 below where two different materials are tested under fixed strain limits. Although strain is fixed, the loads vary significantly in that they converge to different levels.

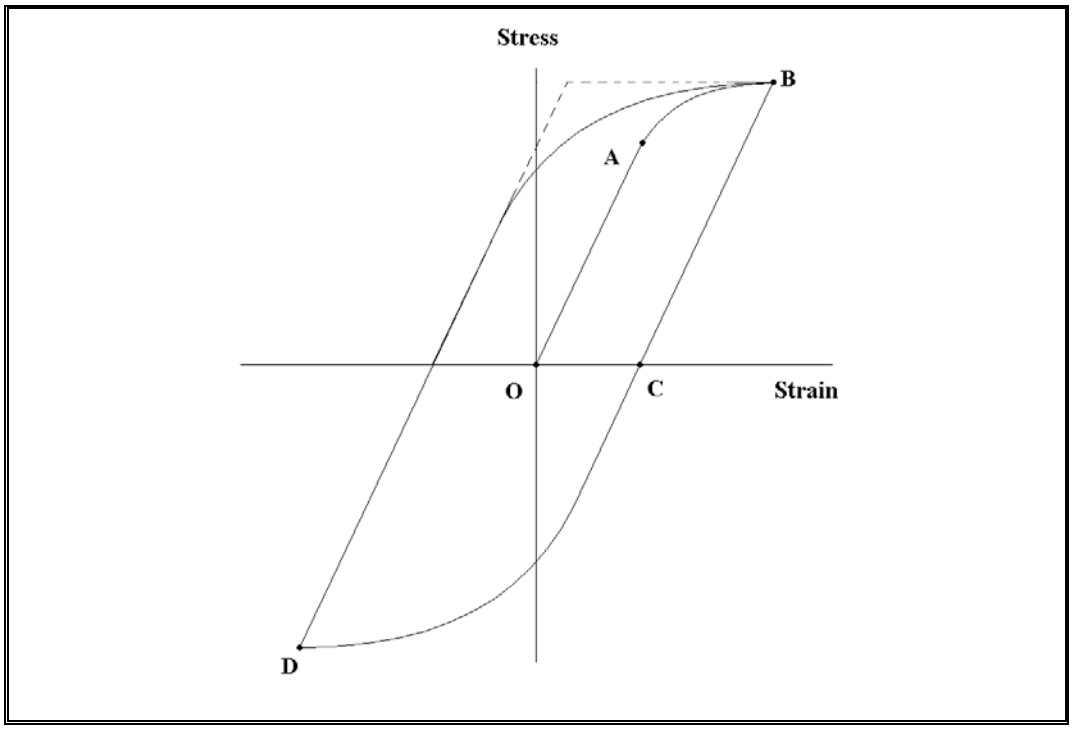


**Figure 2-7 A Complete Stress-Strain Cycle, a Hysteresis Loop[1]**

The discrepancies in load levels demonstrate the material's response to the cyclically induced strain, thus causing the softening or hardening behaviour. It is apparent from figure 2-8 that the maximum stress increases with number of imposed cycles in the case of softening whereby the stress decreases during the

course of hardening [1,2,4]. In both processes, the stresses converge to a certain limit and remain stable until the emergence of a fatigue crack. The hardening and softening behaviour of materials can be mathematically expressed in terms of the ratio of ultimate tensile strength and 0.2% proof strength as follows [1]:

$$\frac{S_u}{S_{0.2}} > 1.4 \tag{2.4}$$

$$\frac{S_u}{S_{0.2}} < 1.2 \tag{2.5}$$

For ratios greater than 1.4, the material cyclically hardens whereas a ratio less than 1.2 demonstrate a softening behaviour. Within the range of 1.2 to 1.4, the material can cyclically soften, harden or exhibit a mixed behaviour [1].

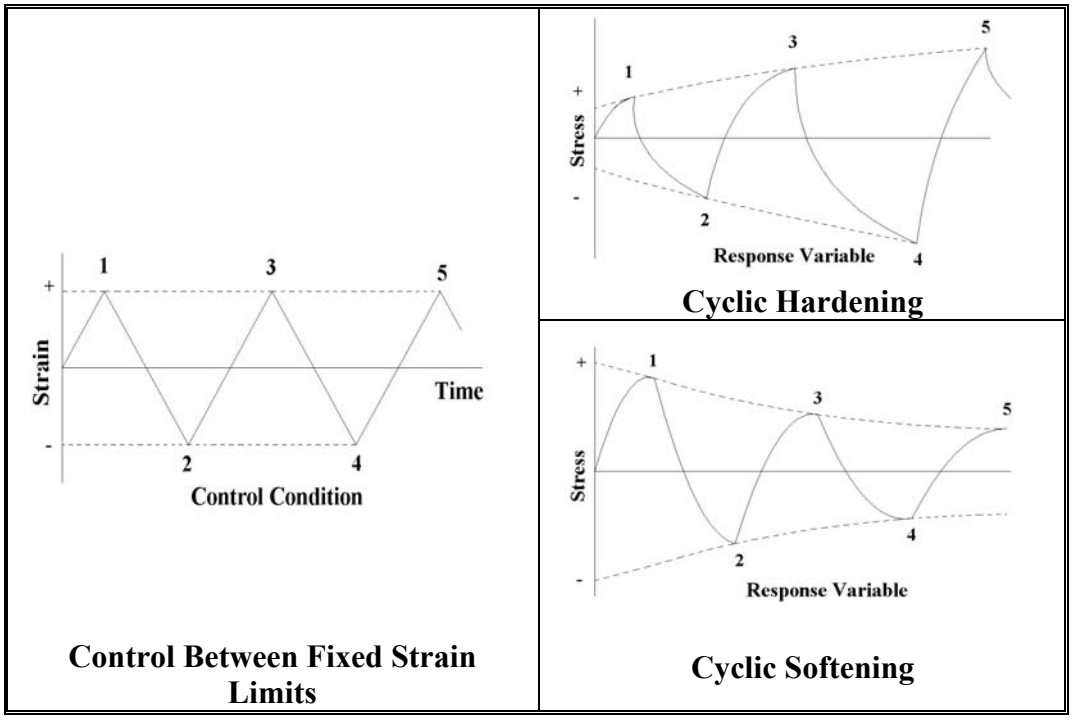


**Figure 2-8 Cyclic Softening and Hardening under Strain Control[1]**

After a relatively small number of cycles, no more than about 10% of the material's total life, the hysteresis loop tend to stabilize, meaning the stress

amplitude remain constant over the entire life portion [1,2,4]. If the stress strain coordinates relating to the tips of the hysteresis loops are plotted, the locus of these points generates the cyclic stress-strain curve (see figure 2-9 below) [1].

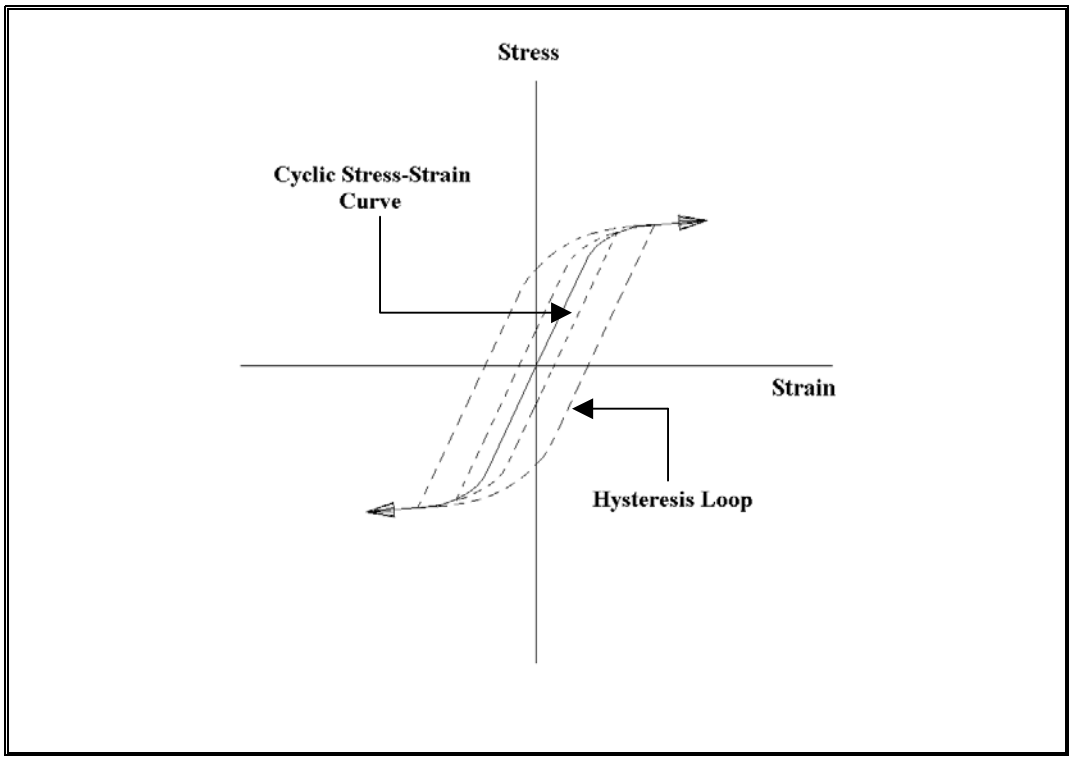


**Figure 2-9 The Cyclic Stress-Strain Curve[1]**

Unlike the true stress-strain curve, the cyclic stress-strain curve defines the material's behaviour under cyclic loading conditions. The cyclic stress-strain curve can be directly compared to its monotonic counterpart to quantitatively assess the softening and hardening behaviour of the material. When a material cyclically softens, the cyclic yield strength is lower than the monotonic yield strength whereas in the case of hardening, the monotonic yield strength is higher than that of the cyclic loading [1,2]. Figure 2-10 (a) through (d) shows a comparison between cyclic and monotonic behaviour.

Although the cyclic stress-strain curve is generated experimentally, it

can also be mathematically expressed as follows [1,2,4]:

$$\varepsilon_t = \frac{\sigma}{E} + \left(\frac{\sigma}{K^1}\right)^{\frac{1}{n^1}} \tag{2.6}$$

where, $\varepsilon_t$ is the total strain, $\sigma$ is the stress amplitude, E is the elastic modulus, $K^1$ is the cyclic strength coefficient and $n^1$ is the cyclic strain hardening exponent.

For a known value of E and coefficients $K^1$ and $n^1$, the cyclic stress-strain curve can be plotted for any material through the above equation.

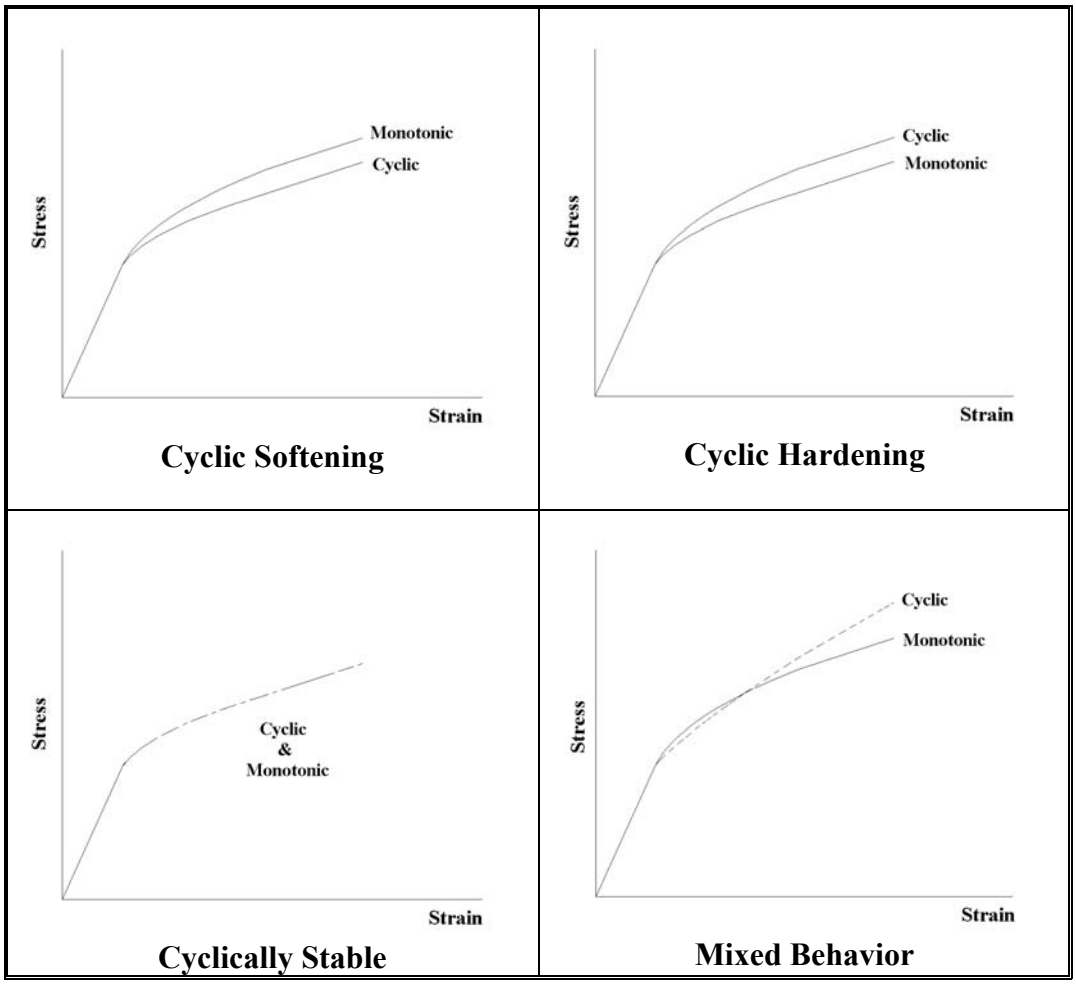


**Figure 2-10 Comparison Between Cyclic and Monotonic Stress-Strain Curves[1]**

### 2.4.2 The Strain-Life Curve

The strain versus fatigue life behaviour is commonly characterized by the strain-life (ε-N) curve. Unlike the S-N curve, the ε-N curve is composed of elastic and plastic strain components. If the elastic and plastic strains are plotted separately against the number of reversals to failure on a log-log scale, a strain-life curve can be generated as shown in figure 2-11 [1,2,4]. Therefore, the strain-life curve represents the total strain against reversals to failure, total strain being the arithmetic sum of elastic and plastic strains [1,2,4].

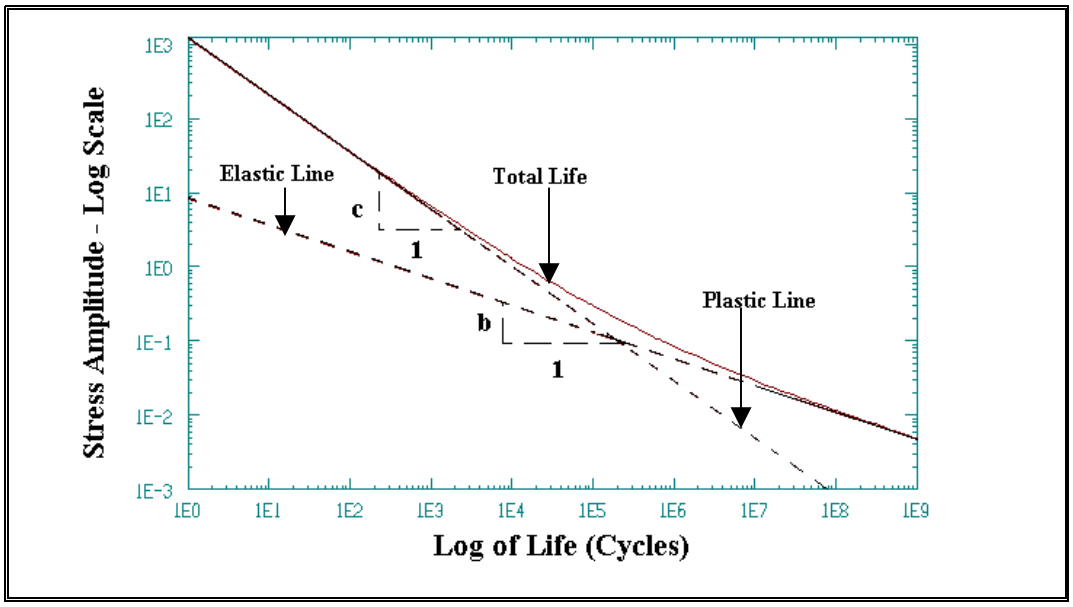


**Figure 2-11 The Strain-Life Curve**[1]

Basquin was the first to derive the mathematical relation between the elastic strain amplitude and number of reversals to failure [1,4]. Similarly, Coffin and Manson established the relation between plastic strain and reversals to failure [1,2,4]. Consequently, Morrow concluded that Basquin and Coffin-Manson elastic and plastic components could be combined to form the total strain amplitude and number of reversals to failure. The strain-life curve based

on Morrow's relation can be expressed as follows [1,4,13]:

$$\varepsilon_t = \frac{\sigma_f^1}{E}\left(2N_f\right)^b + \varepsilon_f^1\left(2N_f\right)^c \tag{2.7}$$

where, the coefficients $\sigma_f^1$ and $\varepsilon_f^1$ are the fatigue strength and ductility coefficients respectively, $2N_f$ is the number of half cycles to failure, and the exponents b and c are the fatigue strength and ductility exponents respectively. The first and second expressions on the right hand side of the equation are Basquin and Coffin-Manson relations respectively.

### 2.4.3 The Influence of Mean Stress

Like the S-N curve, the ε-N is equally affected by mean stress. Hence, to correlate basic fatigue data obtained by testing laboratory specimens under fully reversed loading with realistic service situations, the ε-N should be corrected for mean stress. This can be done by shifting the strain-life curve up or down depending whether the loading is tensile or compressive as illustrated in figure 2-12.

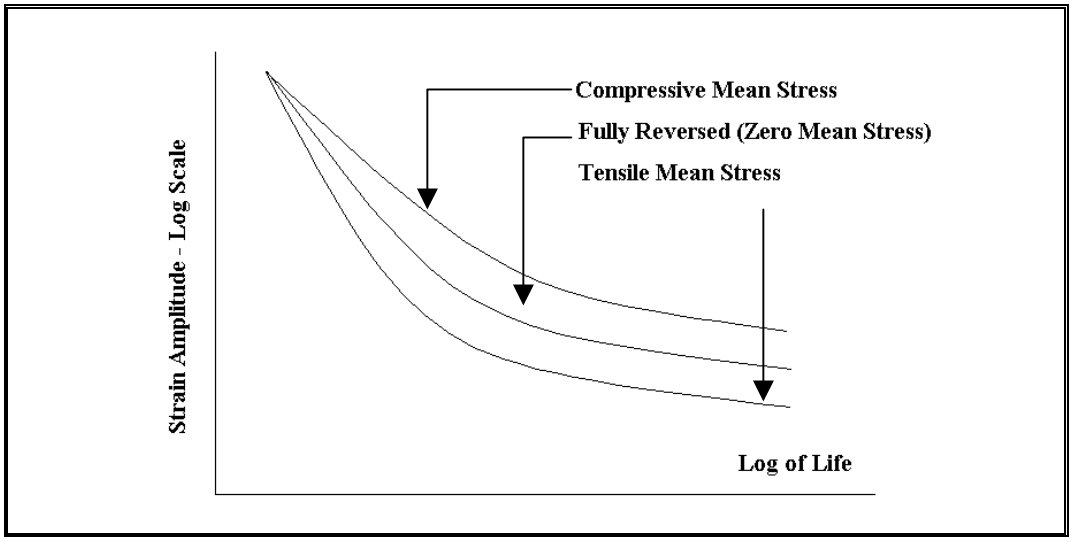


**Figure 2-12 Effect of Mean Stress on the Strain-Life Curve[1]**

The correction for mean stress upon the ε-N was initially proposed by Morrow [1,4,15]. By modifying the elastic part of the ε-N curve, a new relation for the total strain and number of reversals to failure was developed. Hence, the entire ε-N curve can be expressed as [1,15]:

$$\varepsilon_t = \frac{\left(\sigma_f^1 - \sigma_0\right)}{E}\left(2N_f\right)^b + \varepsilon_f^1\left(2N_f\right)^c \tag{2.8}$$

where, $\sigma_0$ is Morrow's mean stress.

On the other hand, Smith-Watson-Topper (SWT) approached the mean stress correction criterion by considering the maximum stress present at any given cycle [1,4,17]. SWT concluded that the product of the maximum stress and the strain amplitude would yield a new ε-N equation including the effect of mean stress. The maximum stress for a fully reversed loading can be characterized as the following power law relation [1,4,17]:

$$\sigma_{\max} = \sigma_f^1\left(2N_f\right)^b \tag{2.9}$$

Thus, the modified ε-N equation can be expressed as [1,4,17]:

$$\sigma_{\max}\varepsilon_a = \frac{\sigma_f}{E}\left(2N_f\right)^{2b} + \sigma_f^1\varepsilon_f^1\left(2N_f\right)^{b+c} \tag{2.10}$$

where, $\sigma_{\max}$ is the maximum mean stress and $\varepsilon_a$ is the strain amplitude.

Based on the approach of SWT, no damage will occur when $\sigma_{\max} \le 0$.

In numerous cases, Morrow and SWT approaches' would generate completely distinct results when applied to a single identical problem. However,

the SWT's approach has proven to yield more conservative results when the loading is tensile while Morrow's method provides more realistic life estimates in the case of a compressive loading sequence [1].

## 2.5 Uni-axial Fatigue Failure

A uni-axial fatigue failure occurs when the magnitude of stress or strains causing the failure is uni-axial in nature. This means that the stress and strain tensors in the component under investigation are aligned in a particular direction. This particular characteristic can be fully understood through a consideration of the principal stresses $\sigma_x$, $\sigma_y$ and $\sigma_z$ together with shear stresses $\tau_{xy}$, $\tau_{yz}$ and $\tau_{xz}$. Consider a particular component where the x-y axes lie in the plane of the component and the z-axis is normal to that plane. A uni-axial stress state will occur when:

- The principal and shear stresses normal to the x-y plane are zero [1]. This means that $\sigma_z = \tau_{yz} = \tau_{xz} = 0$.
- One of the in-plane principal stresses, either $\sigma_x$ or $\sigma_y$ is zero.

The aforementioned methods in sections 2.3 and 2.4 are strictly reserved to uni-axial fatigue analysis. This is because the stress and strain life curves are created using simple uni-axial testing principles. For the case of the S-N curve, the Moore testing machine can be used for either axial, rotating or bending. Similarly, the ε-N curves are created by testing smooth, cylindrical, mirror-polished specimen under simple uni-axial tension.

However, most realistic fatigue situations involve at least two of either axial, bending or torsion. To correlate uni-axial fatigue data with multiple

loading situations, such that the S-N and ε-N curves can be usefully employed to predict life, a new approach was developed. This new approach is commonly known as the equivalent stress-strain approach. The next major section in this chapter gives a thorough description of the equivalent stress-strain approach pertaining to multiple loading. It is however essential to fully understand the extent of multiple loading and its impact on fatigue failure before moving to the equivalent stress-strain approach. Situations where the latter fails are also briefly discussed.

## 2.6 Multi-axial Fatigue Failure

This chapter is dedicated to multi-axial concerns. Multi-axial fatigue failure occurs due to the occurrence of complex multiple loads causing deformation in at least two of axial, bending or torsion. The induced stress state varies over time, hence greatly influencing crack initiation and propagation [1,2,4]. The basic fatigue techniques discussed thus far are based on uni-axial assumptions. However, many practical design situations, including rotating shafts, connecting links, automotive and aircraft components and many others involve a multi-axial state of cyclic stress [1]. Adopting the S-N and ε-N curves in these situations will induce very non-conservative life predictions. Hence, Universities and research departments of some major companies notably in the power generation, ground vehicle and aerospace stream have been actively engaged into research for life predictions under a multi-axial stress state [1]. As a result, new theories have been recently developed. These theories embrace two domains, namely proportional and non-proportional loadings. It should be

noted however, that the onset of non-proportional loading is still in the developing stage such that the mathematical correlations available so far have not been fully validated.

### 2.6.1 Proportional and Non-proportional Loading

Multi-axial loading involves multiple loads. Contrary to a uni-axial cyclic loading, during the course of a multi-axial loading, the direction of principal stresses varies with time. To fully comprehend this behaviour through a consideration of proportional and non-proportional loading, it is important to investigate the two parameters causing it, namely bi-axiality ratio, $a_e$, and angle of spread, $\phi_p$. The bi-axiality ratio and angle of spread indicate whether a loading is proportional or non-proportional based on the assessment of the principal stresses or strains for a given loading. Proportional and non-proportional loadings are distinguished by the magnitudes of $a_e$ and $\phi_p$.

Similar to the uni-axial assessment, the stresses and strains at the surface of the component under investigation are resolved such that the principal and shear stresses normal to the surface are zero. From the values of $\sigma_x$ and $\sigma_y$, $a_e$ and $\phi_p$ can be calculated as follows [1]:

$$a_e = \frac{\sigma_2}{\sigma_1} \tag{2.11}$$

where, $\sigma_1$ and $\sigma_2$ are ordered with $\sigma_1$ being the most positive of $\sigma_x$ and $\sigma_y$. Similarly, $\phi_p$ is the angle between $\sigma_1$ and the local x-axis.

A constant value of $a_e$ denotes a proportional loading with $\sigma_1$ and $\sigma_2$ being proportional to each other. Likewise, proportional loading occurs when

$\phi_p$ is invariant with time. It should be noted that a purely uni-axial loading results when $a_e$ is zero and $\phi_p$ constant. A plot of the principal stresses against the bi-axiality ratio or angle of spread at every reversal through the loading can be equally used to demonstrate proportional and purely uni-axial loadings (see Figures 2-13 and 2-14 below).

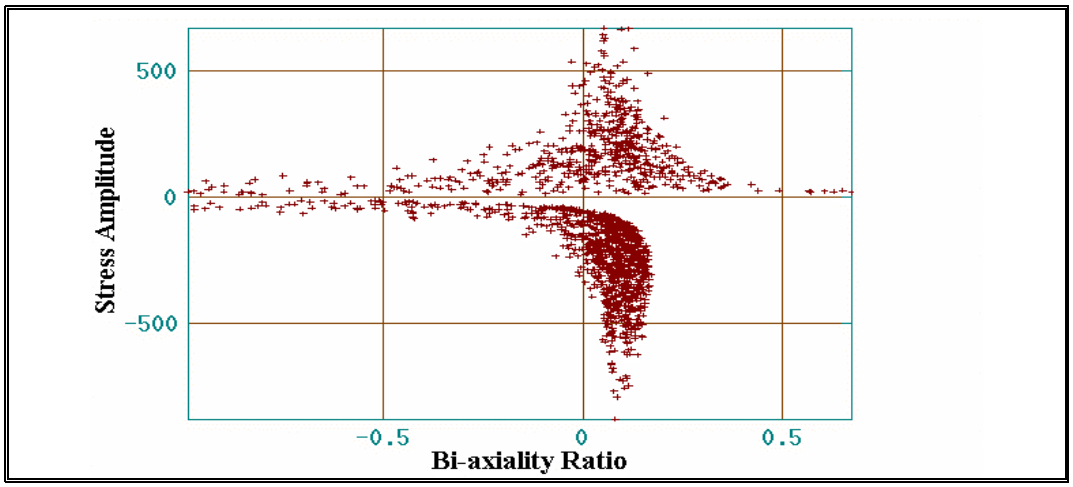


**Figure 2-13 Graphical Display of Proportional Loading Through a Consideration of Bi-axiality Ratio[18]**

Figure 2-13 shows a plot of stress amplitude against bi-axiality ratio. It can be seen from the figure that there is some scatter in the plot. The interesting point to note is that the bi-axiality ratio, $a_e$, tends to align vertically close to zero [18]. This indicates that the loading is proportional since $a_e$ has a constant value [18]. The large scatter happens at low values of stress and has no significant impact on the life. Only high values of stress should be taken into consideration. Likewise, from figure 2-14, the angle of spread, $\phi_p$ tend to align itself at about 45 degrees as indicated by the highest spike in the figure. This indicates the predominant angle with the stress tensor constant at 45 degrees. Again the smaller spikes should be ignored because they occur at lower stress cycles.

The onset of uni-axial loading is portrayed in figure 2-15, from which it can be seen that the stresses line up vertically at a certain value. That approximate value is significantly close to zero. Hence, the loading is purely uni-axial in this case.

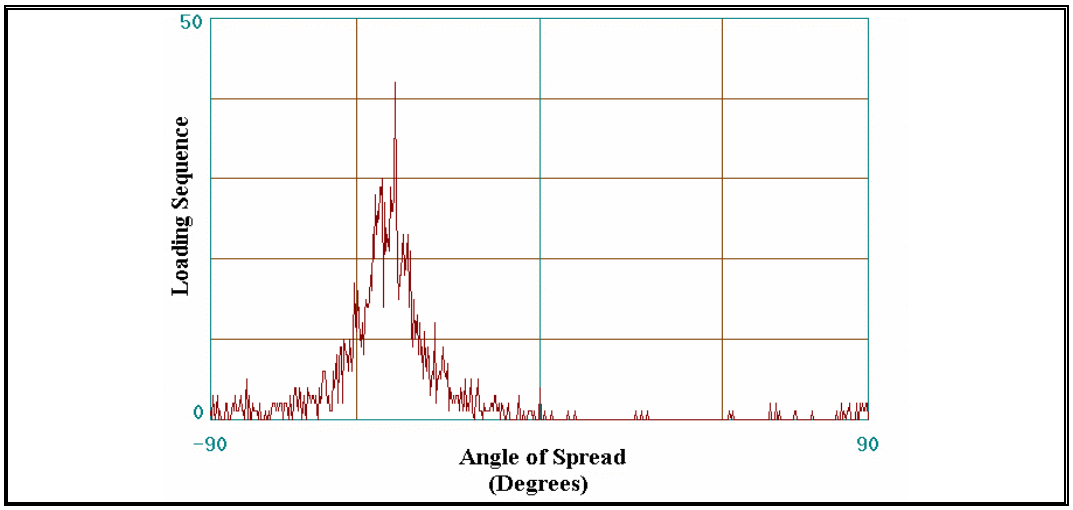


**Figure 2-14 Graphical Display of Proportional Loading Through a Consideration of Angle of Spread[18]**

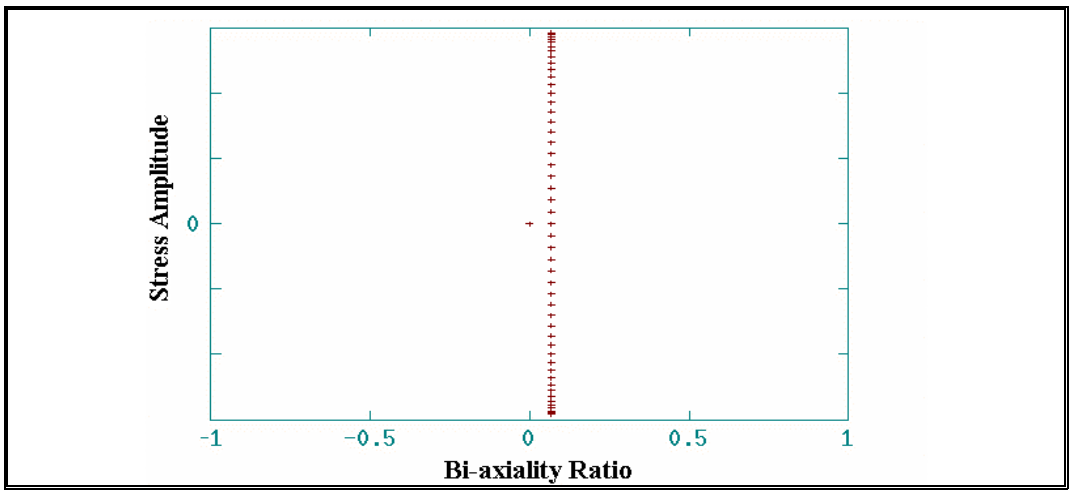


**Figure 2-15 Graphical Display of Uni-axial Loading Through a Consideration of Bi-axiality Ratio[18]**

A multi-axial non-proportional loading condition is illustrated in figures 2-16 and 2-17 below. The graphical display in figure 2-16 shows that for each

value of stress, there is a different value of Bi-axiality ratio. As a result, there is a huge scatter in the plot indicating that the principal stress $\sigma_1$ and $\sigma_2$ are non-proportional to each other at any time during the course of the loading. The other point of interest can be seen from figure 2-17, which shows how the angle oscillates between two predominant angles. This indicates that $\phi_p$ varies with time and that a non-proportional multi-axial condition occurred.

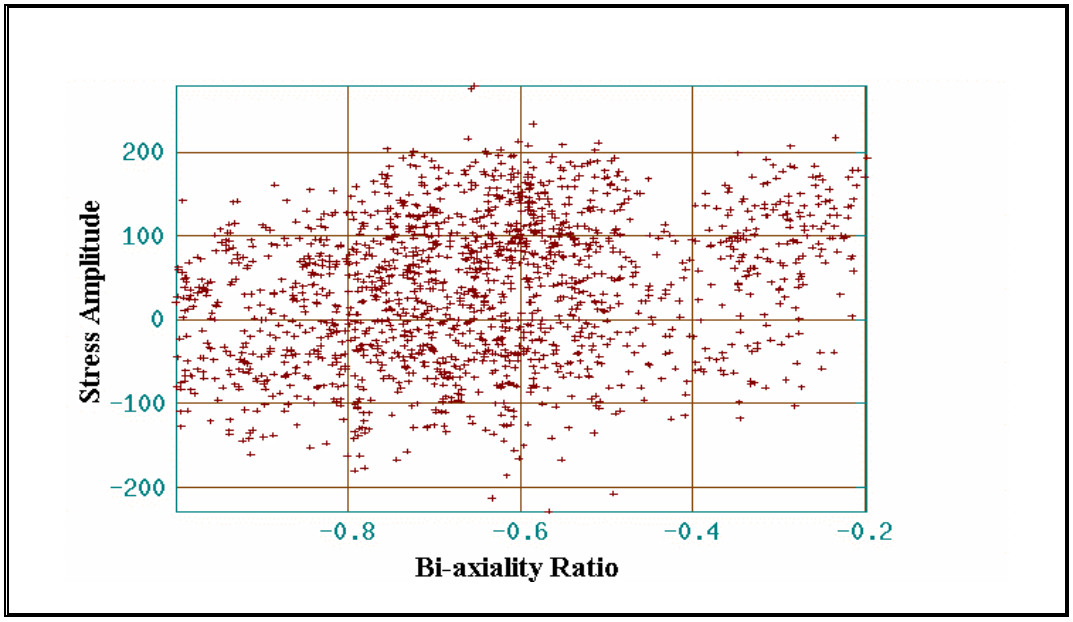


**Figure 2-16 Graphical Display of Non-proportional Loading Through a Consideration of Bi-axiality Ratio[18]**

There is as yet no general agreement about how to fully deal with non-proportional loading conditions [1,18]. Recently, theoretical methods have been developed, but they have not been completely validated [1,18]. Hence, it is strictly recommended to rely on experimental analysis in such cases. The aforementioned methods can be classified as the critical plane approach. For the current research, the latter was reviewed and briefly explained in section 2.8 following the equivalent stress-strain approach.

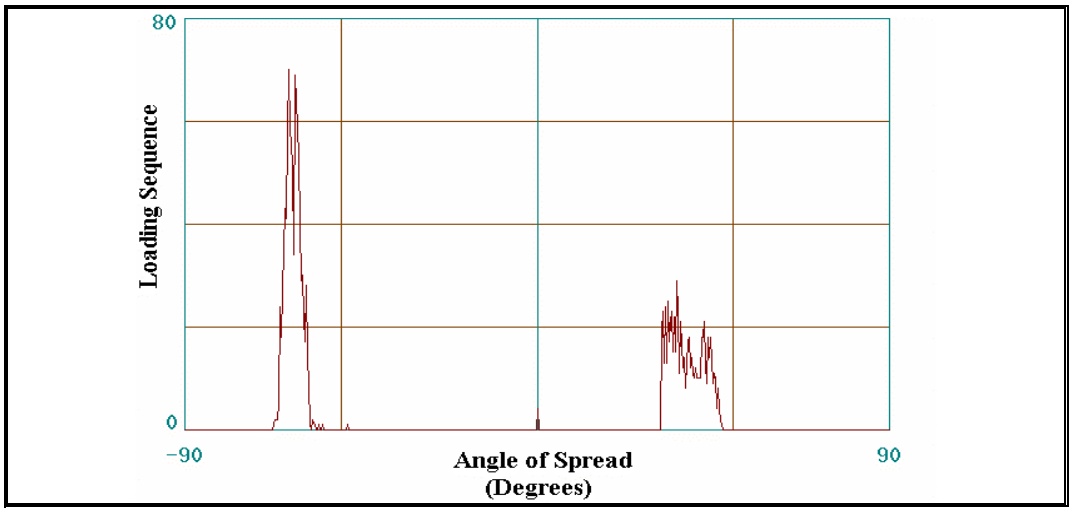


**Figure 2-17 Graphical Display of Non-proportional Loading Through a Consideration of Angle of Spread[18]**

## 2.7 Equivalent Stress-Strain Approach

Failure can be easily predicted if the component under investigation is subjected to purely uni-axial loading. Such analysis can be conducted by referring to the stress-life or strain-life curves only. However, a purely uni-axial state of stress rarely takes place in components rendering the availability of uni-axial test data useless. As a result, a large number of tests would be required in which all of the stress components would have to be varied over an entire range of values in all possible combinations in order to deal with the occurrence of non uni-axial loading [1].

Due the high costs of such tests, it was necessary to develop a theoretical approach. The approach henceforth developed was the equivalent stress-strain approach. As the name suggests, the equivalent stress-strain approach predicts life for fatigue under multi-axial loading by calculating an equivalent uni-axial stress or strain [1]. As a result, the available S-N and ε-N curves can still be

used to predict life. The equivalent stresses or strains used are the maximum principal, the maximum shear and Von Mises [1]. The maximum shear (or Tresca criterion) and the Von Mises (or Octahedral criterion) stress theories have gained the widest acceptance [1]. The empirical correlations behind the aforementioned stress theories are tacitly discussed in the next two sub-sections.

### 2.7.1 The Von Mises Theory

Von Mises predicted that a component would fail under yield when the second invariant of the stress deviator, $J_2$, exceeds a critical value. For example if the monotonic yield stress is the failure mode, then the component will fail when $J_2$ exceeds $\sigma_y$. The stress deviator can be expressed as follows [1]:

$$J_2 = \frac{1}{6}\left[(\sigma_1 - \sigma_2)^2 + (\sigma_2 - \sigma_3)^2 + (\sigma_3 - \sigma_1)^2\right] \tag{2.12}$$

where, $\sigma_1, \sigma_2$ and $\sigma_3$ are the principal stresses in x, y and z direction respectively.

For yielding to occur by tension, $\sigma_1 = \sigma_0$ and $\sigma_2 = \sigma_3 = 0$. Substituting these values into the above equation yields [1]:

$$J_2 = \frac{\sigma_0^2}{3} \tag{2.13}$$

Hence the Von Mises prediction of yield in terms of the principal stress becomes [1]:

$$\sigma_0 = 0.7071\left[(\sigma_1 - \sigma_2)^2 + (\sigma_2 - \sigma_3)^2 + (\sigma_3 - \sigma_1)^2\right]^{0.5} \tag{2.14}$$

Similar correlations can be developed for different failure modes. These correlations will not be further discussed.

### 2.7.2 The Tresca Theory

On the other hand, the Tresca criterion suggests that a component will yield when the maximum shear stress under multi-axial loading reaches the value of the shear stress under uni-axial tension test [1]. The maximum shear stress can be expressed as follows [1]:

$$\tau_{\max} = \frac{(\sigma_1 - \sigma_3)}{2} \tag{2.15}$$

When $\tau_{\max}$ exceeds the shear yield stress $\tau_0$, failure will occur. It is worth noting that the Tresca criterion is much simpler than that proposed by Von Mises [1]. However, there is as yet no general agreement which method prevails over the other. It is all based on the model geometry, number and type of loading and stress distribution.

### 2.7.3 Failure of the Equivalent Stress-Strain Approach

The equivalent stress-strain methods do not take into account the fact that fatigue is essentially a directional process, with cracking taking place on particular planes. In addition to that, the use of multiple loads creates non-proportional loading whereby the applied loads have a non-constant bi-axiality ratio or phase relationship [1,2]. Therefore, researchers emphasized on this particular mechanism of fatigue failure and developed a new methodology known as the critical plane approach [1-4,7,8,10].

## 2.8 Critical Plane Approach

The critical plane approach recognizes that fatigue is a directional process and considers the accumulation of damage on particular planes [1-4,7,8,10]. This is in contrast to the equivalent stress-strain approach, which may be summing damage that is occurring on different planes [1,2]. Typically, the critical plane approach calculates life by summing damage on each plane at 10-degree intervals (see figure 2-18). The worst plane is then selected as the critical plane where crack occurs.

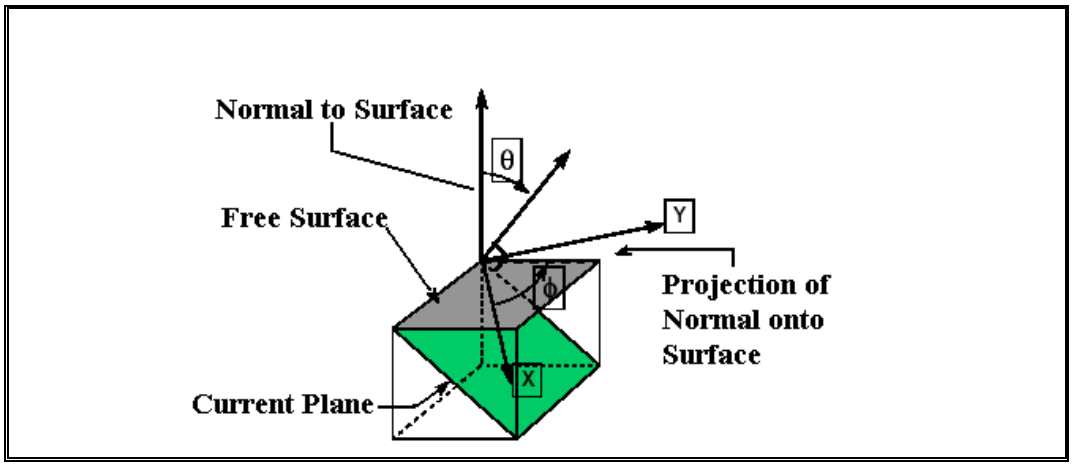


**Figure 2-18 The Critical Plane Approach[1]**

Numerous methods are based on the critical plane approach. As previously mentioned, this approach is still in the research phase. Although available, these methods were not used and will not be further discussed.

## 2.9 Factors Influencing Life

The standardized R.R. Moore testing machine and the strain transducer used to generate the S-N and the ε-N curves respectively based their tests on smooth, cylindrical, mirror-polished specimens under fully reversed loading

conditions. Most components are far from being cylindrical and experience different loading and environmental conditions. The factors listed below influence fatigue life prediction [1].

- Component size
- Type of loading
- Effect of notches
- Effect of surface roughness
- Effect of surface treatment

The effect of loading type has previously been discussed, whereby the stress and strain-life curves were corrected for mean stress or strains. Moreover, the influence of component size can be ignored when finite element is used to obtain the stresses and strains. However, the effects of notches, surface roughness and treatment cannot be neglected.

### 2.9.1 Effect of Notches

The stresses and strains in a component can be either nominal or local. If the component is a flat plate, there is no difference between nominal and local stresses. Many realistic components are far from being flat and include holes and fillets. These holes and fillets can be classified as notches. As a result, there is significant plastic deformation at the notches, which in turn greatly influence fatigue life. In order to translate from elastic strains to elastoplastic strains at the notches, the Neuber's rule are applied [1,2,4,19]. Neuber's rule asserts that to correct elastic to elastoplastic strains, the cyclic stress-strain and strain-life curves can be multiplied by a factor $K_t$ that is mathematically expressed in

terms of the nominal and local stresses and strains as follows [1,2,4,19]:

$$K_t^2 = \left(\frac{\Delta\sigma}{\Delta S}\right)\left(\frac{\Delta\varepsilon}{\Delta e}\right) \tag{2.16}$$

where, $\Delta S$ and $\Delta e$ are the nominal stress and strain respectively and $\Delta\sigma$ and $\Delta\varepsilon$ are the local stress and strain range respectively.

The nominal stress and strain can be directly measured from the component itself. In the case of finite element analysis, the local stress and strains can be obtained by using a fine mesh at the notches [22].

### 2.9.2 Effect of Surface Roughness

A very high proportion of all fatigue failures nucleate at the surface of components implying that surface conditions is an extremely important factor influencing life [1]. Scratches, pits and machine marks affect fatigue strength by acting as stress raisers [1]. These stress raisers aid in significant plastic deformation, reducing the material's resistance to fatigue. Hence, predicting life without considering surface roughness is very non-conservative. It is therefore important to measure the arithmetic average surface roughness on a component and calculate the surface factor before estimating life.

### 2.9.3 Effect of Surface Treatment

As in the case of surface roughness, surface treatment can have a profound influence on fatigue strength [1]. Mechanical, thermal and plating processes greatly influence the fatigue strength by altering the residual stress at

the free surface [1]. Mechanical and thermal processes create a compressive layer whereas plating creates a tensile residual stress layer at the free surface [1]. To properly estimate the life of a surface treated component, it is important to implement the effect of residual stresses on that component. For the current research, the specimen was not surface treated. Hence, the mechanical, thermal and plating processes will not be further discussed.

## 2.10 Application of Finite Element Analysis

In this chapter, the traditional and advanced fatigue mechanisms were discussed. Whether it is the S-N or ε-N approach in the uni-axial case and equivalent stress-strain or critical in the multi-axial case, they all require stresses and strains. To facilitate this process, finite element analysis (FEA) can be used. FEA is certainly a great advantage when the lives of complex geometries are being estimated. It also aids in the estimation of local stresses and strains. Chapter four is entirely dedicated to FEA, from the modeling aspect to static analysis, on the specimen under research.

# CHAPTER 3 FATIGUE, AN EXPERIMENTAL APPROACH

## 3.1 Overview

This chapter focuses on the experimental aspect of fatigue life prediction. Experimental procedures are widely used nowadays for fatigue life prediction. However, they have proven to be very costly and time consuming. At the preliminary design stage, engineers tend to rely solely on numerical simulation rather than experiments. At the final stage of the design, it is necessary to conduct experiments to validate the simulation results. In this chapter, both uni-axial and multi-axial fatigue experiments are conducted prior to numerical simulation. As such, the experimental set-up is copied through FEA and fatigue. This exercise is done in this manner to verify whether FEA can be applied to fatigue life estimation in the door hinge. This chapter is composed of two major different parts, uni-axial and multi-axial experiments respectively.

## 3.2 Uni-axial Fatigue

Uni-axial fatigue tests are usually conducted when full-scale multi-axial tests are unavailable or too costly. In the demanding and extremely competitive automotive industry, full-scale multi-axial tests are very time consuming. In many occasions, the time is very limited for product design engineers to meet customer demands and design an efficient reliable product. In such cases, uni-axial fatigue tests have proven to be very successful. In the current

investigation, a uni-axial fatigue test is conducted on the hinge such that the experimental results can be used as guidelines to model and simulate a proper FE based fatigue analysis.

### 3.2.1 Description of Apparatus and Experimental Procedure

This uni-axial loading experiment is designed to approximate the highest severity loading conditions that the hinge is expected to be subjected to in its duty life cycle. The uni-axial fatigue test is a hyperextension load against the full open stop face of the hinge. The experimental set up is shown in Figure 3-1. This set up consists of the door hinge, the lever bar for load transmission, and a loading device that is connected to a computer for controlling the magnitude of the applied load.

**Figure 3-1 Uni-axial Loading Apparatus**

In the configuration shown in figure 3-1 above, the hinge is in the fully-

opened position, whereby, the BS bracket rests freely on the DS bracket. A load is induced through the computer, where the former is gradually increased from zero to a maximum value of 110 Nm. At that maximum value, the load is instantly removed and the value drops down to zero. As such, the brackets are in full hyperextension. This procedure is repeated at a rate of 25 cycles per minute. The component is checked for any evidence of crack initiation at every 5,000 cycles.

### 3.2.2 Experimental Results

Five sets of experiments are conducted. The results are illustrated in table 3-1 below.

| Sample number | Number of cycles till crack initiation | Crack length (mm) |
|---|---|---|
| 1 | 287,000 | 3.5 |
| 2 | 292,000 | 5.0 |
| 3 | 295,000 | 4.5 |
| 4 | 280,000 | 1.5 |
| 5 | 290,000 | 1.5 |

**Table 3-1 Experimental Uni-axial Results**

It is seen that the average number of cycles till crack initiates is 289,000. The crack length shown propagates at a very fast rate from a 1 mm length, in the order of 10 cycles. As such, the life obtained is taken as the value at a 1 mm crack length. Moreover, the critical location for crack initiation is around the

edge of the oval hole in the DS bracket (see figure 3-2).

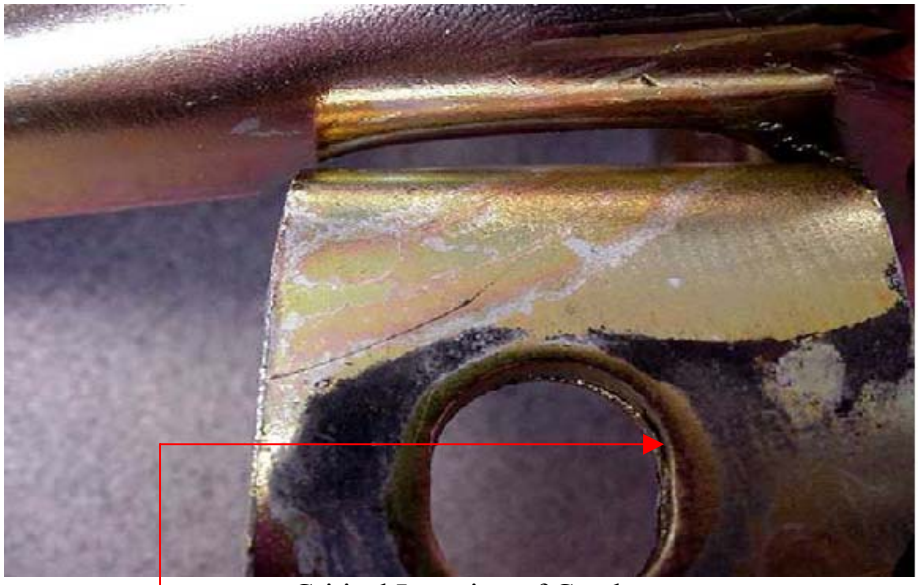


**Figure 3-2 Crack Location Site From Uni-axial Experiment**

## 3.3 Multi-axial Fatigue

This section describes the full-scale multi-axial fatigue tests on the door hinge simulating the actual vehicle environment. However, such tests are very time consuming. In this case, the door hinge is cycled for an average of 30 days until crack initiated.

### 3.3.1 Description of Apparatus and Experimental Procedure

The multi-axial fatigue set-up consists of the vehicle's door (figure 3-3). The latter is attached to the vehicle's body by the upper and lower hinges. The hinge fixtures, shown in figure 3-4, rigidly attach the doorframe to the vehicle. The door is driven by a motor that simulates the open/close door cyclic movement. The rate of motion of the motor is controlled by a computer, in

which the load is induced. The load is applied at 135 Nm for the first 23 cycles and at 320 Nm on the 24$^{th}$ cycle. The 135 Nm load represents the average torque required to open the door from a fully-closed to a fully-opened position. On the other hand, the 320 Nm torque is a hyperextension load when the door swings abruptly to a fully-opened position. The abrupt motion of the door represents a stop-check load when the driver suddenly applies on the brakes.

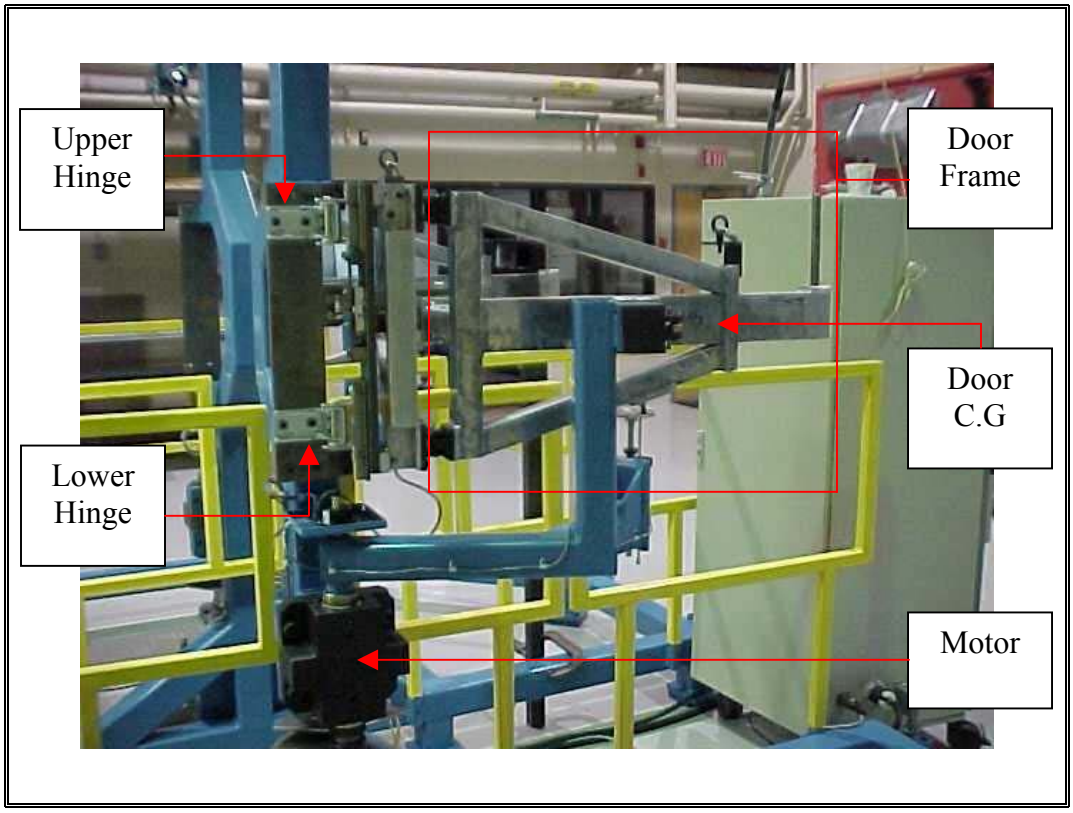


**Figure 3-3 Multi-axial Loading Apparatus**

Moreover, at all times during the full cyclical movement, a door weight of 480 N is included. This experimental set-up represents the most severe environment the door hinge is subjected to in its duty life. The hinge is cycled at a rate of 9 cycles/min until the initiation of crack. As such, the experiment is checked everyday.

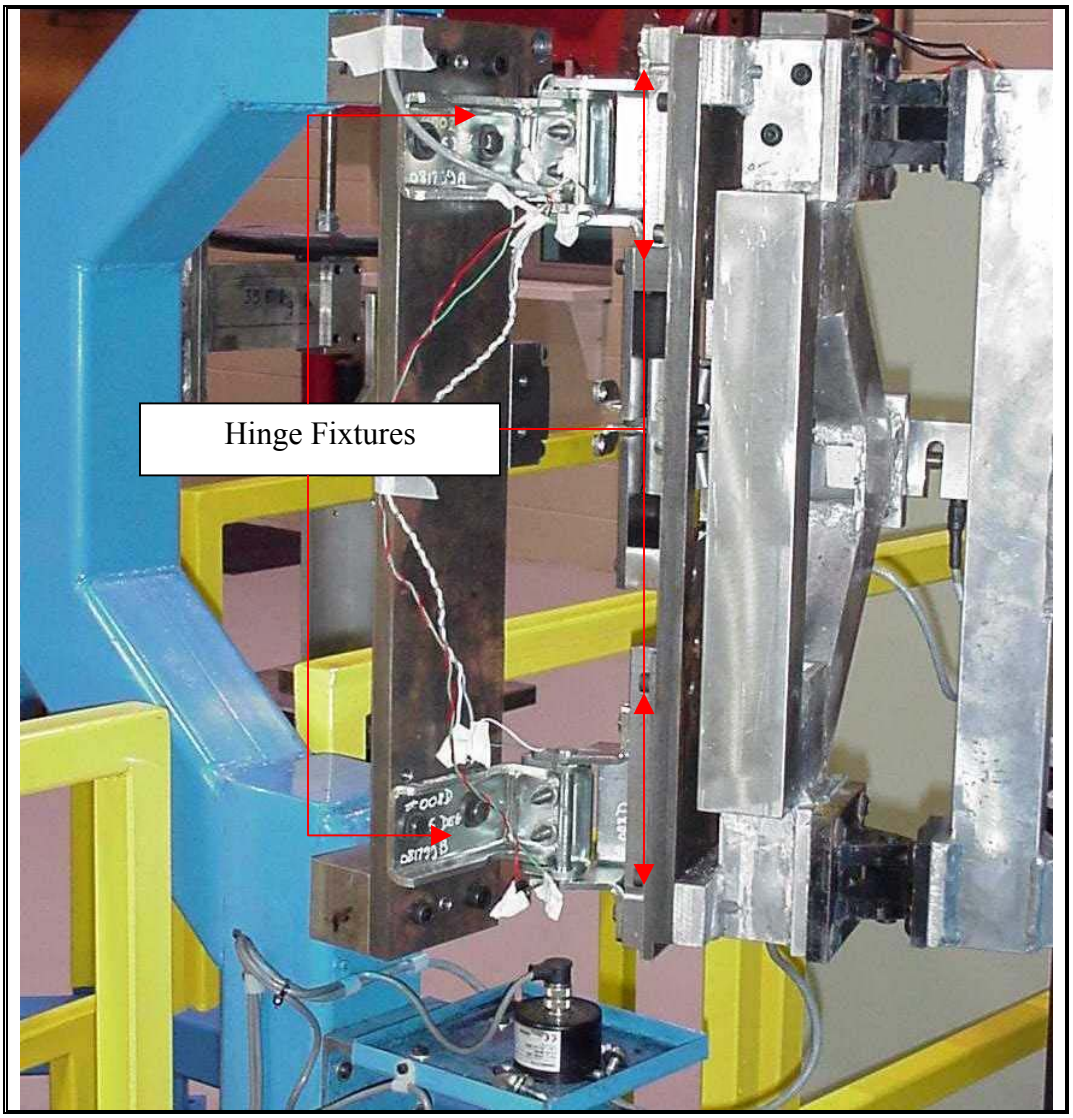


**Figure 3-4 Hinge Fixtures**

### 3.3.2 Experimental Results

Five sets of experiments are conducted. The results are illustrated in table 3-2 below. In the multi-axial case, the average value for crack initiation is 72,000 cycles. Similarly, the crack propagates at a very fast rate. The interesting point here is the occurrence of crack after only 31,600 cycles in sample four. This occurrence clearly demonstrates the statistical nature of fatigue. The location of the crack is at the root of the notch in the BS Bracket (see fig. 3-5).

| Sample number | Number of cycles till first evidence of cracking (Cycles) | Crack length (mm) |
|---|---|---|
| 1 | 88,400 | 4.0 |
| 2 | 72,000 | 5.0 |
| 3 | 92,700 | 9.0 |
| 4 | 31,600 | 3.0 |
| 5 | 72,000 | 5.0 |

**Table 3-2 Experimental Multi-axial Results**

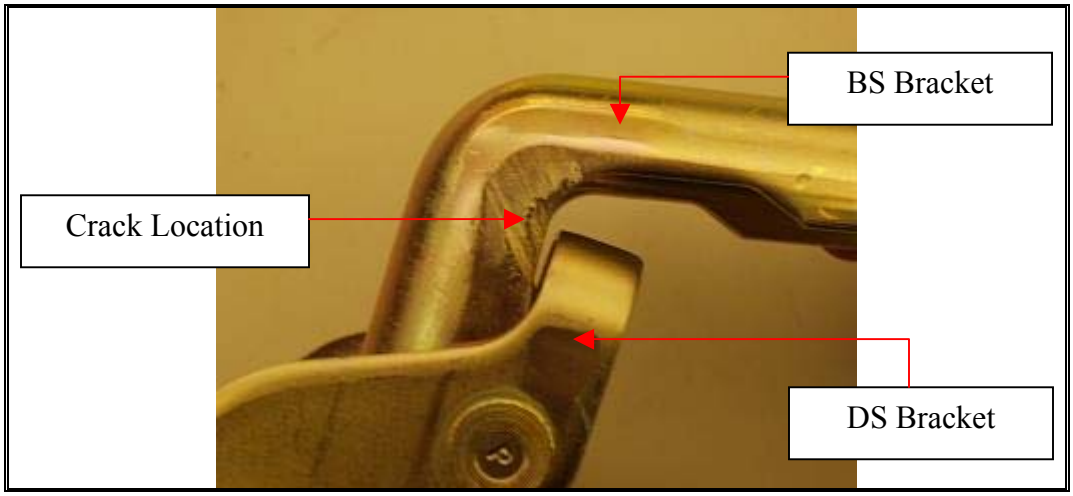


**Figure 3-5 Crack Location Site From Multi-axial Experiment**

## 3.4 Results Summary and Conclusions

The average life obtained from the uni-axial fatigue test was 289,000 cycles whereas the multi-axial fatigue test yielded an average life of 72,000 cycles. As previously stated, the life resulting from a uni-axial test is not as important as the one from a multi-axial test. The latter reflects the actual loading environment in the door hinge. On the other hand, the former only gives an

approximate solution to fatigue life prediction. In the preliminary design stage, the uni-axial fatigue test results are adequate for the product design engineers. Uni-axial fatigue test results are reliable when the component is still in the development phase. However, in the validation phase, results from full-scale multi-axial tests are imperative. The results clearly showed that the life and crack location are very dissimilar in each case. At this point, from a validation point of view, the uni-axial fatigue life should be disregarded. However, for the current research, the uni-axial result was used as a guideline in the FE modeling of the hinge. This is because in the early phase of this research, the full-scale multi-axial fatigue test was unavailable. Hence, the uni-axial fatigue result was used to refine the gap that existed between numerical and experimental models. The experimental multi-axial fatigue result was then used to validate that obtained from numerical simulation.

# CHAPTER 4 NUMERICAL ANALYSIS: FE STATIC

## 4.1 Overview

In this chapter, Finite Element (FE) is used to model the 60-degree door hinge. Two models are considered, one for uni-axial loading and the other for multi-axial loading. The uni-axial model consists of a single hinge whereas the multi-axial one consists of the entire door hinge system, which includes two hinges and the doorframe. A static analysis is conducted on both models to obtain the stresses and strains to be used as input for fatigue life prediction.

A thorough analysis is also performed on a simple cantilever beam that is subjected to a bending load to demonstrate the accuracy and effectiveness of certain element types. The result from the aforementioned analysis is then used as a guideline to select the proper element type for the hinge under investigation. This chapter also demonstrates the importance of geometry check in FE. This is achieved by modeling the uni-axial hinge with two different mesh options and comparing the effectiveness of both models with the use of geometry check parameters and the static results. It is observed that the combination of proper element type and mesh selection would yield static results that are close to realistic solutions.

## 4.2 Analytical vs. Numerical Methods for FE Static Analysis

Engineering systems can be categorised as either discrete systems or continuous systems. In the case of a static problem, the stiffness in a discrete

system is assumed to be present at certain discrete points or degrees of freedom (DOF), as in the case of a single DOF spring-mass system. However, for a continuous system, the stiffness is considered to be distributed as a series of infinitely small decretized domains called elements. They move relative to each other in a continuous fashion under an applied load [22].

The governing equations of motion of the discretely modeled system are easily solvable ordinary differential equations. In contrast, continuous system yields partial differential equations, which in most cases, do not have mathematical closed-form solution. Therefore, complicated systems such as the hinge have to be solved by numerical procedures.

The Finite Element Method (FEM) is an example of a numerical procedure for solving a set of complex equations that describes the physics of the problem of interest [21,22]. The basic idea behind the FEM is piecewise approximation whereby the solution of continuous is obtained by dividing the entire system into a finite number of small elements, and then approximating the solution over each element by a simple interpolation function [23]. The primary solution in a static case is the displacement, u, whereas the stresses and strains are secondary solutions.

The correct selection of elements is important in FEA. Elements can be classified as 1D, 2D or 3D. Some of the elements are only applicable to certain situations and some work better than others in a particular situation. The next section discusses how elements can be selected based on the simple cantilever beam example.

## 4.3 Element Selection: The Cantilever Beam Example

In this section, the maximum bending stress of different element types are approximated through a FE based static analysis with the intention of demonstrating the usefulness and accuracy of FE modeling. Moreover, a qualitative assessment is performed on the element types to demonstrate their applicability to particular situations. These situations are axial, bending and torsion or a combination of at least two of the aforementioned situations (e.g., a comparison between the response and effectiveness of element X and Y when both are subjected to a bending load). A cantilever beam as shown in figure 4-1 below is used as an example for this assessment.

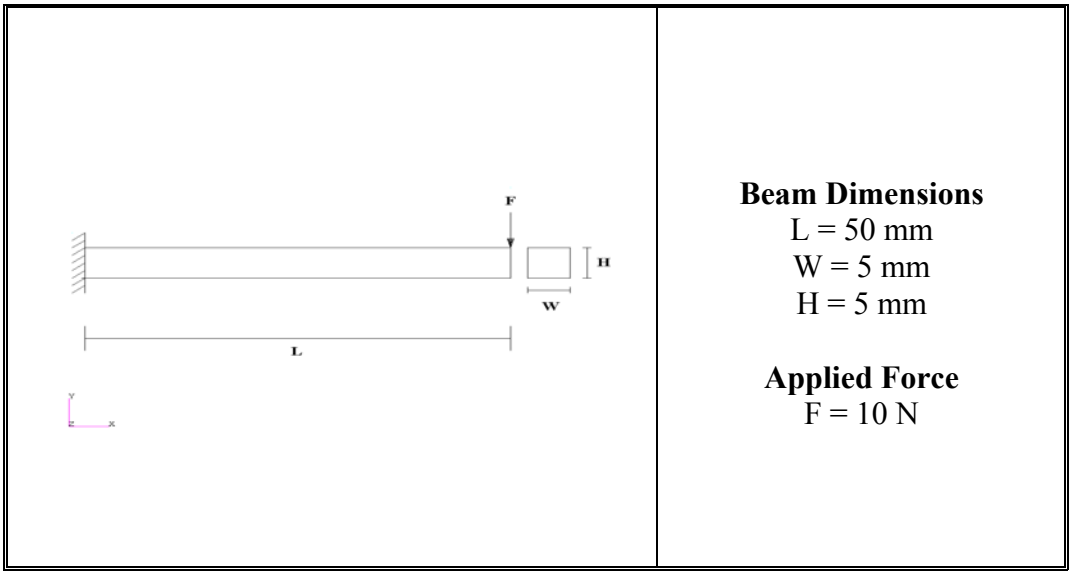


**Figure 4-1 The Cantilever Beam**

The exact solution is calculated by means of the Euler-Bernoulli beam theorem. This solution is then compared to solutions obtained from finite element. In the latter case, 1D, 2D and 3D elements are used. Table 4-1 below lists the element types and their applications.

| Types | Topology | Number of Nodes | DOF at each Node | Applications |
|---|---|---|---|---|
| 1D Bar | Linear | 2 | 3 (2 translations + 1 rotation) | One-dimensional beam problems where torsional rigidity is required. |
| 2D Shell | Tria | 3 | 6 (3 translations + 3 rotations) | Three-dimensional thin-walled structures. – Should be avoided due to high stiffness. |
| | Quad | 4 | 6 (3 translations + 3 rotations) | Three-dimensional thin-walled structures. |
| 3D Solid | Wedge | 6 | 3 (3 translations) | Solid structures. |
| | Hex | 8 | 3 (3 translations) | Solid structures. |

**Table 4-1 Typical Element Types and their Applications**

Using the Euler-Bernoulli beam equation, the maximum bending stress can be calculated as follows:

$$\sigma_{max} = \frac{My}{I} \tag{4.1}$$

where,

$$M = FL \tag{4.2}$$

$$y = \frac{H}{2} \tag{4.3}$$

$$I = \frac{WH^3}{12} \tag{4.4}$$

where, I is the moment of inertia and y is the maximum vertical distance from the beam's neutral axis.

The exact solution is compared to a beam, shell and solid element respectively. It can be seen from figure 4-2 below that the value obtained for the maximum bending stress is equal to the one from the Euler-Bernoulli theorem. However, most structures are three-dimensional. In such cases, these structures are approximated by a 2D element topology such as a shell element.

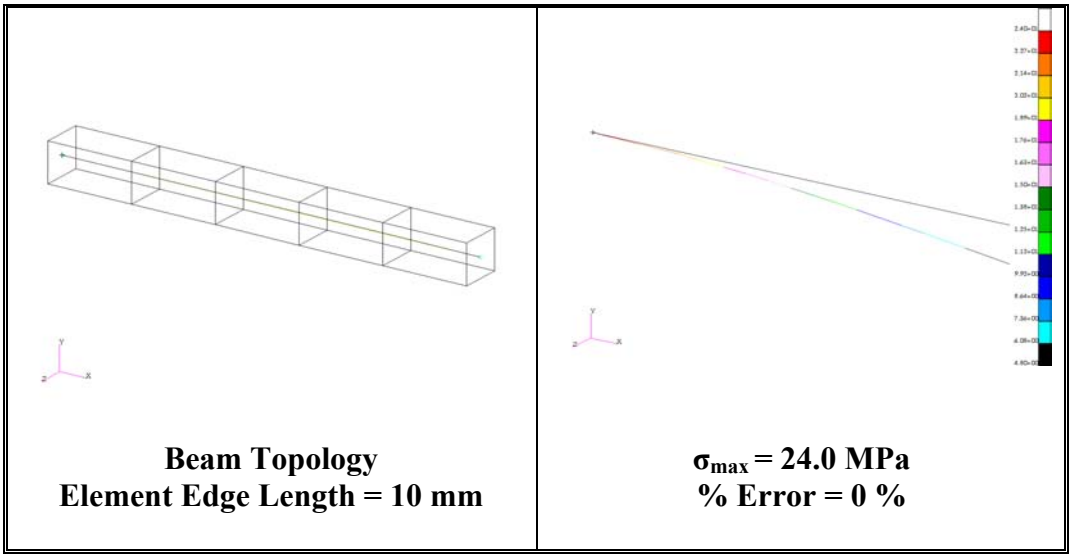

**Beam Topology**
**Element Edge Length = 10 mm**

**$\sigma_{max}$ = 24.0 MPa**
**% Error = 0 %**

**Figure 4-2 Maximum Bending Stress for Beam Element**

Although ideal for modeling bending situations, the beam element is very

limited in the hinge application, such that it is only used in certain structures to transfer loads from two unconnected 2D-shell or 3D-solid elements.

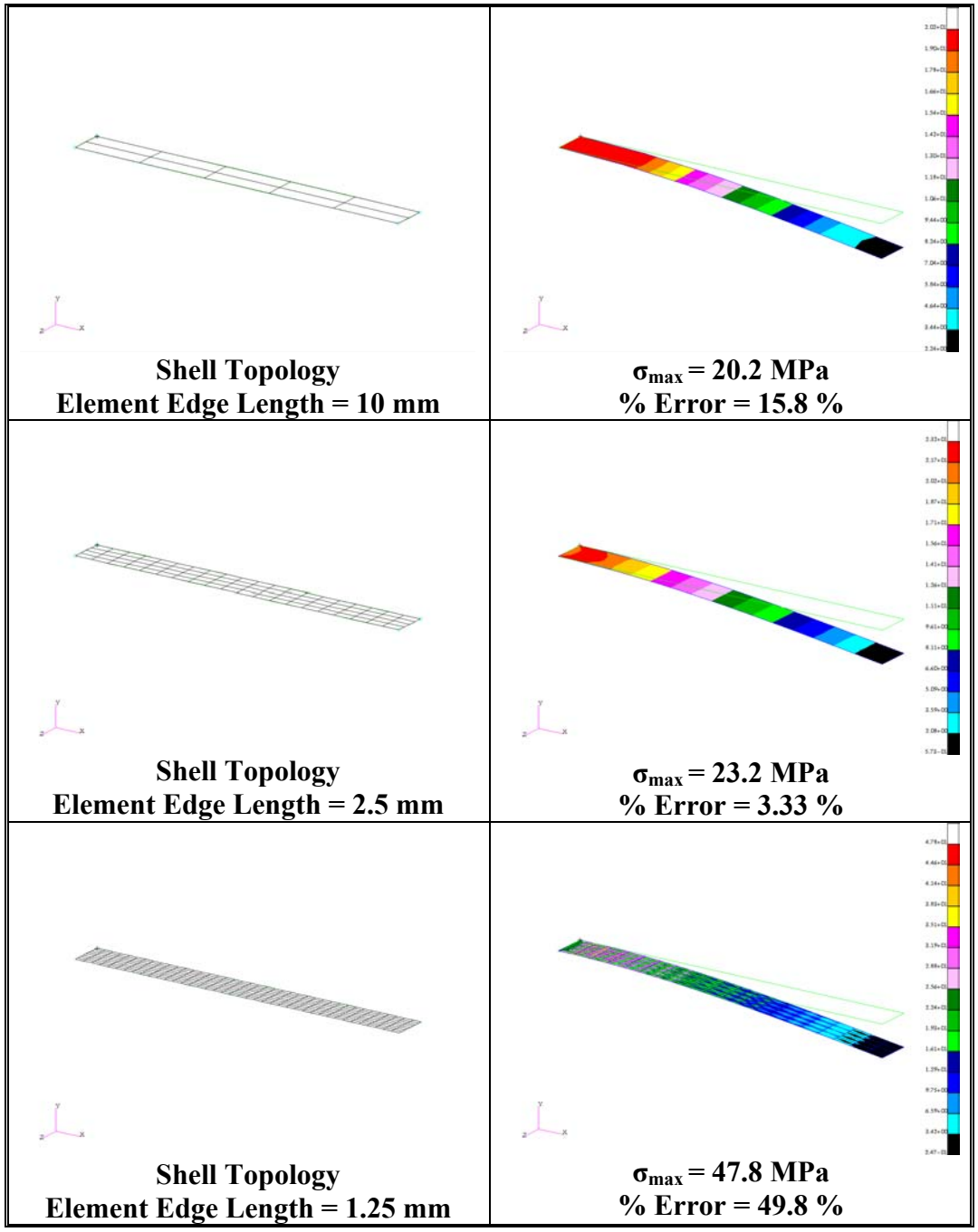


**Figure 4-3 Maximum Bending Stress for Shell Element (Quad4-node)**

As a result, shell and solid elements are widely used in place of beam elements. Indeed, shell elements themselves cannot be universally applied. As

previously mentioned, shell elements are used as an approximation to solid elements. The popularity of the former comes from its six DOF capability. Since most components are subjected to both forces and moments in realistic situations, the shell is an ideal choice. Shell elements also reduce the amount of computation time as compared to solids. However, there are situations where shell elements fail. One of the most important situations where shell elements fail is depicted below in figure 4-3. This investigation is based on the same cantilever beam, whereby the element topology is altered to shell elements. Figure 4-3 shows the effect of refining the element edge length on the maximum bending stress.

The effect of altering the element edge length from 10mm to 2.5mm causes the maximum bending stress to approach the exact solution. Indeed, from finite element theory, discretizing the structure into smaller elements should cause the solution to converge to the exact value. However, further refinement of the mesh from 2.5mm to 1.25mm causes a drastic change in the stress. Instead of converging to a value close to the exact solution, the maximum bending stress almost doubled from its original value. Furthermore, the contour plot of the stress distribution as seen from the spectrum is irregular and very distinct from the previous ones. The occurrence of this result can be explained by comparing the length to thickness ratio of the shell element. In general, a length to thickness ratio of 1:2 is appropriate. In this case, the ratio is 1:4 and is therefore unacceptable. Hence, solid elements should be used.

Generally, structural designers tend to avoid using solid elements

because most solids, except for tet4-node elements, do not have rotational stiffness. In addition to that, solids increase the analysis run-time when compared to shells. However, as seen in the previous example, shells fail when the length to height ratio exceeds 1:2.

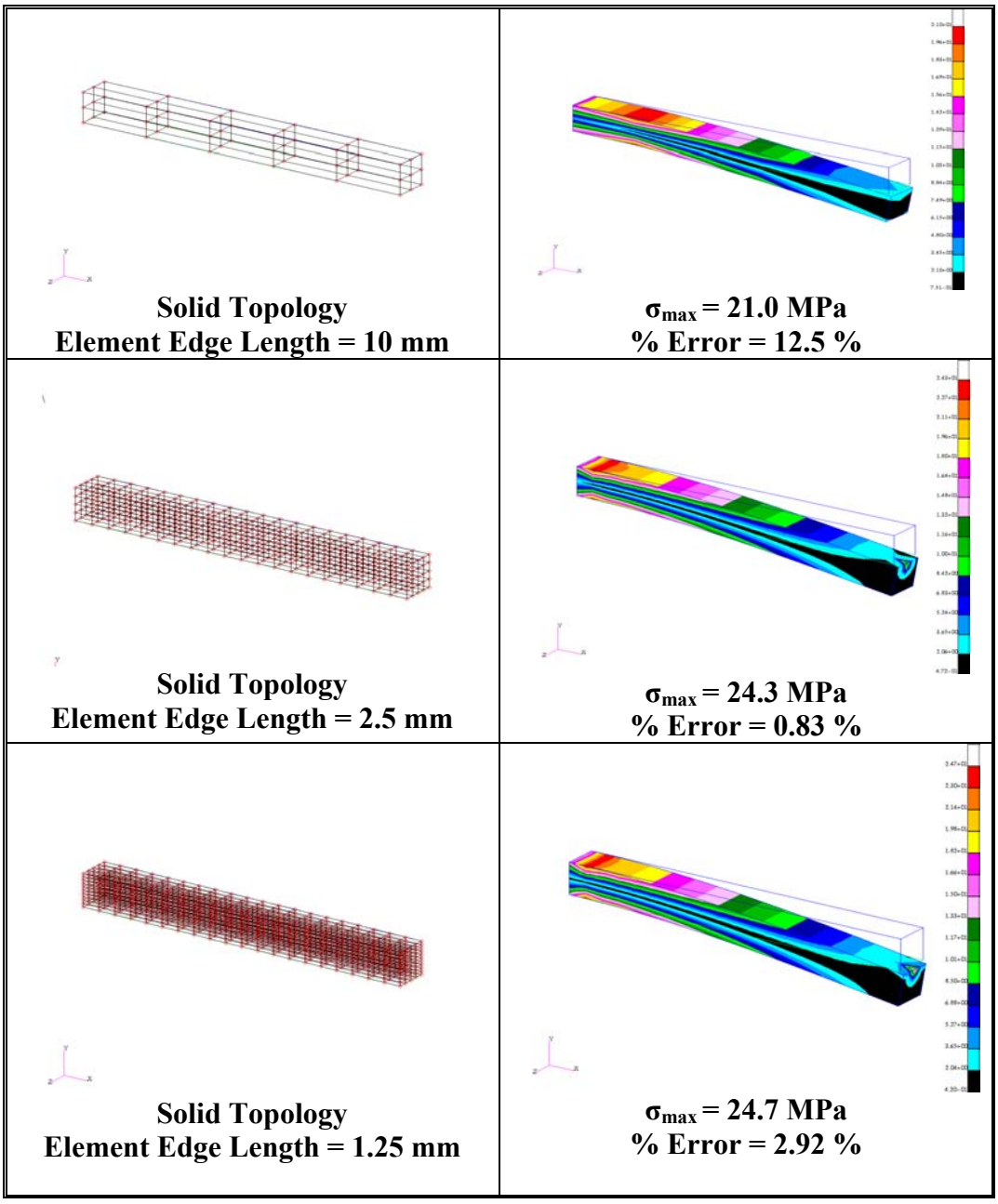


**Figure 4-4 Maximum Bending Stress for Solid Element (Hex8-node)**

Moreover, structures consisting of irregular thickness (e.g. a tapered

beam) cannot be modeled using shell elements. The use of solids is unavoidable in those situations. The next example shows the cantilever beam modeled as a solid or commonly known as the brick element. The results show that using a refined mesh through the length and thickness cause the solution to converge to the exact value. The interesting point to note here is how the unavailability of rotational stiffness is compensated by the use of a refined mesh through the thickness. These observations are crucial as it enables the structural designer to properly select the type of element applicable to a particular analysis.

The results based on this exercise are used to model the hinge system. Before discussing the detailed finite element modeling and analysis of the hinge system, it is important to understand the difference between effective and improper elements. The next section discusses, and provides acceptable data that characterize, effective and improper elements.

## 4.4 Geometry Check for Solid Elements

Generally, the distortion of a solid element can be measured according to its skew and warp angles, together with aspect, taper and jacobian ratios. All these measures represent the amount that the solid element deviates from its ideal shape. In practice, highly skewed and warped elements, as elements with a very high aspect, taper and jacobian ratios should be avoided.

The skew angle of solid elements, brick or wedge, are calculated by referring to each face in the element. More precisely, the skew angle is measured on each face as if it is a tria or quad element. Figure 4-5 below shows the measurement of skew angle for a tria and quad element respectively. Hence,

the skew angle for a brick or wedge is taken as the highest angle resulting from the respective quad or tria element. In practice, this angle should be smaller than 30 degrees [22,23].

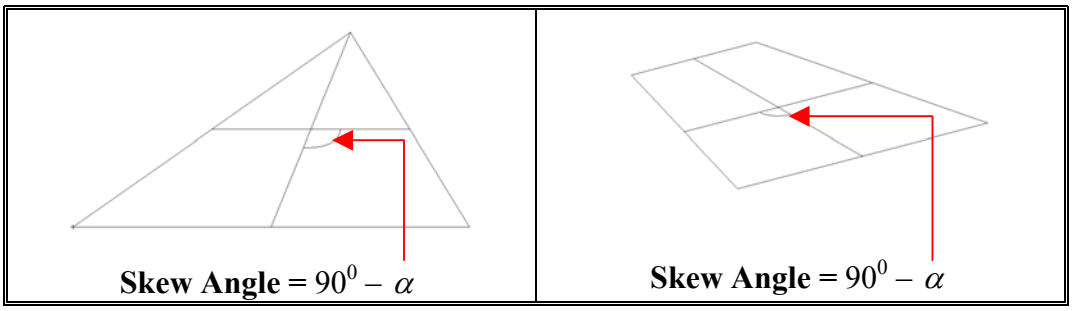


**Figure 4-5 Skew Angle Measurements in Tria and Quad Elements**

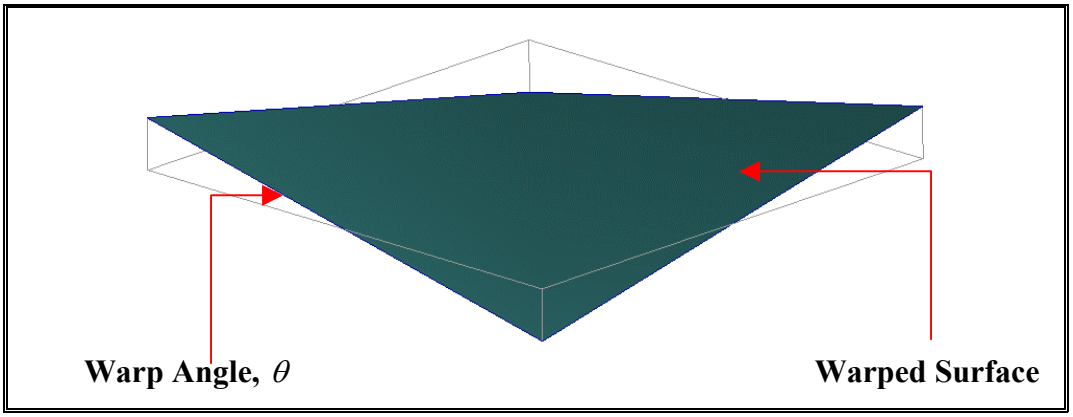


**Figure 4-6 Warp Angle Measurements in a Quad Element**

Similarly, the warp angle of a brick or wedge element is measured by referring to each face in the element, whereby the highest angle is reported as the warp angle. Figure 4-6 shows a highly warped quad element with θ as the warp angle. The warp angle should be smaller than 5 degrees [22].

The aspect ratio is calculated as the ratio of the distance between opposing faces. Unlike the skew and warp angle, the aspect ratio is calculated differently for a brick and a wedge elements. For a wedge element, the two triangular faces are averaged to obtain a mid-surface. The aspect ratio of the

latter is then calculated. For the remaining quad faces in the wedge element, the ratio of the maximum to minimum length are measured and multiplied by the aspect ratio of the mid-surface tria element [22]. The resulting solution is the aspect ratio of the wedge element (see figure 4-7 below). The maximum acceptable ratio is 5:1.

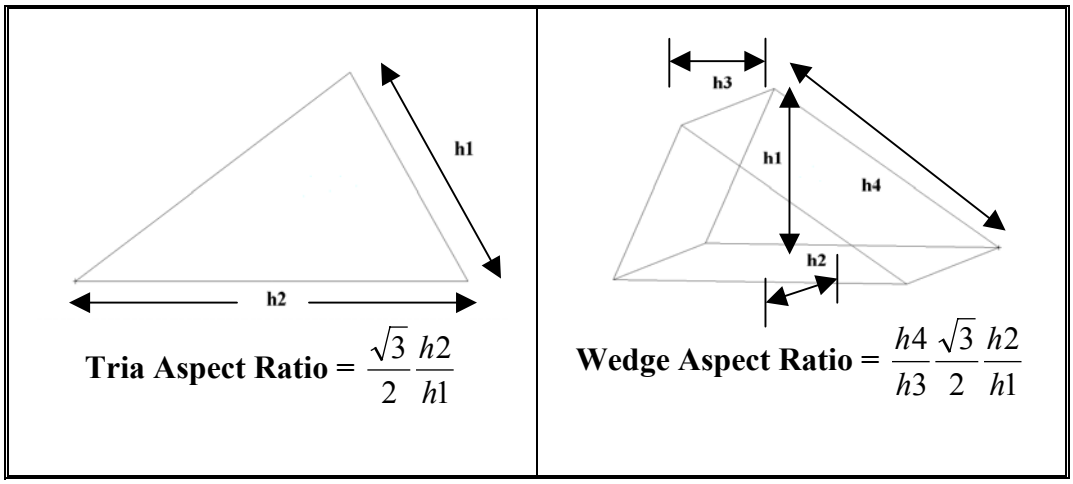


**Figure 4-7 Aspect Ratio Measurements in Tria and Wedge Elements**

The Aspect Ratio (AR) in a brick element is calculated as the ratio of the distance between opposing faces. The distances between the centerpoints of all three pairs of opposing faces are compared and the maximum value taken as the AR (see figure 4-8) [22]. The maximum acceptable ratio is 5:1.

The taper and jacobian ratios only exist for quad or brick elements. The former is calculated by splitting the quad element into four triangles connected at the mid-point of the quad. The area of each triangle is calculated. The ratio of the smallest to the total area is the taper ratio. Therefore, for the brick element, the aforementioned procedure is repeated for each face and the largest value is reported as the taper ratio of the brick element (see figure 4-9 (a)). A minimum value of 4:5 is acceptable [22].

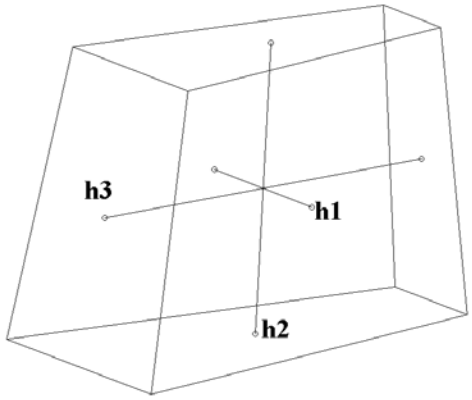


h1, h2 and h3 are distances between the mid-point of each opposite faces.

$$\textbf{Brick AR} = \frac{\max(h1, h2, h3)}{\min(h1, h2, h3)}$$

**Figure 4-8 Aspect Ratio Measurements in Brick Elements**

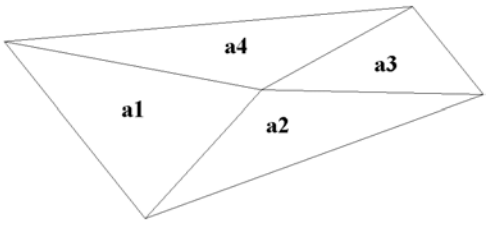


$$\textbf{Taper Ratio} = \frac{4\min(a1, a2, a3, a4)}{a1 + a2 + a3 + a4}$$

**(a)**

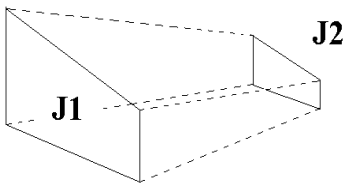


**J1**=Jacobian of Face 1; **J2**=Jacobian of Face 2

$$\textbf{Jacobian Ratio} = \frac{|J2|}{|J1|}$$

**(b)**

**Figure 4-9 Taper and Jacobian Ratio Measurements in Brick Elements**

The jacobian ratio is a measure of the deviation of a quad element from its ideal rectangular shape. The jacobian is calculated for each face in the brick element. The jacobian ratio is the maximum ratio of jacobian between the opposite faces. An ideal element has a jacobian ratio of 1.0. Generally, jacobian ratios of 0.7 and above are acceptable (see figure 4-9 (b)) [22].

## 4.5 FE Modeling of the Door Hinge System

The FE model of the door hinge system is developed using the

commercial FE package MSC.PATRAN. The modeling process of the structure involves three steps, namely geometry modeling, FE discretizing and structure assembling. Two distinct models are considered. The first model (model A) is discretized by a combination of hexagonal eight node and pentahedral six node elements and the second (model B), a bi-parametric solid, consists solely of hexagonal eight node elements. The effectiveness of each model is crucial to fatigue life prediction, is compared based on the FE static results. Two separate static analyses are then performed on each model. The first one is to compute the stresses and strains and use them as input data for a uni-axial fatigue analysis whereas the other is for a multi-axial fatigue analysis. The uni-axial and multi-axial models are quite dissimilar from each other in the sense that the former consists of a single hinge whereas the latter, the entire door hinge system. All static analyses are performed using MSC.NASTRAN.

### 4.5.1 Geometry Modeling

The hinge model, created in the Computer Aided Design (CAD) package IDEAS, is imported into MSC.PATRAN as a PARASOLID. The PARASOLID format contains the solid geometry of the hinge (see figure 4-10 below).

The hinge is a three-piece component consisting of a Body-Side (BS) bracket, a Door-Side (DS) bracket and a circular cross-section Pin. The BS bracket and Pin are symmetrical components unlike the DS bracket that has an oval and a circular shaped hole on each side of the component. The Pin is removed from the model since it does not contribute directly to the FEA. The pin mechanism allows rotation of the DS about the BS bracket, thus transferring

loads from one bracket to the other. A different approach, as will be seen later in section 4.5.3, is used to transfer the loads.

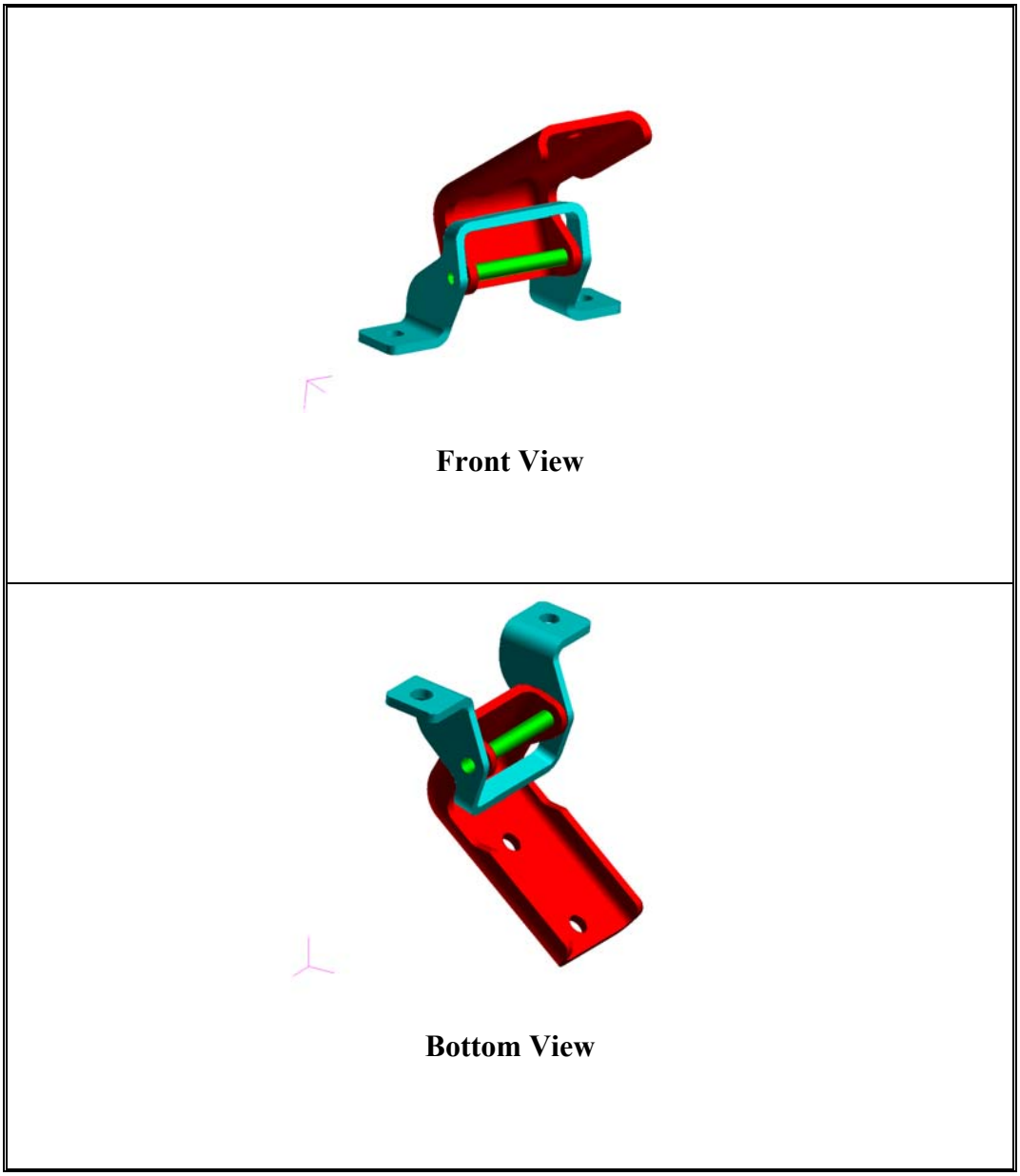


**Figure 4-10 CAD Model of Door Hinge**

For both models A and B, a surface model is created from the PARASOLID. It is important to create a mid-surface from the solid geometry. The mid-surface being equidistant from the top and bottom surfaces of the CAD model. Model B is split into bi-parametric surfaces for reasons that will become

obvious later. A bi-parametric surface is one enclosed by no more than four curves. Figure 4-11 compares models A and B.

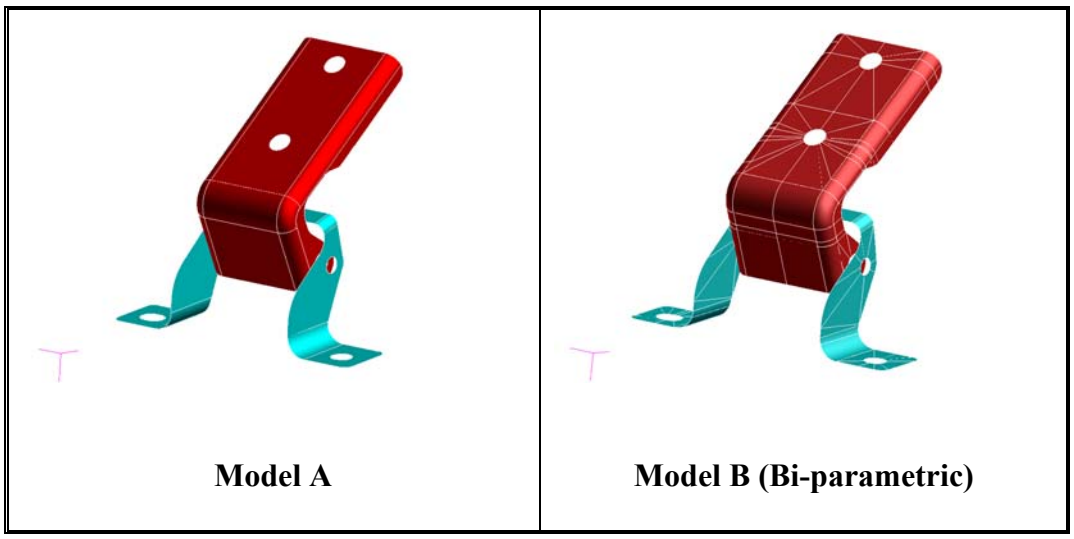


**Figure 4-11 Comparison between Models A and B**

### 4.5.2 FE Discretizing

After the surfaces are created, each bracket is separately discretized. Model A is initially meshed using a combination of Quad4-node and Tria3-node shell elements. In general, Triangular elements (Tria3) should be avoided due to excessive stiffness. Rectangular elements (Quad4) are ideal for shell mesh. However, in components consisting of holes, fillets and curvatures, it is very difficult to avoid Tria3 elements. It should be noted that a model in which the total number of Tria3 is less than five percent of the total number of elements in the model yields conservative results [22]. Figure 4-11 shows the discretized shell model with Quad4 and Tria3 elements with an element edge length of 3 mm. It can be seen from figure 4-12 that Tria3 are indeed formed at curvature and holes.

The shell elements are then extruded to create solid elements. This

procedure is done by extruding the mid-surface by ½ the total thickness of the model in each direction normal to the surface of the shell element. As a result, Tria3 and Quad4 become Wedge6 and Hex8 solid elements respectively. It should be noted that the original surfaces couldn't be meshed directly by solid elements, unless tetrahedral elements are used. Like triangular elements, tetrahedral elements are excessively stiff. Moreover, when tetrahedral elements are used, gaps are induced in the FE model. This is because at curvatures, the tetrahedral elements do not geometrically fit to the surface. Hence, if the original surfaces are to be used for meshing, extruding a shell mesh (model A) is a better option. Otherwise, a bi-parametric solid geometry (model B) has to be created.

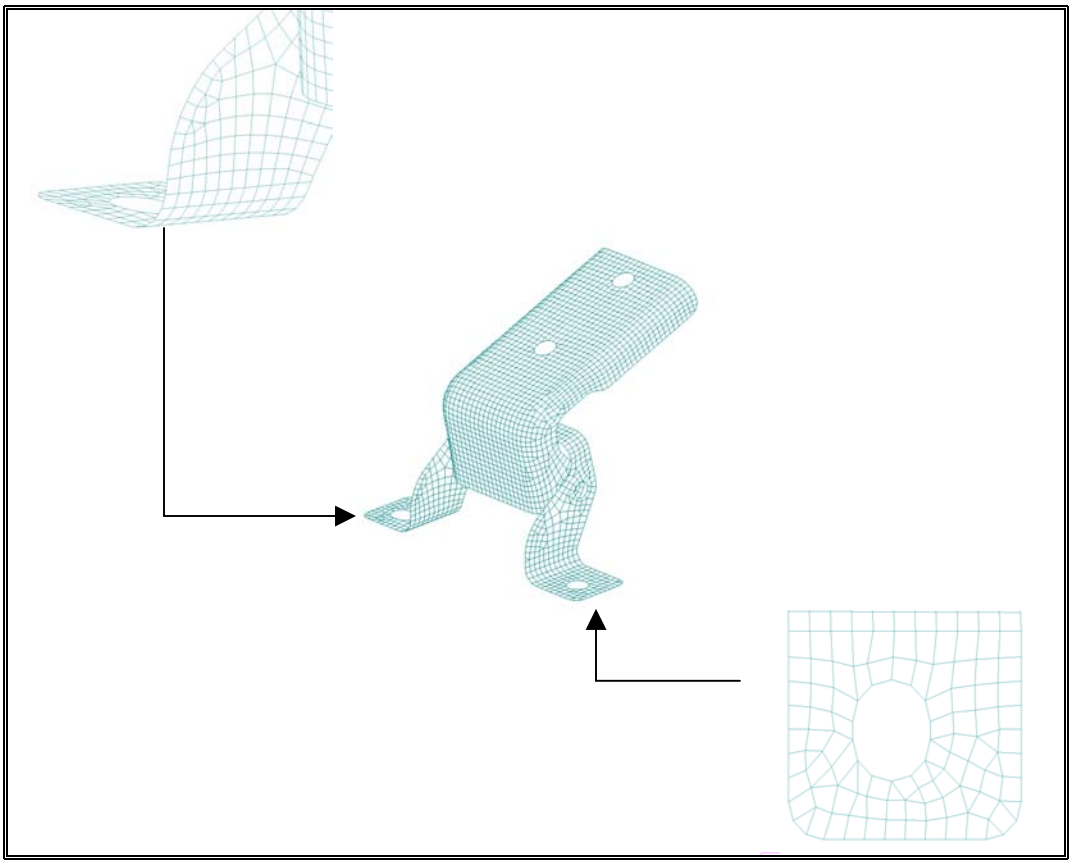

**Figure 4-12 Shell Discretization with Quad4 and Tria3 Elements**

To create a bi-parametric solid geometry, the bi-parametric surface of model B is extruded. The bi-parametric solid can then be discretized by using an isomesh with hex8 elements. From section 4-3, it was seen that to take into account bending, the solid elements had to be refined through the thickness. At least 3 solid elements should be used through the thickness, if proper bending effects are to be included [22]. Figure 4-13 shows a comparison between the meshes of models A and B respectively.

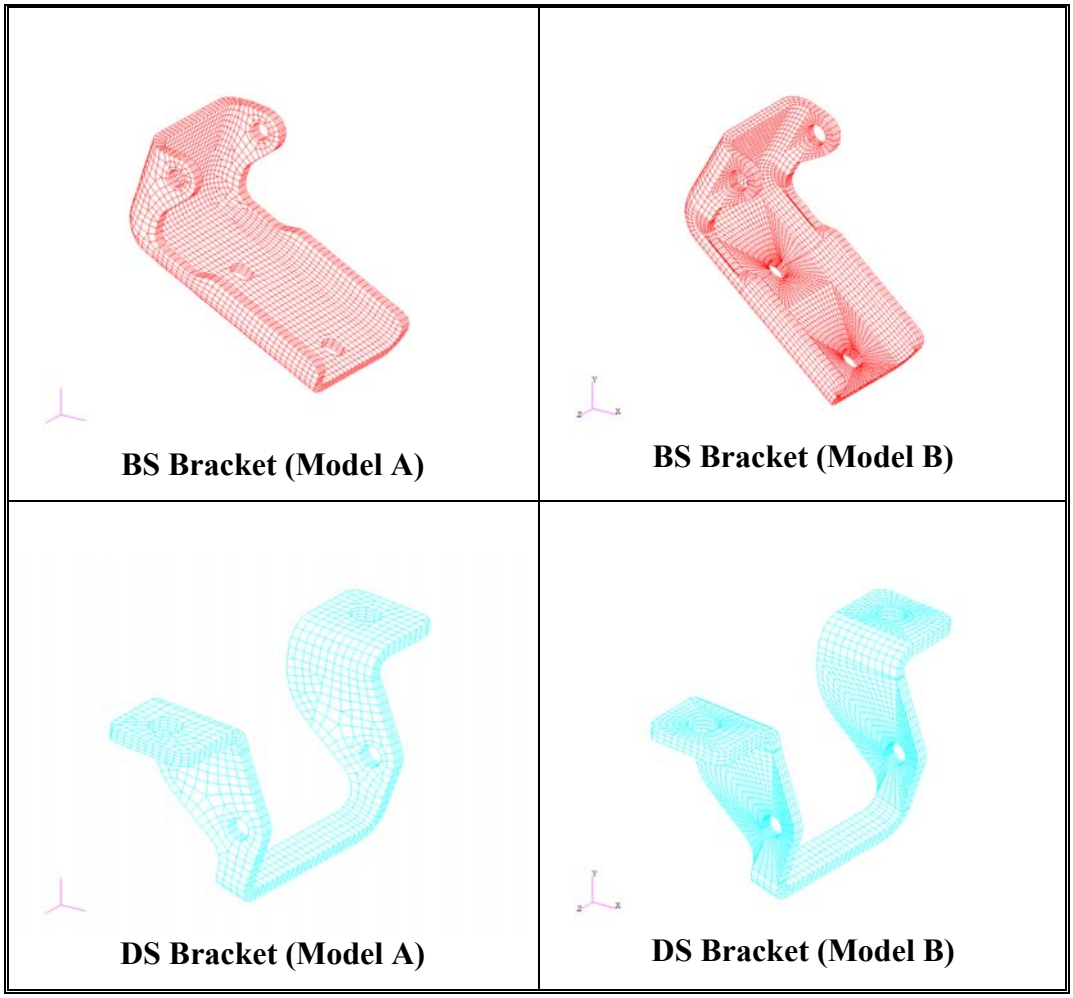


**Figure 4-13 A Comparison between the FE Models A and B**

After discretization of the model is completed, several geometry checks are performed to verify whether the elements qualities are acceptable. Figure 4-

14 below shows the potential areas where the elements failed the skew angle geometry tests. The shaded areas are the distorted elements.

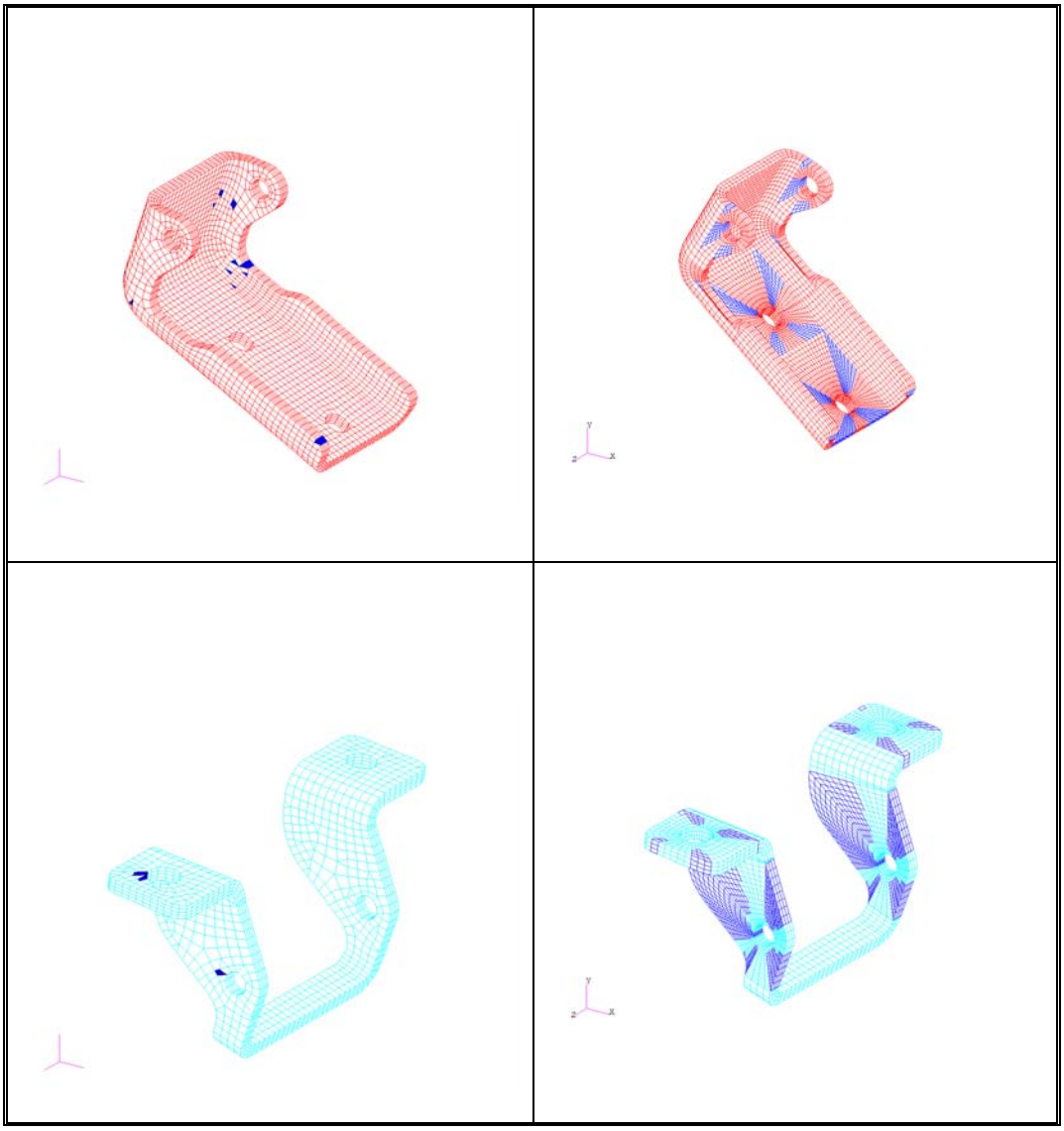

**Figure 4-14 Distorted Elements in BS and DS Brackets**

When performing geometry checks on the brackets for both models, error messages are also issued showing the extent by which the element failed. Referring to section 4-4, where the minimum or maximum acceptable values for each parameter are listed, the extent by which the failed element deviated from the acceptable values can be calculated. Table 4-2 below displays the outcome

of the geometry check on each bracket for both models.

| Bracket type and model | Total number of elements | % Failure in jacobian ratio test | % Failure in aspect ratio test | % Failure in taper ratio test | % Failure in skew angle test | % Failure in warping test |
|---|---|---|---|---|---|---|
| BS (A) | 7476 | 0% | 0% | 93.3% Worst: 0.748 | 0.56% Worst: $34.3^0$ | 96.9% Worst: $15.0^0$ |
| DS (A) | 2688 | 0% | 0% | 92.6% Worst: 0.753 | 0.47% Worst: $36.7^0$ | 92.2% Worst: $15.0^0$ |
| BS (B) | 9774 | 0% | 0% | 92.9% Worst: 0.130 | 19.8% Worst: $83.3^0$ | 98.8% Worst: $15.0^0$ |
| DS (B) | 6153 | 0% | 0% | 93.9% Worst: 0.693 | 41.3% Worst: $77.2^0$ | 97.5% Worst: $15.0^0$ |

**Table 4-2 Percentage of Failure in Geometry Tests**

Although not all the elements in the models satisfied the geometry check criteria, when meshing the structure, the goal is to minimize the number of distorted elements and to obtain values for these distorted elements that are close to the acceptable value. It can be seen from table 4-2 that all the elements pass the jacobian and aspect ratios. Moreover, the percentage failure in taper ratio arising from models A and B are very close. However, the value for the worst element in model A is very close to the acceptable value. On the other

hand, in model B, the taper ratio for worst element deviate quite a lot. The skew angle check can be analyzed in a similar fashion. It can be seen that the elements in model B are highly skewed with skew angles significantly larger than the minimum. Eventually, element warping cannot be avoided in both models because of the highly curved surfaces. The percentage of warp angle failure is similar in both models.

The objective behind the geometry tests in the two models is to compare the effectiveness of model A over B or vice-versa. Based on the results, it is seen that model A is more accurate. The accuracy of the FE model can also be verified by analyzing the stresses in a static case. A sharp transition in stress at a certain point in the model other than notches and loading areas arise from distorted elements. This can result in the prediction of wrong stress values. This feature is demonstrated in section 4.6.

### 4.5.3 Components Assembly

The final step involves assembling all the discretized components of the hinge. To this end, the two components of the hinge, the BS and DS brackets, are joined using multi-point constraints (MPC). MPC acts as a rigid bar between two nodes and constrains all DOF, three translational in his case, so that the nodes move by the same amount in every direction. One of the two nodes is called a dependent node and the other, an independent node. If the independent node is displaced by a certain amount, the dependent node will undergo a similar displacement. Therefore, MPC can be used to transfer loads from one node to the other. In this case, the MPC is used to replace the Pin connecting the

two brackets. An induced load on BS is therefore transferred to DS and vice-versa. Since MPC is rigid, it will not deform under external load and does not require any physical or material properties as analysis input.

The interesting point to note here is the mechanism behind the motion of the brackets in the hinge. In reality, the DS bracket rotates about the Pin with the BS bracket fixed. The DS bracket rotates up to a maximum angle of 60 degrees. This motion simulates the open/close door movement. Hence, at the zero-degree position, the door is fully-opened and at the 60-degree position, the door is closed. Figure 4-15 shows the range of motion of the hinge.

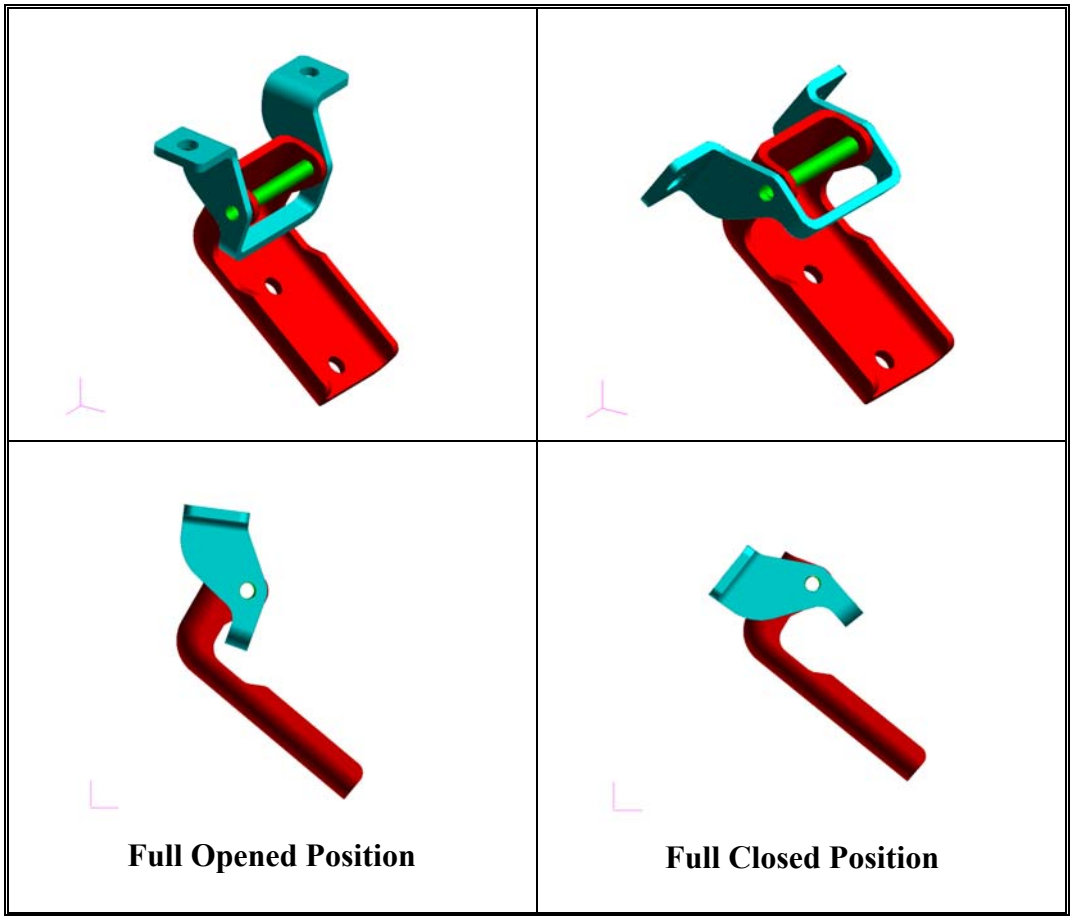


**Figure 4-15 Range of Motion for the 60-Degree Hinge**

The mechanism of the hinge motion from the fully-closed to the fully-

opened position is very complex to model through FE. This is because contact points have to be defined at subsequent points throughout the entire motion. MSC.MARC was used to model the contact points. Two types of contacts were used, rigid and sliding contacts. This exercise proved to be very tedious, time consuming and unsuccessful. The following assumptions were then made.

- If the rigid body motion of the hinge is considered, the stress is negligible until the BS and DS brackets come directly into contact.
- A rigid contact can then be used to constrain the BS and DS brackets when they come into contact.

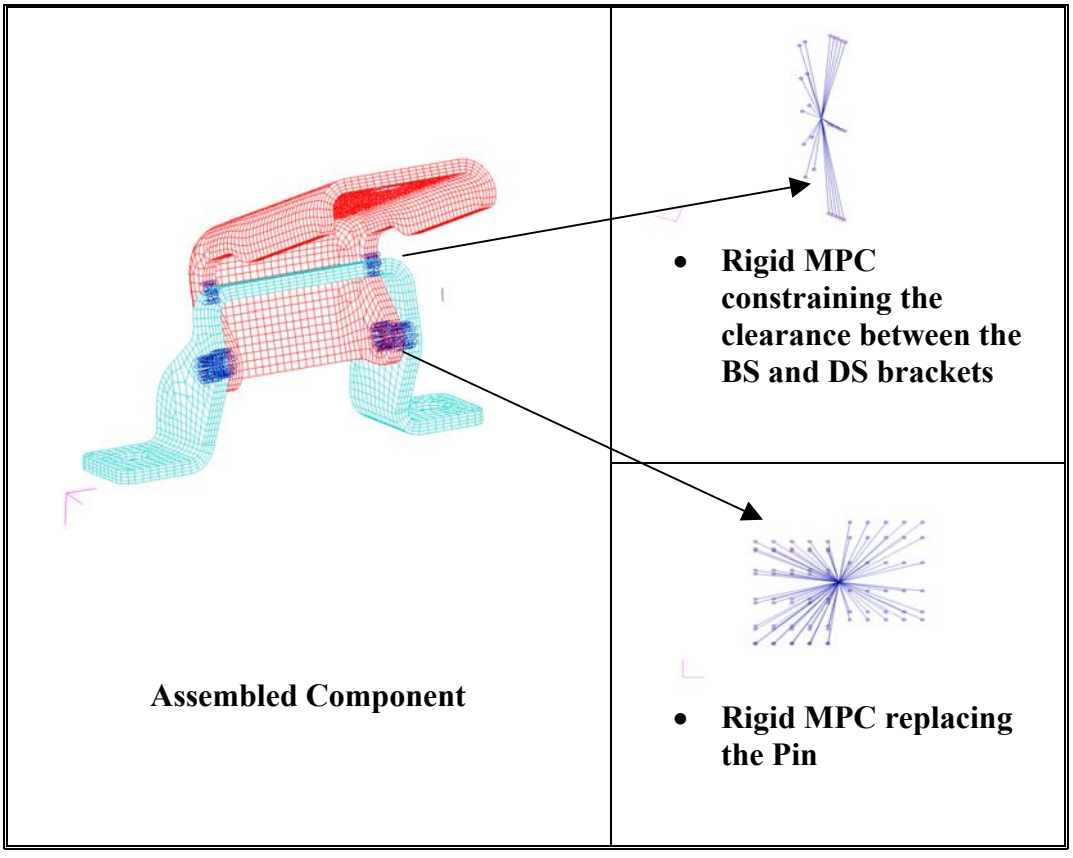


**Figure 4-16 Assembled FEM with MPC**

Based on these assumptions, MPC were used to model the rigid contact. These rigid MPC ties the nodes on the BS and DS brackets together at the

contact area. Hence, a load induced to the DS bracket is transferred to the BS bracket through the MPC. Figure 4-16 displays the use of MPC to constrain the hinge.

### 4.4.4 Boundary Conditions

The hinge is subjected to both uni-axial and multi-axial loading conditions. Therefore, two separate models are built for the different loading conditions. In the uni-axial model, the circular and oval holes in the DS brackets are fixed and a force is applied via a block on top of the BS bracket. Although MPC could be used to apply the load, a meshed block is used instead to reflect a more realistic loading. The block is attached to the BS bracket using rigid MPC.

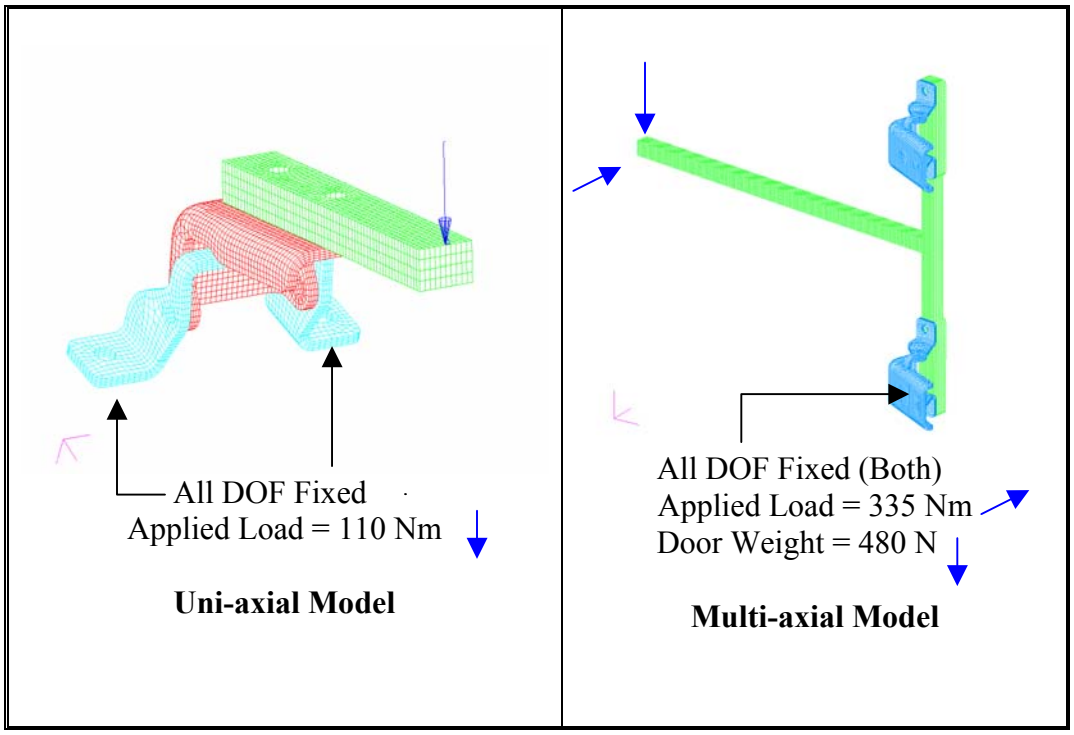


**Figure 4-17 Applied Loads and Constraints**

The multi-axial model consists of two hinges and a T-shaped support to reflect the entire door-hinge system. In this model, the upper circular holes on the BS

brackets are fixed. Two separate load cases are applied to the multi-axial model, namely an applied torque and the weight of the door. The applied torque is converted to a force because solid elements do not have rotational DOF. The uni-axial and multi-axial models are shown in figure 4-17. When constraining the holes in both the uni-axial and multi-axial models, a certain area around the holes was fixed instead of the circumference only. Hence, the correct bolt and washer environment is simulated.

## 4.5 FE Static Analysis: Analysis Parameters

As previously mentioned, the objective of this research is to predict fatigue life in the door hinge subjected to uni-axial and multi-axial stress states. It is therefore necessary to calculate the stresses and strains in a static analysis and use these as input to calculate fatigue life. Before implementing a static analysis, geometric and material properties need to be assigned to all the elements in the hinge. The geometric properties in this case are self-defined when solid elements with a constant gauge are used (E.g., if shell elements are used instead of solids, the thickness needs to be entered as a geometric property). On the other hand, material properties have to be defined in all cases. In this case, the material used is steel (SAE Grade 1008-1010). The desired static results from Finite Element Analysis (FEA) are used as input data to calculate fatigue life. Therefore it is important to use the elasto-plastic properties of the material, since it is unknown at this point whether the stresses and strains will fall in the high or low cycle region. The cyclic and monotonic-true stress-strain curves for SAE1008 are shown in figure 4-18.

The question here is whether to use the monotonic or cyclic curve. From a static analysis point of view only, the monotonic curve should be used. However, since the stress and strain values are used as input data to calculate fatigue life, the cyclic curve is used. This feature is explained in chapter 5. Based on the material non-linearity, a non-linear static analysis is conducted. MSC.NASTRAN is used to solve for the stresses and strains. This analysis is conducted on both models A and B. The results are discussed in the next section.

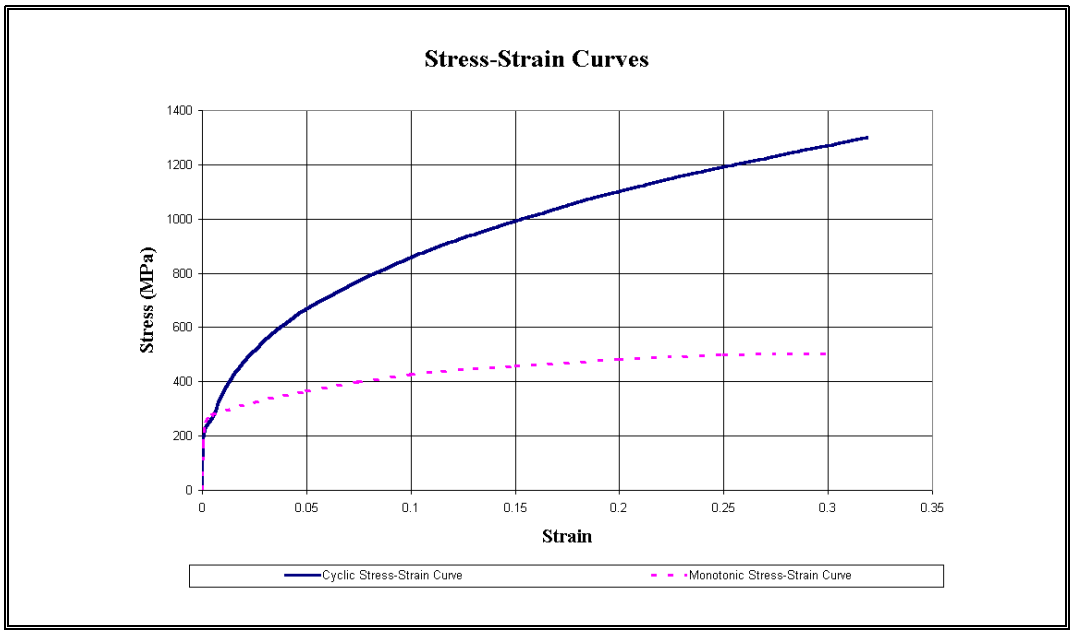


**Figure 4-18 Stress-Strain Curves for SAE1008**

The question here is whether to use the monotonic or cyclic curve. From a static analysis point of view only, the monotonic curve should be used. However, since the stress and strain values are used as input data to calculate fatigue life, the cyclic curve is used. This feature is thoroughly explained in chapter 5. Based on the material non-linearity, a non-linear static analysis is conducted. MSC.NASTRAN is used to solve for the stresses and strains. This

analysis is conducted on both models A and B. The results are portrayed in the next section.

## 4.6 Simulation Results

In this section, the stress contour plots for both the uni-axial and multi-axial models are displayed. FEA generates maximum and minimum principal stresses (i.e., tensile and compressive stresses) together with the equivalent Von Mises and shear stresses. It is important at this point to analyse each stresses effectively and use the most critical one as input to calculate life. The rule of thumb is that the critical stress will have the most adverse effect on fatigue life. Using improper stress values will result in inaccurate fatigue life prediction.

The accuracy and effectiveness of both models A and B are now investigated. The most appropriate model can be selected (see figure 4-19) by examining the distribution of the Z-component of stress in the uni-axial loading. In a uni-axial stress state, the X- and Y- components of the stresses lie in the plane of the model with the Z-component being close to zero.

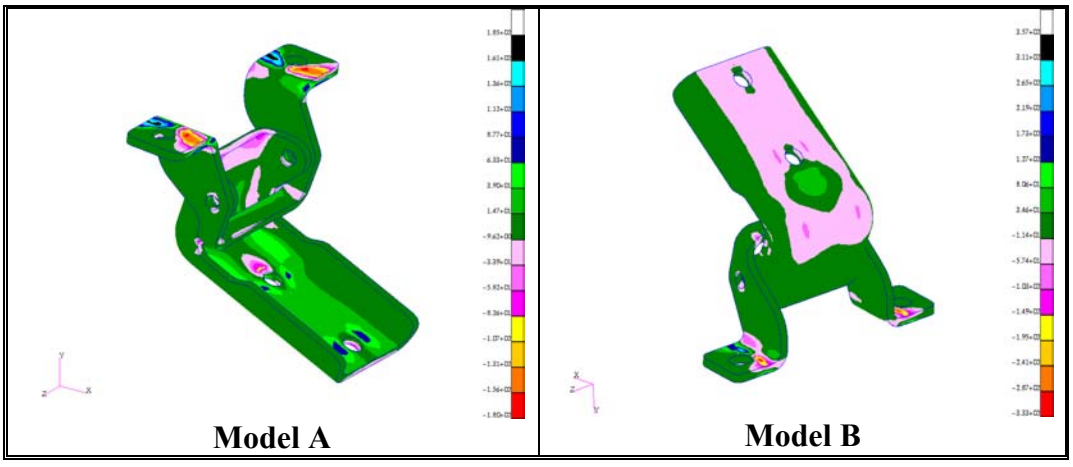


**Figure 4-19 A Comparison between the Z-Component of Stress In Models A and B based on a Uni-axial Loading**

It can be seen from figure 4-19 that the stress is uni-axial in nature in both models except at the holes on the DS brackets. The sharp transition in stresses in these areas is due the constraints. The hinge was fixed in all DOF at these locations, thus the high stress values are really artificial stresses. In an experimental analysis, the stresses will be close to zero at these locations. One of the drawbacks of FEA is that artificial stresses are created at loading and constrained points. These stresses should be ignored. However, looking at the spectrum on the right hand side of both models, it can be seen that the stresses are excessively higher in model B than in model A. The maximum stress in model B is 357 MPa, whereas in model A, the stress is 185 MPa.

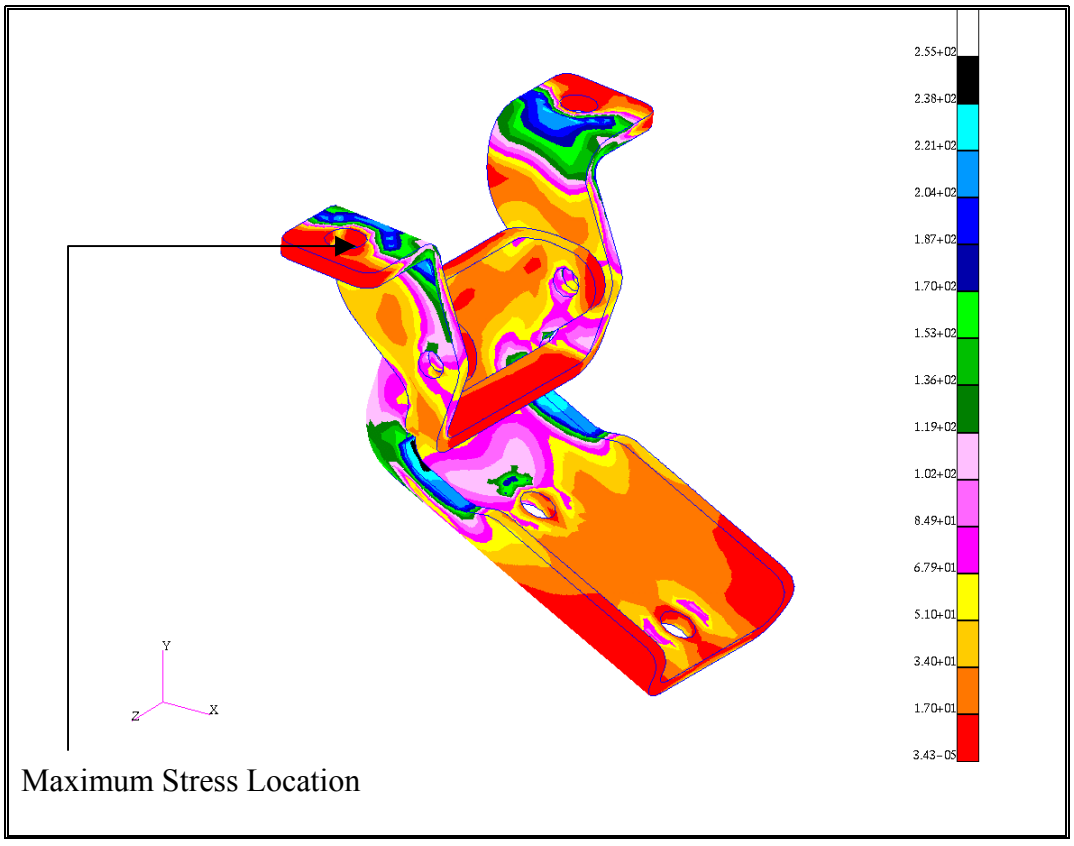


**Figure 4-20 Maximum Principal Stress Contour in the Uni-axial Model**

Since the maximum Z-component of stress is higher than the tensile strength, it is concluded that model B is inaccurate. The occurrence of the high stresses is certainly due to distorted elements. Hereafter, only model A is used for uni-axial and multi-axial fatigue analysis. Figures 4-20 and 4-21 display the maximum principal stress based on the uni-axial and multi-axial loading cases respectively. In the uni-axial model, the maximum stress is 255 MPa, and in the multi-axial model, the maximum stresses are 343 MPa and 142 MPa for the torque and weight cases respectively. The maximum principal stress is the most critical stress in both loading cases.

## 4.7 Results Summary and Conclusion

It is concluded that the most appropriate FE model is model A. Model A has an equal element edge length and thickness of 2.5 mm. A mesh size of 3.5 is initially used, and subsequently reduced to 3 mm and 2.5 mm. Although, the results are not reported here, the stress results tend to converge. However, the attainment of convergence cannot be definitively reported as the mesh size could not be further refined. This is because the high mesh density required a more powerful computational tool (Random Allocated Memory). Hence, the stress values were taken as the converged results. At this point, it is assumed that a correct life prediction by fatigue analysis implies that converged stress values are employed. The most important observation from the static analysis is the location of the maximum stress in the model for both the uni-axial and multi-axial models.

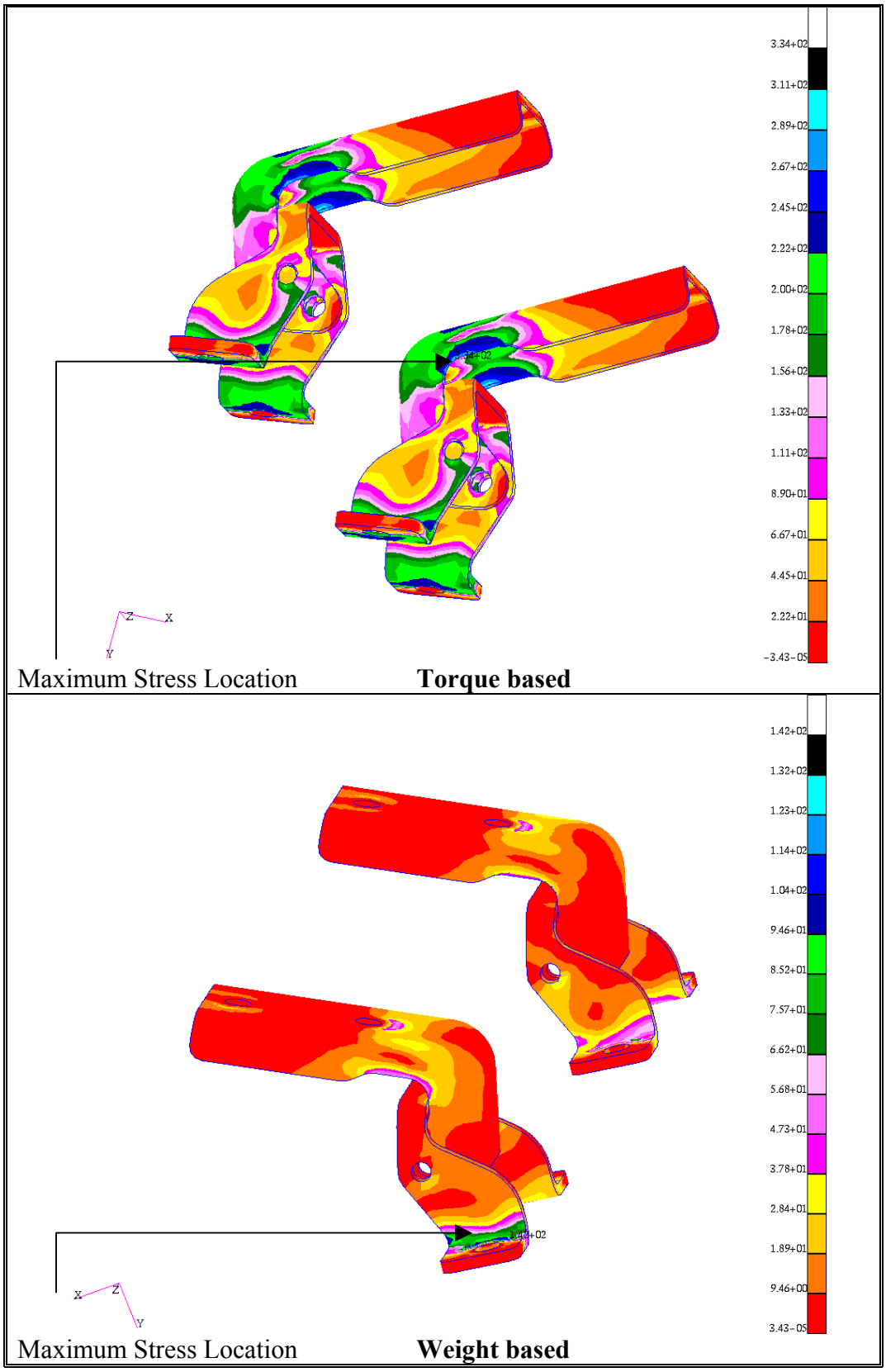


**Figure 4-21 Maximum Principal Stress Contour in the Multi-axial Model**

Firstly, in the uni-axial model, the maximum stress occurred at the inner edge of the oval-shaped hole. Although this is the constrained area, only the stresses at the top and bottom surfaces can be ignored (i.e. surfaces in contact with the washer). It will be seen later that crack is initiated at the oval hole. At this stage, no further explanation will be given until confirmation from the fatigue analysis is obtained. Secondly, the maximum stresses in the multi-axial model are at different locations for the torque and weight cases respectively. It will be seen afterwards that the stresses in both cases are superimposed to simulate the multi-axial environment of the hinge. Similarly, it will be seen that the crack occurs at the location of the maximum stress.

Indeed, this is the real advantage of FEA. It is not only efficient in the analysis of complex models, but it also generates local stress-strain information at the root of notches if a sufficient small size mesh is used. The maximum principal stresses are therefore used as input data in the numerical fatigue analysis.

# CHAPTER 5 FE BASED FATIGUE ANALYSIS

## 5.1 Overview

In this chapter, the fatigue life of the door hinge is predicted using computational methods under both uni-axial and multi-axial loading. In the former, the hinge is subjected to a single load and the stress results associated with this load are cycled until crack initiates. In the latter, a hinge system is analyzed, whereby results from two separate loads are superimposed and used to predict life. Moreover, the bi-axiality ratio and angle of spread are evaluated and plotted at the critical location in the multi-axial case to assess whether a proportional or non-proportional loading exists.

## 5.2 High Cycle vs. Low Cycle Domains

The onset of high and low cycle fatigue are explained in chapter two. It is stated that if the maximum stress in a component is lower than the yield strength of the material, the component fails under high cycle fatigue. This means that the life cycles to failure is greater than 100,000 cycles. In contrast, when the maximum stress is higher than the yield strength, the component fails under low cycle fatigue with life between 100 to 100,000 cycles. As a matter of fact, knowing the failure mechanism before running the fatigue analysis is very important. This is because in the high cycle region, using parameters based upon the S-N curve yields conservative results. Similarly, in the low cycle region, using parameters based upon the ε-N curve is preferred.

Consider the maximum stress in the hinge in the uni-axial loading case and the S-N curve for the material used, SAE1008 hot-rolled (see figure 5-1). The maximum stress obtained from FEA is 255 MPa while the stress range on the vertical axis of the S-N curve is varying from 80 MPa to 256 MPa. Since the maximum principal stress is right at the yield point and lies within the stress range, using the S-N curve would result in the prediction of conservative fatigue life (line LA1 in figure 5-1). On the other hand, consider the maximum principal strain and the ε-N curve (see figure 5-2). The corresponding maximum principal strain is 3.63E-3. If this strain value is applied to the ε-N curve (i.e., using the Strain-Life approach), the number of life cycles to failure will be infinite (line LB1 in figure 5-2). Hence, the S-N approach is the most appropriate in the uni-axial fatigue case.

Likewise, consider the maximum principal stress and strain in the multi-axial loading case. Since the torque yields the highest stress and strain, it is solely used to assess whether the S-N or ε-N approach is to be adopted. The maximum principal stress and strain are 343 MPa and 8.5E-3, respectively. If a horizontal line is drawn from the stress value of 343 MPa to the far right vertical axis on the S-N curve, it is seen that the line does not cross the curve (line LA2 in figure 5-1). Therefore, an infinite life will be predicted if the S-N curve is used. On the other hand, if the corresponding strain value is used on the ε-N curve and a similar line drawn from the maximum principal strain, the line crosses the curve at a finite value (line LB2 in figure 5-2). This shows that the ε-N approach is more suitable in the multi-axial case.

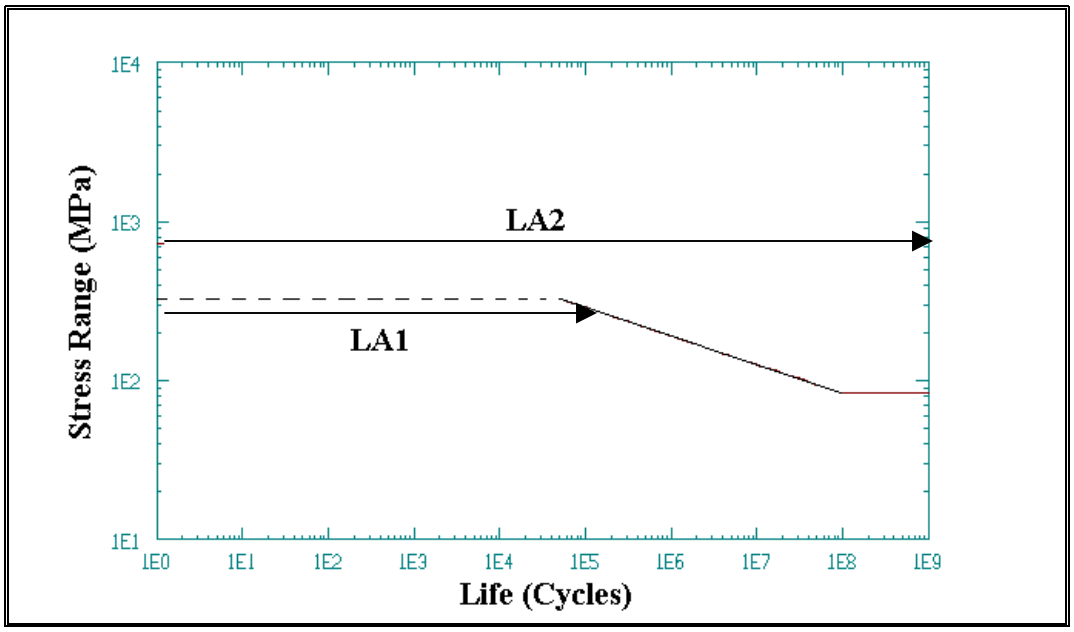


**Figure 5-1 S-N Plot for SAE1008 Hot-Rolled[18]**

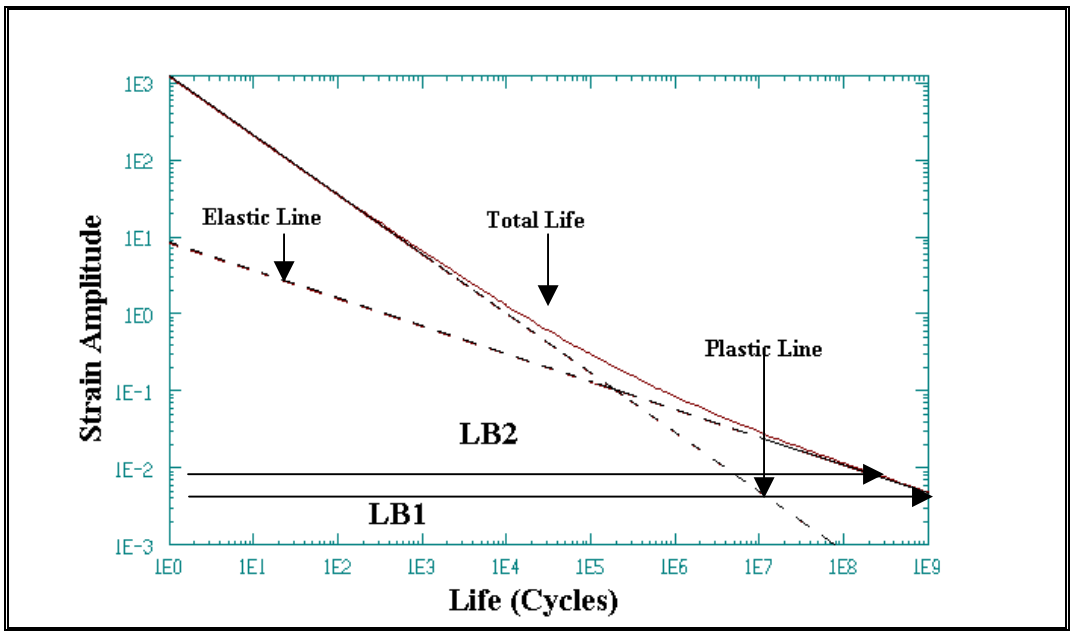


**Figure 5-2 ε-N Plot for SAE1008 Hot-Rolled[18]**

At this stage, it is necessary to deal with the uni-axial and multi-axial fatigue analyses separately, since they require different analysis parameters. The next two sections describe the uni-axial and multi-axial fatigue analyses,

respectively.

## 5.3 Uni-axial Fatigue

In this section, a uni-axial assessment is conducted on the hinge. The chart below (figure 5-3) shows the required path for a successful prediction of life. Based on the observations in the previous section, the S-N approach is used for the uni-axial fatigue analysis. The available S-N curve is characterized from tests performed on a smooth cylindrical hourglass specimen at fully reversed loading. The hinge differs significantly from the test specimen in geometry, loading environment and surface finish. These differences have a significant impact on fatigue life. Hence, the S-N curve is modified accordingly so that it can be used to predict life.

The modification of the S-N curve is solely dependent on the loading history, which is the service environment the hinge is subjected to in the experimental process. This means that the static load applied to the hinge is cycled, based upon the loading history.

### 5.3.1 Loading History

The loading history for the hinge in the uni-axial fatigue analysis is obtained experimentally. Figure 5-4 shows the loading history. In general, the range of any loading history is from –1 to +1. For a fully tensile loading, which is the case here, the minimum value should be greater than zero and the maximum value no greater than +1. In the uni-axial experiment, the applied load was increased up to a maximum value of 110 Nm and released.

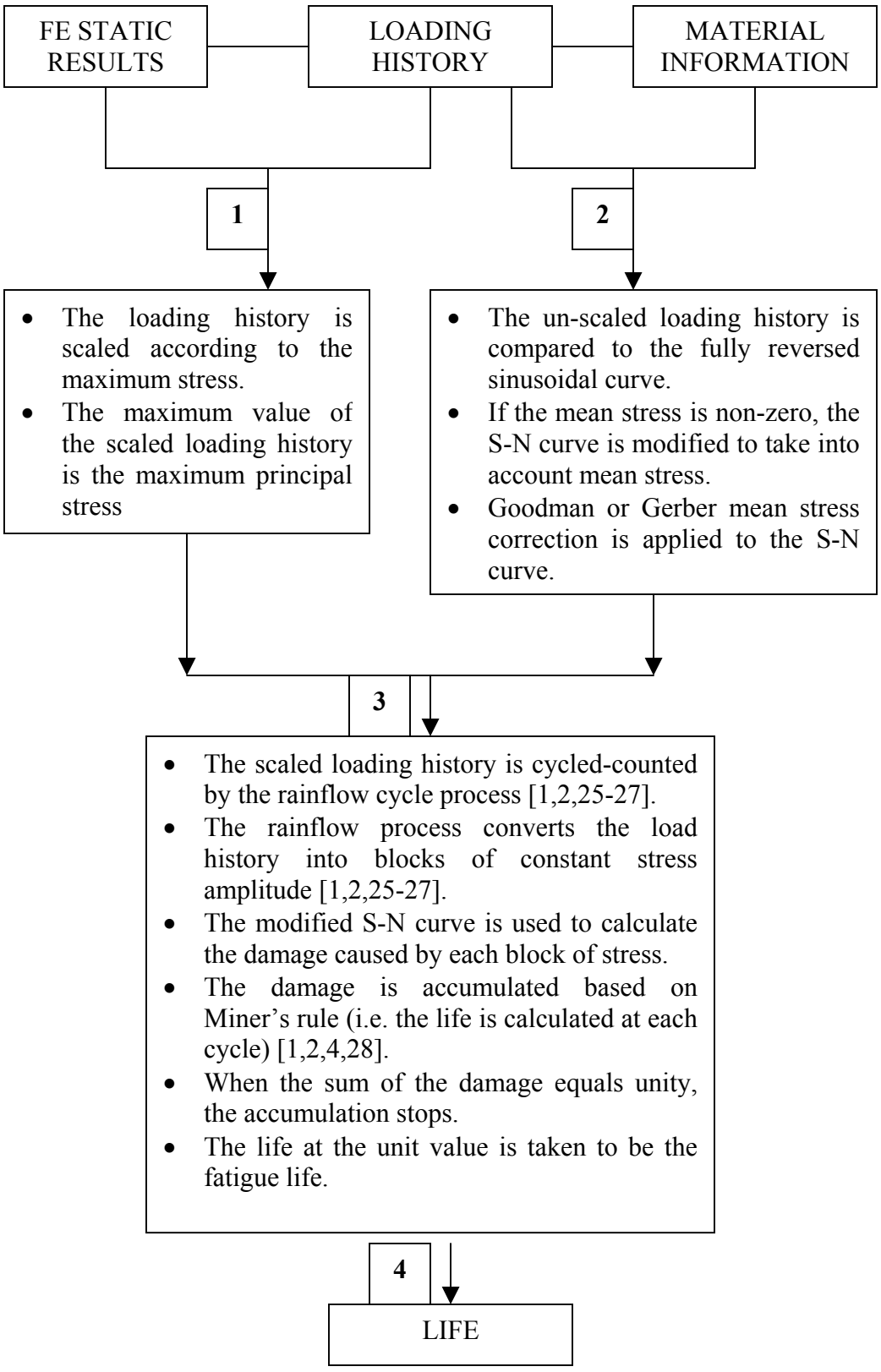


**Figure 5-3 Flow-Chart for Uni-axial Fatigue Life Calculation**

Hence, the true loading history has a minimum and a maximum value of 0 Nm and 110 Nm respectively. However, in FEA, the curve defining the loading history is normalized (i.e. the true loading history is divided by the maximum value of 110 Nm). The static stress resulting from the applied load of 110 Nm is then superimposed with the normalized loading history. As such, the true service the hinge is subjected to in the experiment is properly reflected by this superposition method.

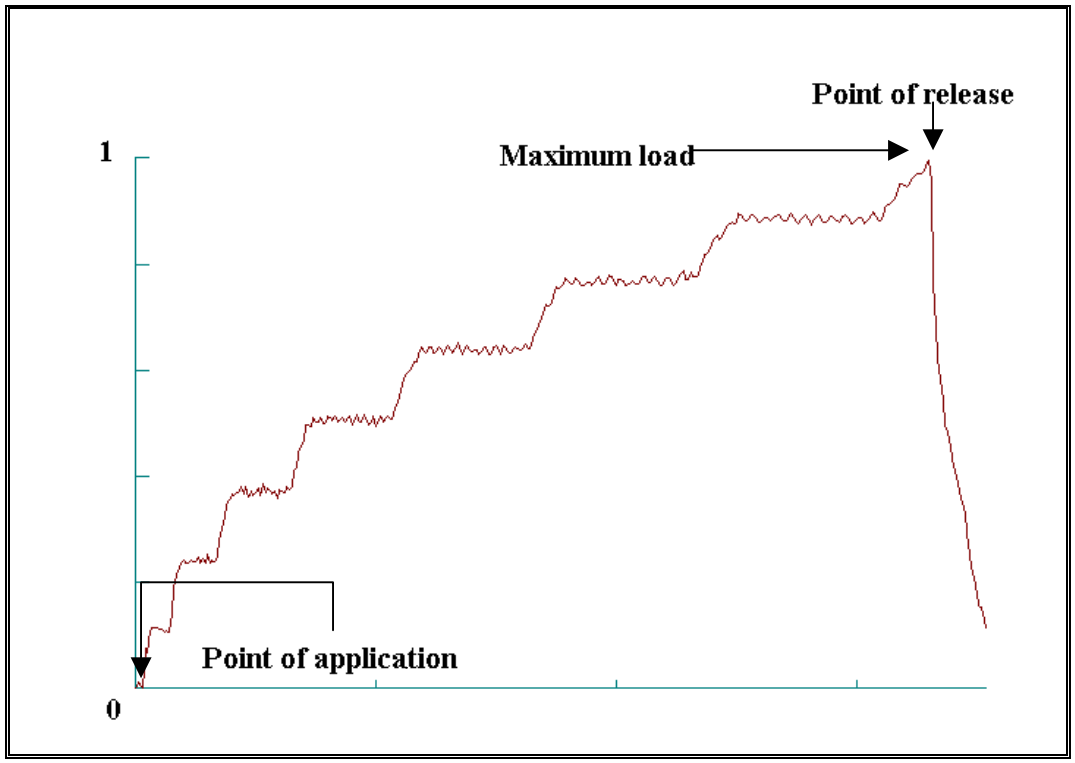


**Figure 5-4 Normalized Loading History for the Uni-axial Analysis**

### 5.3.2 Analysis Parameters

The next step in the analysis is the implementation of the S-N curve. As previously mentioned, the latter has to be modified in case mean stresses are present. When the loading history is compared to a sinusoidal waveform, it is

clearly seen that mean stresses are present. Therefore, based on either Goodman or Gerber mean stress correction factors, the S-N curve is modified. This can be done by pivoting the elastic line about the intersection point on the horizontal life axis (see figure 5-5).

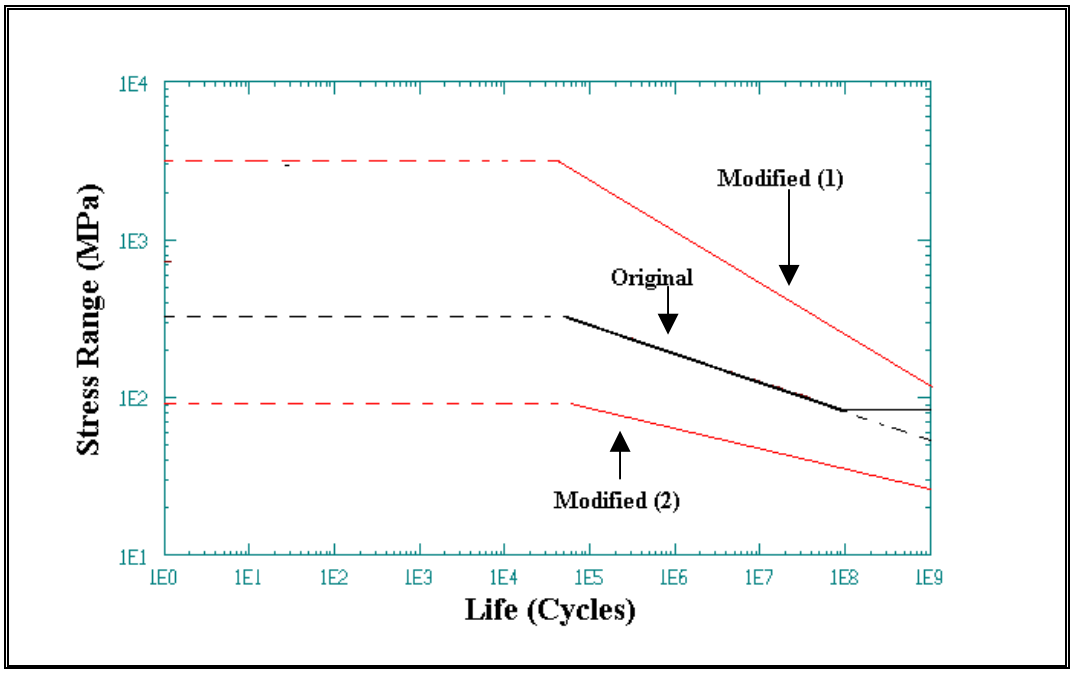


**Figure 5-5 Mean Stress Correction in the S-N Curve**

To date, little or no experimental data exist to support one approach over the other. Therefore, both Goodman and Gerber corrections are used and the one yielding the most conservative result is taken as the appropriate correction factor. The final step involves combining the scaled loading history and the modified S-N curve. The loading history is converted to constant blocks of stress amplitudes such that it can be used on the S-N curve. This conversion is done from the rainflow cycle counting process.

The rainflow cycle counting is an algorithm commonly used in fatigue whereby an irregular load history is converted to blocks of constant amplitude

like a histogram [1,2,25-27]. Figure 5-6 shows a sketch of this process.

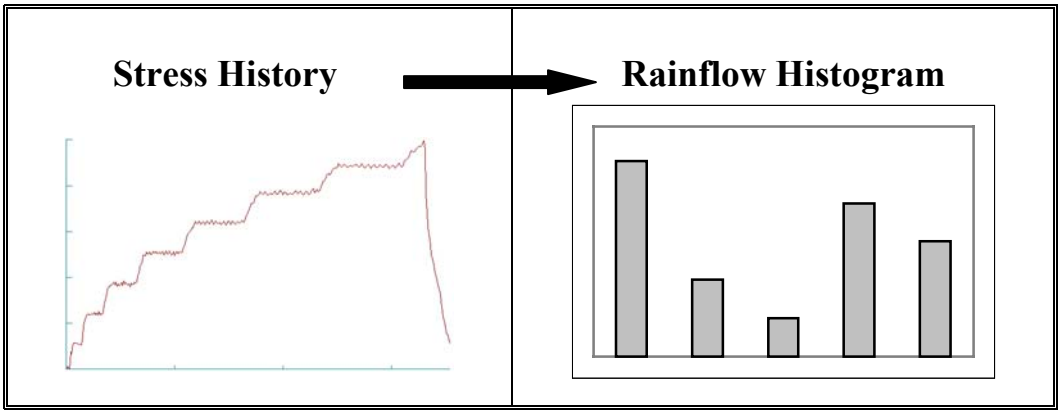


**Figure 5-6 Histogram Illustrating the Rainflow Procedure**

After the rainflow histogram is created, the life is calculated via the linear damage summation based upon Miner's rule [1,2,4,28]. Miner calculated the life by summing the damage after each cycle. For each block in the histogram, the corresponding life is extracted from the S-N curve and a damage parameter is calculated (see figure 5-7).

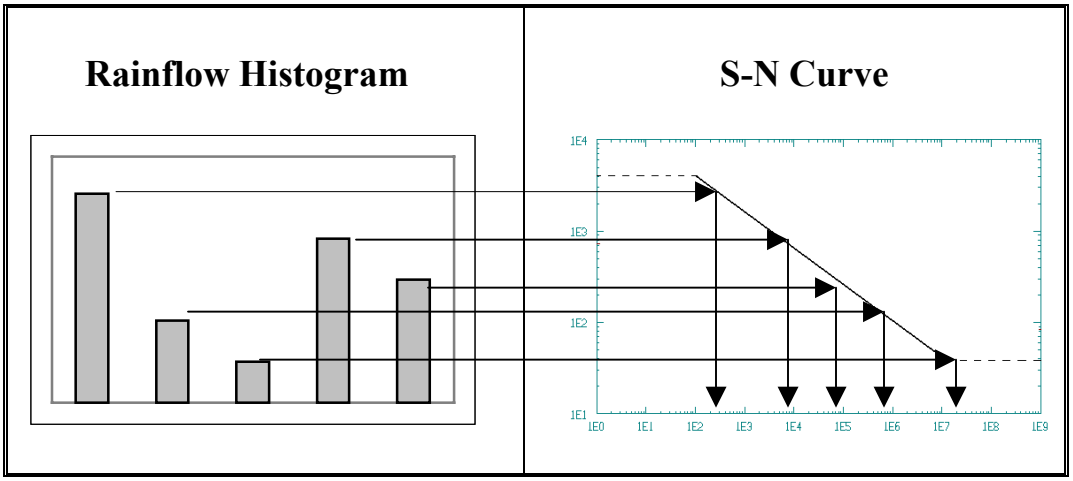


**Figure 5-7 The Linear Damage Summation Procedure**

Henceforth, the damage parameter at stress $S_1$ is denoted by the ratio of the number of cycles of operation to the total number of cycles to cause failure at that stress level [1]. This can be mathematically expressed as follows [1]:

The damage parameter $D_1$:

$$D_1 = \frac{n_1}{N_1} \tag{5.1}$$

where, $n_1$ is the first cycle and $N_1$ , the corresponding life cycles to failure obtained from the S-N curve from $S_1$. Hence, failure is predicted when the sum of the damage parameter equals unity.

$$\sum_{i=1}^{n} D_i = 1 \tag{5.2}$$

Furthermore, the number of life cycles to failure is the inverse of the damage parameter at which the accumulation stops (i.e., if the damage sum approaches unity at $D_{1000}$, then the corresponding life cycles to failure is 1/ $D_{1000}$).

All the steps herewith mentioned are included in MSC.FATIGUE. These procedures can be done in a few easy steps by selecting the appropriate stress/strain combination, material curve and mean stress correction. The uni-axial fatigue results are reported in the following sub-section

### 5.3.3 Simulation Results

In summary, the maximum principal stress of 255 MPa from FE is superimposed with the loading history and the latter is cycle-counted by the rainflow procedure to create a set of blocks with constant stress amplitude called the rainflow histogram. Moreover, the loading history is compared with a sinusoidal waveform to assess the presence of mean stresses in the hinge. The corrected S-N and the rainflow histogram are simultaneously used to calculate

damage using Miner's rule. The fatigue life cycles to failure is then evaluated from the accumulation of damage. Figure 5-8 below shows the fatigue life contour in the hinge. The minimum life cycles to failure is shown in a log scale on the bottom right corner of the figure.

The weakest spot is around the edge of the oval hole in the DS bracket. The minimum life cycles to failure is 309,000 cycles. It should be noted that if the analysis is conducted as described, the minimum life is 383,000 cycles. This is because the hinge is considered to have a perfectly polished surface. In reality, the edge of the hinge has a rough surface due to manufacturing processes. The surface roughness was measured at different locations in the hinge and the average value implemented in the analysis. That average value is 353 microns. The inclusion of surface roughness yielded a life of 309,000 cycles (the inverse logarithmic of the value shown in figure 5-8).

As previously mentioned, the location of the hot spot is around the oval hole of the DS bracket. More precisely, crack occurs at the contact surface between the bolt and the edge of the bracket. This can be explained by considering the sliding motion of the bolt around the oval hole.

In contrast to the circular hole, the bolt does not fit perfectly around the edge of the oval hole. The clearance is to allow easy placement and removal of the hinge from the vehicle. Thus, when the load is applied and cycled, the bolt slides across the oval hole. Although the sliding movement is not very significant, it causes the occurrence of scratch marks, on a microscopic scale, which eventually turn into crack. Such mechanisms are carefully modeled

in the FEA. The maximum stress located on the top or bottom surface of the hole (i.e., areas in contact with the washer) were ignored in the analysis.

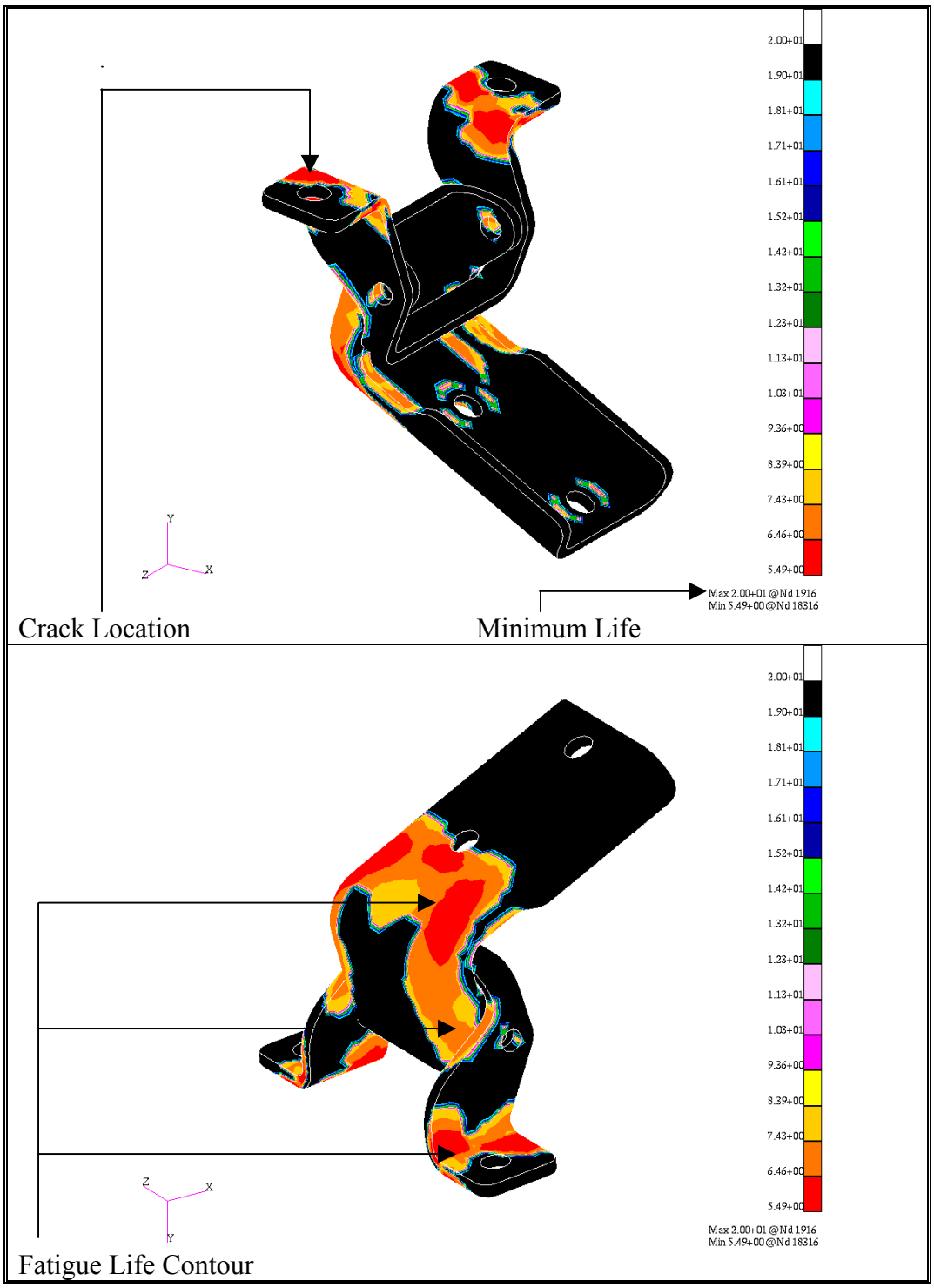


**Figure 5-8 The Uni-axial Fatigue Life Contour in the Hinge**

### 5.3.4 Results Summary and Conclusions

The life predicted from the numerical analysis was 309,000 cycles compared to 289,000 cycles tested experimentally. From a theoretical or numerical point of view, fatigue is usually predicted in the order of two or three times the realistic value. In this case, life was predicted accurately. The required fatigue life is 260,000 cycles was reached. However, the environment in which the hinge operates is far from being strictly uni-axial. The service environment of the hinge is multi-axial. Hence, a multi-axial fatigue analysis needs to be conducted.

## 5.4 Multi-axial Fatigue

In this section, a multi-axial assessment is conducted in the door hinge system. To conduct such assessment, the equivalent stress-strain approached is used. This assumes a uni-axial stress state when calculating life. The bi-axiality ratio and angle of spread is evaluated at critical locations in the hinge system in order to decide in the existence of a state of proportional of non-proportional loading exist. For proportional loading, the uni-axial assumption is valid and the predicted life is correct. In case a state of non-proportional loading exists, life has to be re-evaluated by the critical plane approach. Figure 5-9 shows a flow chart adopted in the equivalent stress-strain approach.

Moreover, from static FE results, it is seen that the stress and strain values fall in the low cycle region. Hence, the equivalent stress-strain approach uses the σ-ε and ε-N curves to evaluate life. In the next section, it is seen how the multiple load cases and their respective loading histories are combined.

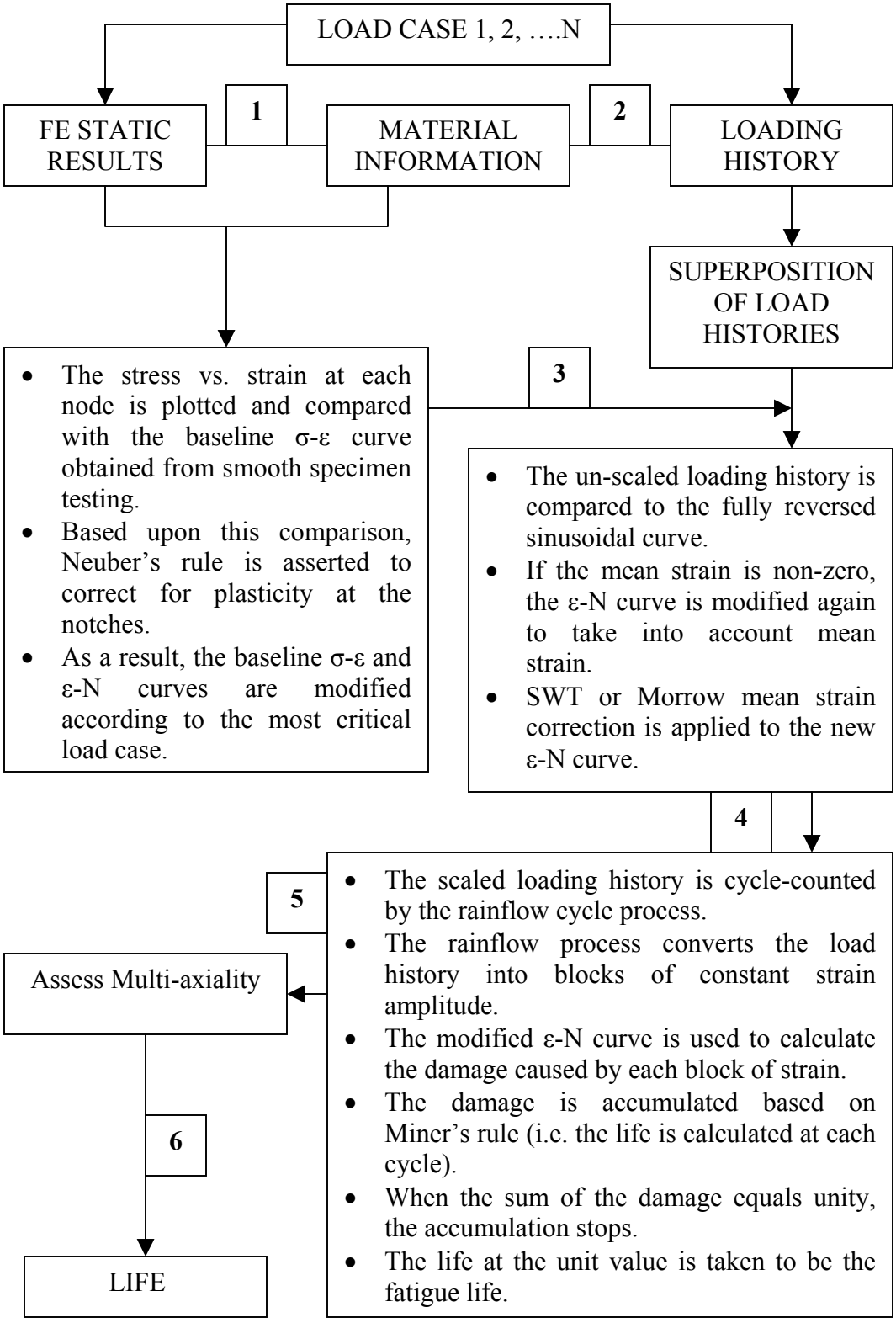


**Figure 5-9 Flow Chart for Multi-axial Fatigue Life Calculation**

### 5.4.1 Loading History

The loading history is the service environment the hinge system is subjected to in its duty life cycle. The loading history for the hinge system is the open/close door movement. This means that the loading history starts at the fully-closed position and stops at the fully-opened position of the door. However, since the full range of motion of the door is not considered, the loading history was modified. The loading histories shown in figure 5-10 are the outputs from the actual testing process. The loading histories in the multi-axial case consist of two dissimilar cases. Referring to the experimental testing process, the induced loading consists of two torques. The first torque (T1) is at 135 Nm and the other (T2) at 335 Nm. As such, T1 is cycled 23 times before T2, and this process repeats itself.

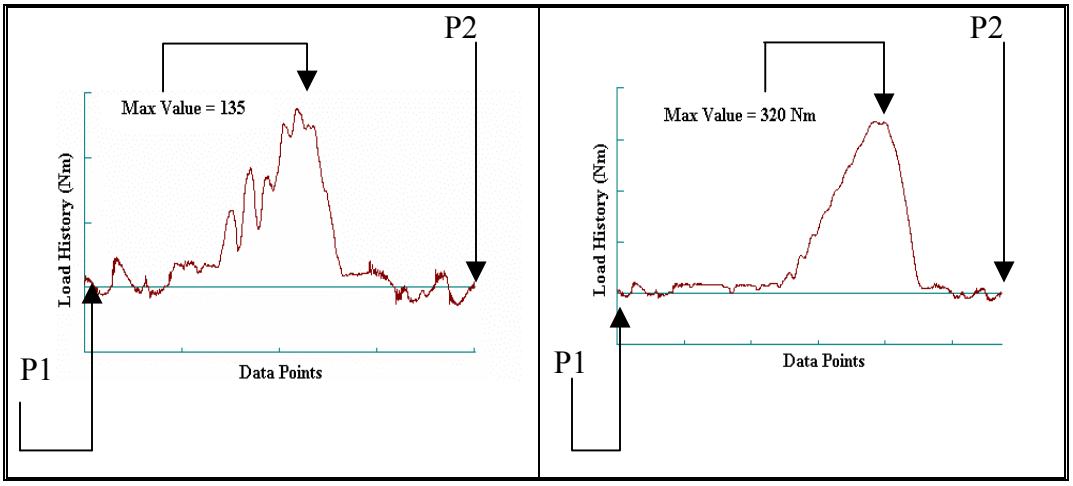


**Figure 5-10 Loading Histories for the Applied Torque, T1 and T2**

In FEA, the loading histories are combined, normalized and input as a single loading history. This is done by cumulatively adding 23 cycles of T1 and 1 cycle of T2. Hence the entire loading history consists of 24 cycles. Henceforth, the unit of life cycles to failure is entered as 24 cycles. Hence, each

calculated life in the linear damage summation is divided by 24.The complete loading consisting of a total of 24 cycles is shown in figure 5-11. P1 and P2 are the closed position of the door whereas the maximum point on each curve represents the full opened position of the door.

The combined loading history has close to a million data points. As seen in figure 5-11, each loading torque has small spikes. Those spikes are the result of vibration in the hinge when the door swings from a closed to an opened position. If the damage is summed at each data point, the simulation time will be very lengthy. To reduce the simulation time, a process called peak valley slicing is used [1,2]. Peak Valley Slicing (PVS) is a fairly simple mechanism, which tracks and extracts the peaks and valleys of all signals to be used in the analysis. Figure 5-11 shows the process of PVS, whereby the original complete loading consisting of one million data points is converted to one with only 292 points. When a gate value is entered, which is usually a small percentage of the load, the peaks and valleys that fall within that gate value are deleted. Hence, the number of data points is reduced.

This procedure accelerates the analysis and is useful when complex loading histories are involved in a fatigue analysis. The combined loading history is afterwards normalized and implemented in the analysis. In contrast to the torques, the weight does not change throughout the open/close door movement. Therefore, the weight history is entered as a simple static offset of the stress results from FE and need not be normalized.

Similar to the S-N approach in the uni-axial fatigue analysis, the load

history is compared to the sinusoidal waveform and corrected for mean strain. Prior to that, the loading histories are combined with their respective static load case strain results. Furthermore, the two load histories from the combined torques and weight are superimposed and resolved to a single scalar loading history.

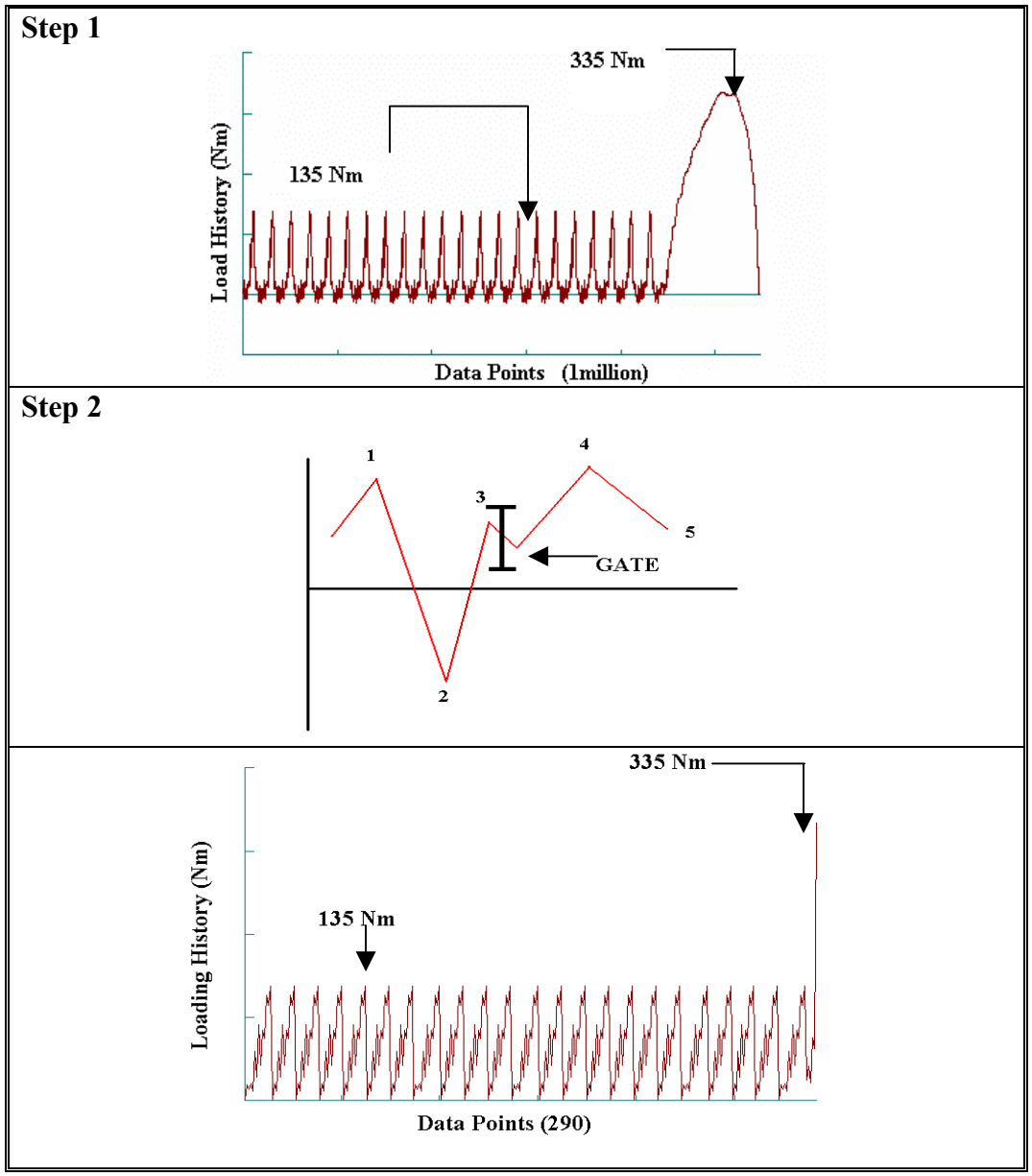


**Figure 5-11 Combined Loading Histories from PVS**

### 5.4.2 Analysis Parameters

Unlike the S-N approach, the equivalent stress-strain approach involves the use of the σ-ε and ε-N curves. In addition, Neuber's rule is used in the low cycle region to correct for plasticity by shifting both σ-ε and ε-N curves upward. [1,2,4,19]. The amounts the curves are shifted depend on the extent of plasticity involved. Henceforth, the stress and strain results from FE are used to determine the amount of plastic deformation in the hinge. The stress vs. strain result is plotted at each node from the FEM and the resulting plot compared with the baseline σ-ε curve obtained from the smooth specimen testing. This is the main reason behind the use of cyclic stress-strain in the FE static analysis. Hence, the stress vs. strain plot has the shape of the predefined σ-ε curve and can be accurately compared with the corresponding baseline curve (see figure 5-12). The ε-N curve is modified by the same amount.

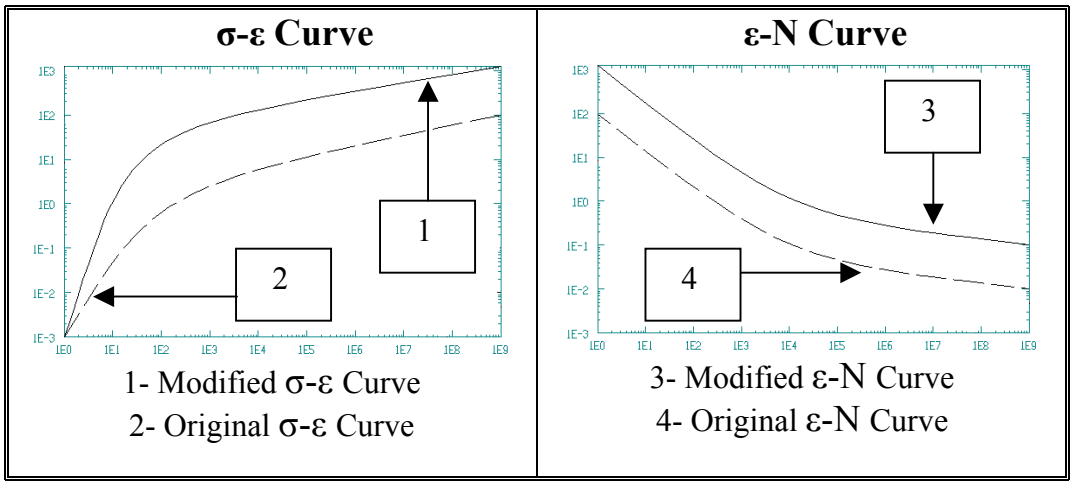


**Figure 5-12 Neuber Correction Procedure**

The modified ε-N curve is further corrected for mean strain. This process is similar to the uni-axial S-N approach, where the loading history is compared to the sinusoidal waveform. Since the loading history is tensile, the

SWT correction factor is used. SWT corrects for mean strain by pivoting the ε-N curve about the zero-life vertical axis (see figure 5-12). Miner's rule is then used to sum the damage and predict life (see figure 5-13).

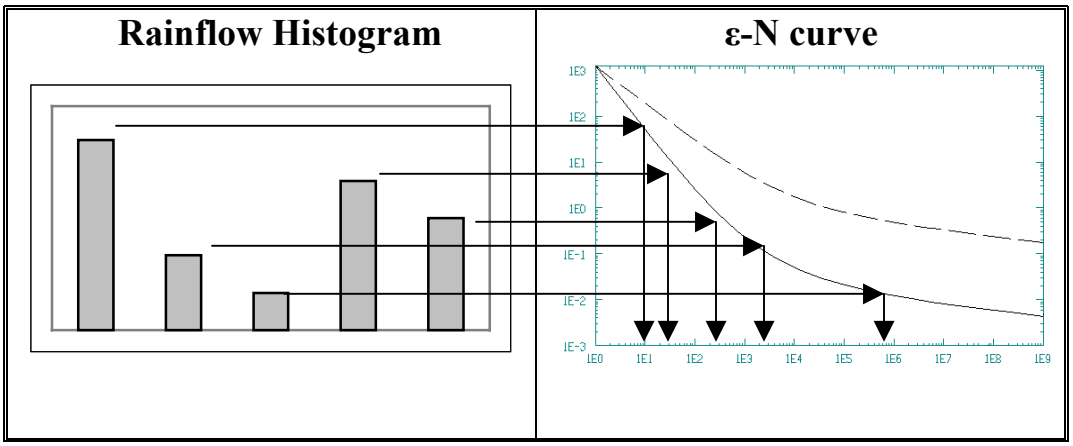


**Figure 5-13 SWT Curve and The Linear Damage Summation Procedure**

### 5.4.3 Simulation Results

In summary, the maximum principal strain for each load case (applied torque and weight) is combined with the respective loading histories. The loading histories are superimposed by the principle of linear superposition and cycle counted by the rainflow procedure. The resulting rainflow histogram of constant strain and the modified ε-N are used to predict life. A multi-axial assessment is then conducted at critical locations in the hinge system to determine whether a state of non-proportional loading exists. Figure 5-14 below shows the fatigue life contour in the hinge system. It is seen that the crack location is on the bottom surface of the DS bracket with a life of 10,470 cycles to failure. The log of life is shown on the bottom right corner of figure 5-14.

The shortest life appears to be around the oval-hole surface, which is in contact with the washer. The location of crack at that location is spurious since a

surface in contact with a washer cracks only in the presence of machine marks or extrusions. This is not the case here, meaning the location and estimation of life is incorrect. The occurrence of a crack at that location is due to the presence of artificial stresses from FE static analysis. The contact surface of the washer and the doorframe was constrained with rigid MPC. As a result, the MPC acts as links that concentrate loading at specific nodes, thus causing the high stresses. The stresses and strains at loading and constrained nodes should be ignored in any FE static analysis.

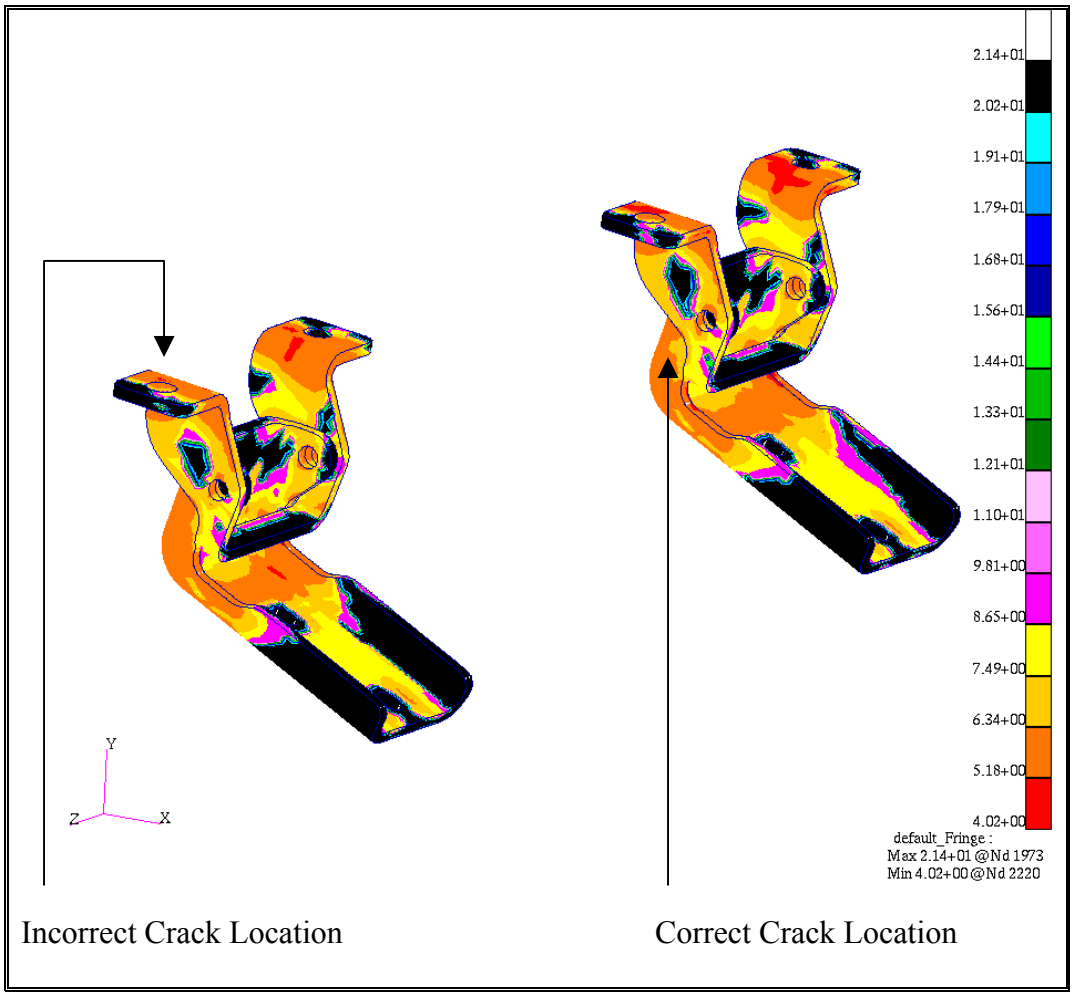


**Figure 5-14 Fatigue Life Contour Under Multi-axial Stress State**

The real hot spot is around the flange in the BS bracket. More precisely, the crack location is at the notch radius. The minimum life cycles to failure at that location is 99, 600 cycles. The initial value was calculated as 119,000 cycles. With the inclusion of an average surface roughness value of 213 microns, the life reduced to 99, 600 cycles.

The next step in the analysis is to assess multi-axiality by calculating the bi-axiality ratio and angle of spread at the critical location. Figure 5-15 (a) displays the plot of Maximum principal strain vs. bi-axiality ratio at every reversal in the loading history. Similarly, figure 5-15 (b) shows a plot of reversal vs. angle of spread.

It can be seen from figure 5-15 (a) that the bi-axiality ratio tends to line up vertically, not equal but close to zero at the most critical node. This indicates that a proportional state of stress exists. As such, the assumption on the equivalent stress-strain approach is valid. This observation is further supported by examining at the angle of spread (figure 5-15 (b)), which shows that the angle is at a constant value. Hence, the predicted life is correct.

### 5.4.4 Results Summary and Conclusions

The life predicted from FEA is 99,600 cycles compared to the experimental value of 72,000 cycles. Moreover, it can be seen that the accepted standard value of 260,000 cycles was not reached. This means that the hinge has to be replaced after 72,000 cycles. The solution to this problem is to conduct a sensitivity analysis in the hinge to improve the life. The sensitivity analysis was conducted and the results are illustrated in the appendix.

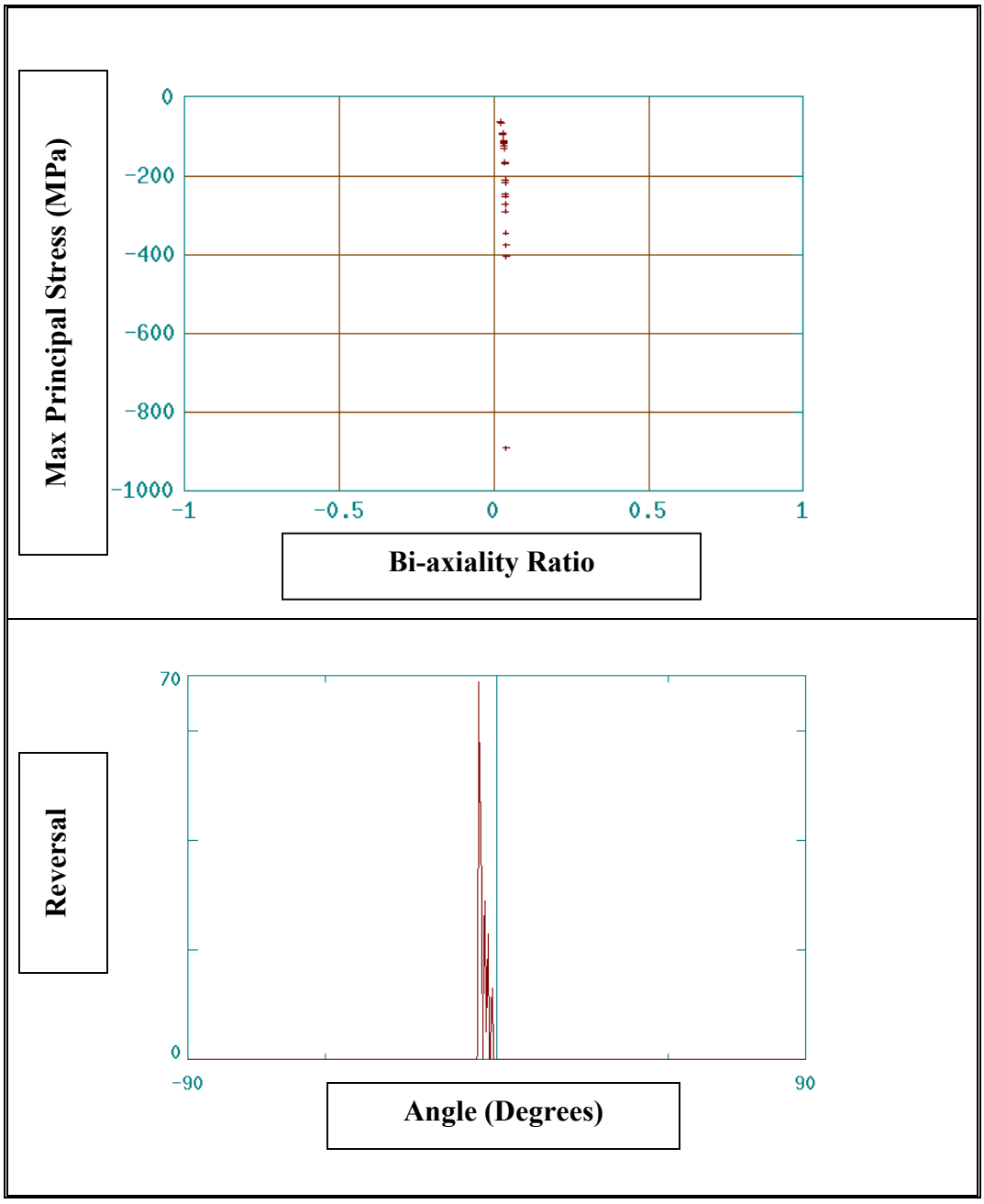


**Figure 5-15 Bi-axiality Ratio and Angle of Spread Plots**

# CHAPTER 6 CONCLUSION AND RECOMMENDATIONS

## 6.1 Conclusion

FE based fatigue was used to locate the critical point of crack initiation and to predict the life in a door hinge system. Both uni-axial and multi-axial fatigue analyses were conducted. The simulation results were experimentally validated through full-scale uni-axial and multi-axial fatigue tests conducted at Van-Rob Stampings Inc. For the computational approach, two dissimilar FE models were built, for uni-axial and multi-axial loading cases, respectively. Also, two separate FE analyses were conducted in each loading case; static and fatigue. The static analyses were conducted prior to fatigue and the stress and strain results were then used as input to fatigue life prediction. The simulation results for the uni-axial loading case yielded a life of 309,000 cycles compared to 292,000 cycles obtained experimentally. Similarly, a life of 99,600 cycles was obtained compared to the experimental value of 72,000 cycles for the multi-axial loading case.

The accuracy of the simulation results showed that the FE based fatigue life prediction approach was very effective. Hence, this approach can be efficiently employed in place of costly, time-consuming fatigue experiments at the preliminary design stage. The simulation results also provide the product design specialists with substantial savings, enabling fewer prototypes to be tested at the preliminary design level.

The standard requirement for the durability of such a hinge in the ground

vehicle industry is 260,000 cycles. From the multi-axial results, it is seen that the life of the hinge was distinctly lower than the standard requirement. Hence, traditional optimization techniques were used to improve the life expectancy of the hinge. However, due to the strong influence of cost in design optimization, it was seen that the life could only be altered by modifying the notch radius of the hinge. The life was only increased to 189,000 cycles under the multi-axial loading case. Although the required design life was not attained, the improvement in fatigue life enables the replacement of the door hinge only once instead of four times during the in-service monitoring phase.

## 6.2 Recommendations for Future Work

As stated previously, the simulation results were experimentally validated. However, it should be noted that fatigue is essentially a statistical quantity. Presently, numerical or theoretical approaches can only predict fatigue life up to a factor of two. Accurate results are obtained in very few cases, as is for the door hinge. The statistical nature of fatigue is illustrated in chapter three, where it is seen that the lives evaluated experimentally varies from 72,000 to 92,700 cycles for the multi-axial loading case. The cause for this discrepancy is mainly the surface roughness in the hinge. During the manufacturing process, each hinge has a different surface roughness associated with it. Therefore, for future research, more hinge samples should be tested and their surface roughness measured prior to testing. Furthermore, the surface roughness values should be implemented in the simulation procedure. As such, a correlation can be found between the experimental and simulation results (see figure 6-1). This

correlation can then be used to evaluate fatigue life in different hinge designs or other components and structures.

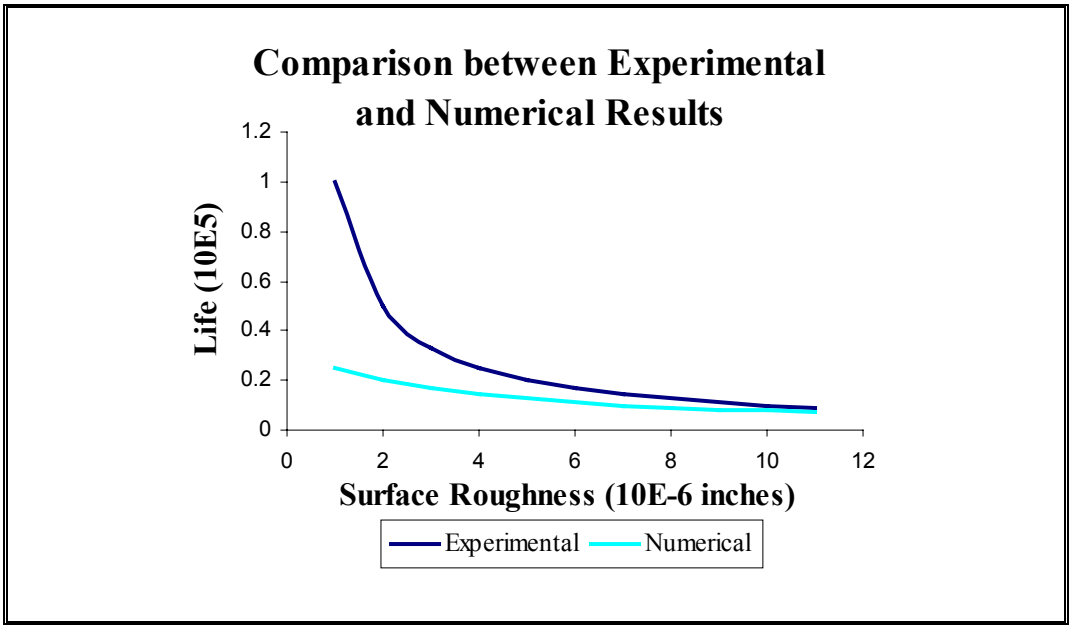


**Figure 6-1 Chart of Fatigue Life vs. Surface Roughness**

Moreover, the minimum required life of 260,000 cycles was not obtained. Hence, computational optimization techniques have to be used to improve the life of the hinge. Hereafter, a sensitivity analysis was conducted on the hinge. The analysis included the effects of thickness, material's UTS, surface treatment and notch radius. The results, illustrated in the appendix, demonstrate how the life of the hinge can be increased. Hence, it is recommended to optimize the hinge taking into account these sensitivity factors.

# APPENDIX

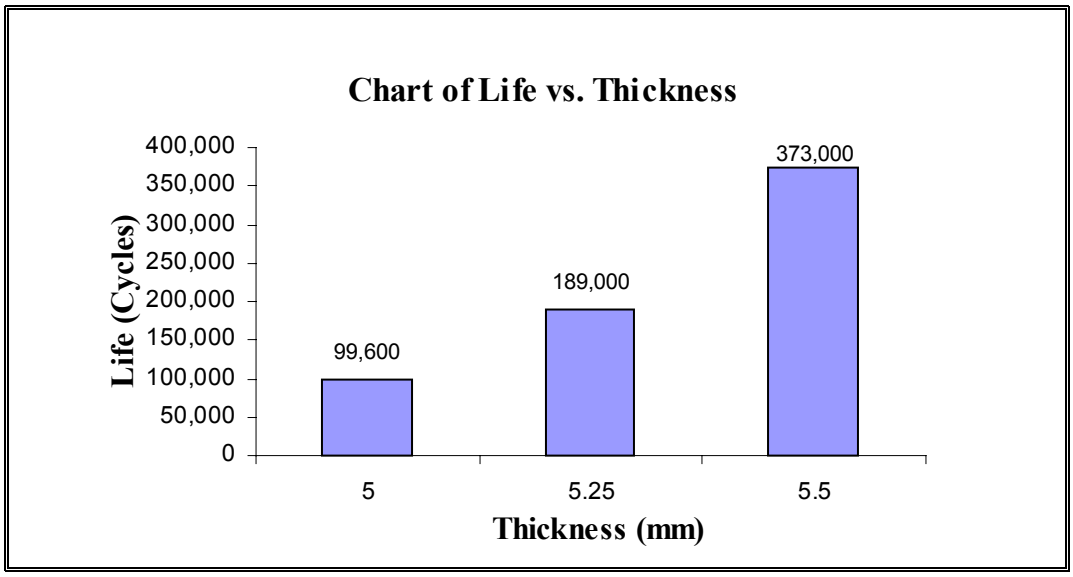


**Figure A-1 Effect of Thickness on the Fatigue Life of the Hinge**

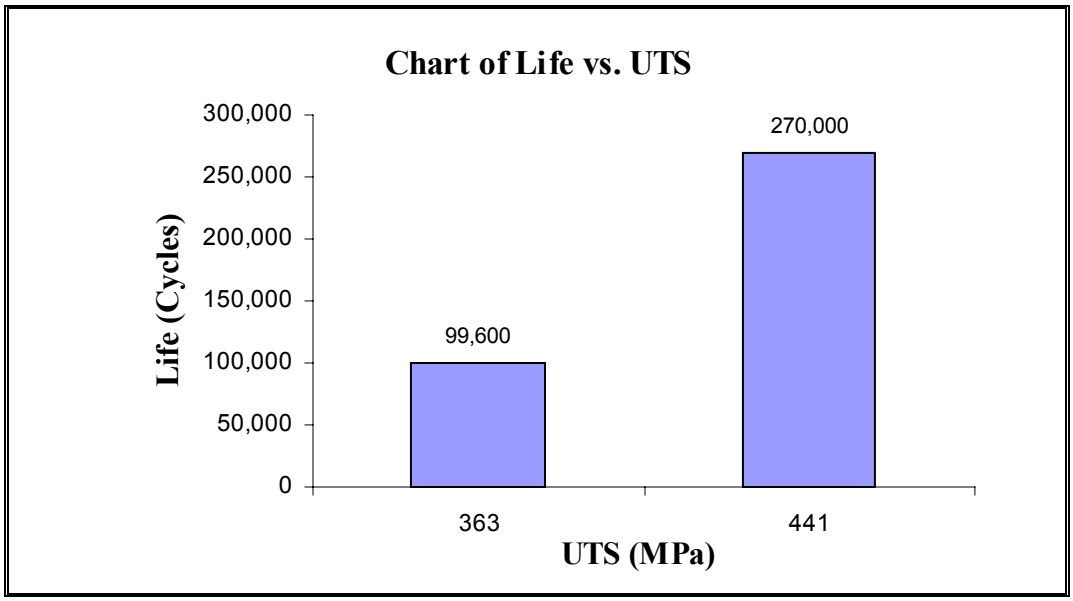


**Figure A-2 Effect of Steel's UTS on the Fatigue Life of the Hinge**

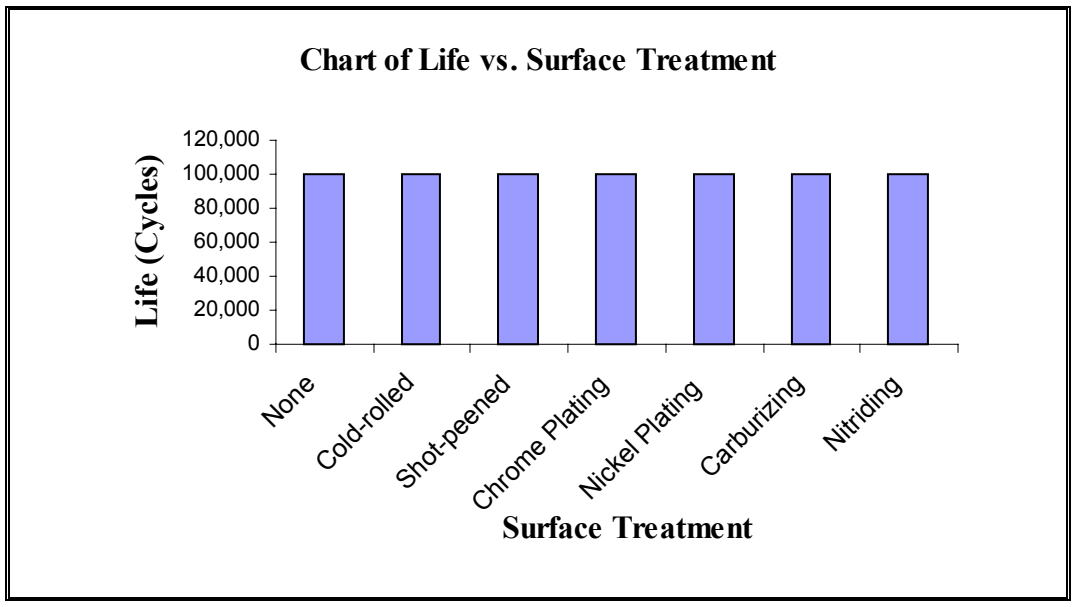


**Figure A-3 Effect of Surface Treatment on the Fatigue Life of the Hinge**

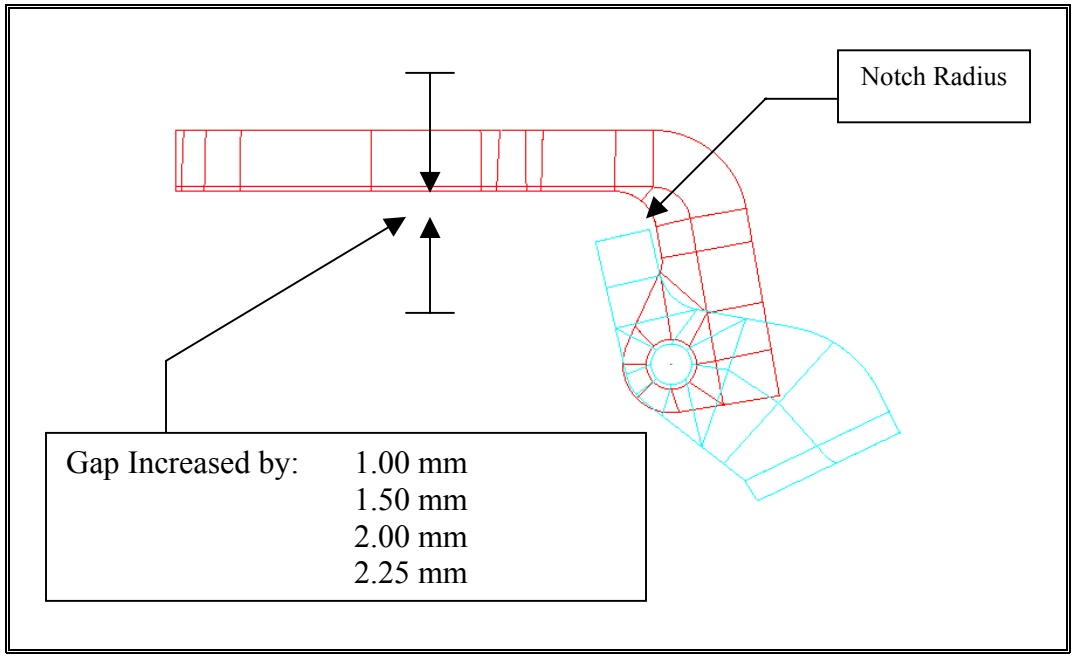


**Figure A-4 Notch Radius Increase**

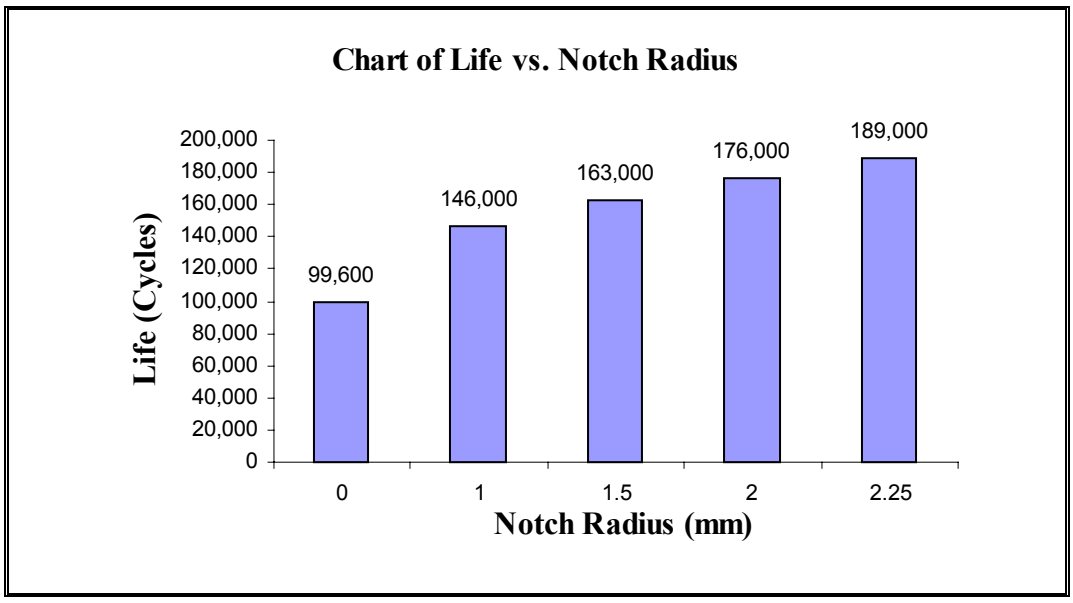


**Figure A-5 Effect of Notch Radius on the Fatigue Life of the Hinge**

# REFERENCES

[1] MSC.Fatigue [Encyclopedia]. Los Angeles (CA, USA): MacNeal Schwendler Corporation, 2003.

[2] SAE International, SAE Fatigue Design Handbook, Third Edition, AE-22, Prepared under the auspices of the SAE Fatigue Design and Evaluation Committee, 1997.

[3] Miller, K. J., "Metal Fatigue- Past, Current and Future," *Proceedings of the Institution of Mechanical Engineers*, Vol. 205. 1991.

[4] Ellyin, Fernand, Fatigue Damage, Crack Growth and Life Prediction. New Delhi: Chapman & Hall, 1997.

[5] Raske, D. T., and Morrow, J., Mechanics of Materials in Low Cycle Fatigue Testing. ASTM. 1969. pp. 1-25.

[6] Bannantine, J. A., "A Variable Amplitude Multi-axial Fatigue Life Prediction Method," Ph.D. Dissertation. The University of Illinois, Champaign, Illinois. 1989.

[7] Socie, D. F., "Multi-axial Fatigue Damage Models," *J. of Engineering Materials and Technology*, ASME, Vol. 109. October 1987. pp. 293-298.

[8] Socie, D. F., and Morrow, J., "Review of Contemporary Approaches to Fatigue Damage Analysis," in Risk and Failure Analysis for Improved Performance and Reliability, J. J. Burke and V. Weiss. Plenum Publishing Corp. 1980. pp. 141-194.

[9] Fatemi, A., and Socie, D. F., "A Critical Approach to Multi-axial Fatigue Damage Including Out-of-Phase Loading," *Fatigue and Fracture of Eng.*

*Matls. and Structures*, Vol. 11, No. 3. 1988. pp. 149-165.

[10] Wang, C. H., and Brown, M. W., "Life Prediction Techniques for Variable Amplitude Multi-axial Fatigue- Parts 1 and 2," Journal of Engineering Materials and Technology, Vol. 118. 1996. pp. 367-374.

[11] Landgraf, R. W., "Fundamentals of Fatigue Analysis," *SAE Technical Paper*, No. 820677. 1982. pp. 11-18.

[12] Callister, W. D., Materials Science and Engineering: An Introduction. Toronto: John Wiley & Sons Inc. 1994.

[13] Gerber, T. L., and Fuchs, H. O., "Analysis of Non-propagating Fatigue Cracks in Notched Parts with Compressive Mean Stress," *Journal of Materials*. JMLSA, Vol. 3, No. 2. June 1968. pp. 359-379.

[14] Goodman, J., Mechanics Applied to Engineering. Longmans, Green and Co. 1899.

[15] Morrow, J., "Fatigue Properties of Metals," Fatigue Design Handbook. SAE. 1968. pp. 21-30.

[16] LaPointe, N. R., "Monotonic and Fatigue Characterizations of Metals," *SAE Technical Paper*, No. 820679. 1982. pp. 23-37.

[17] Smith, K. N., Watson, P., and Topper, T. H., "A Stress-Strain Function for the Fatigue of Metals," SMD Report 21. University of Waterloo. October 1969.

[18] MSC.Fatigue [Computer Software]. Los Angeles (CA, USA): MacNeal Schwendler Corporation, 2003.

[19] Neuber, H., "Theory of Stress Concentration for Shear Strained

Prismatical Bodies with Arbitrary Non-linear Stress-Strain Law," *Journal of Applied Mechanics*. ASME. December 1961. pp. 544-550.

[20] MSC.Patran [Computer Software]. Los Angeles (CA, USA): MacNeal Schwendler Corporation, 2003.

[21] MSC.Nastran [Computer Software]. Los Angeles (CA, USA): MacNeal Schwendler Corporation, 2001.

[22] MSC.Patran [Encyclopedia]. Los Angeles (CA, USA): MacNeal Schwendler Corporation, 2003.

[23] Zienkiewicz, O. C., The Finite Element Method. McGraw-Hill Book Co. 1977.

[24] Kwon, Y. W. and Bang, H., The Finite Element Method Using MATLAB. CRC Press LLC, 1997.

[25] Downing, S.D. and Socie, D.F., "Simplified Rainflow Counting Algorithms," *Int. Jnl. Of Fatigue*, Vol. 4, No. 1, January 1982, pp. 31-40.

[26] Khosrovaneh, A. K. and Dowling, N. E., "Fatigue Loading History Reconstruction based on the Rainflow Technique," *Int. Jnl of Fatigue*, Vol. 12 No. 2. pp. 90-106.

[27] Matsuishi, M. and Endo, T., "Fatigue of Metals Subjected to Varying Stress," *paper presented to JSME,* Fukuoka, Japan, March 1968.

[28] Barron, G. E., "A Finite Element and Cumulative Damage Analysis of a Keyhole Test Specimen," *SAE Technical Paper*, No. 750041. SAE. 1975.

[29] Coffin, L. F., "A Study of Cyclic-Thermal Stresses in a Ductile Metal," *ASME Transactions*, Vol. 76. ASME. 1954. pp. 931-950

[30] Lynn, A. K., DuQuesnay, D. L., "Computer simulation of variable amplitude fatigue crack initiation behaviour using a strain-based cumulative damage model," *Int. Jnl. of Fatigue* 2001:27(11): 977-986.

[31] Mitchell, M. R., "Fundamentals of Modern Fatigue Analysis for Design," *ASM, Fatigue and Microstructure*. 1979. pp. 385-437.

[32] Tucker, L. E., Landgraf, R. W., and Brose, W. R., "Proposed Technical Report on Fatigue Properties for the SAE Handbook," *SAE Technical Paper*, No. 740279. SAE 1974.

[33] Peterson, R.E., Stress Concentration Factors. New York: John Wiley & Sons, 1974.